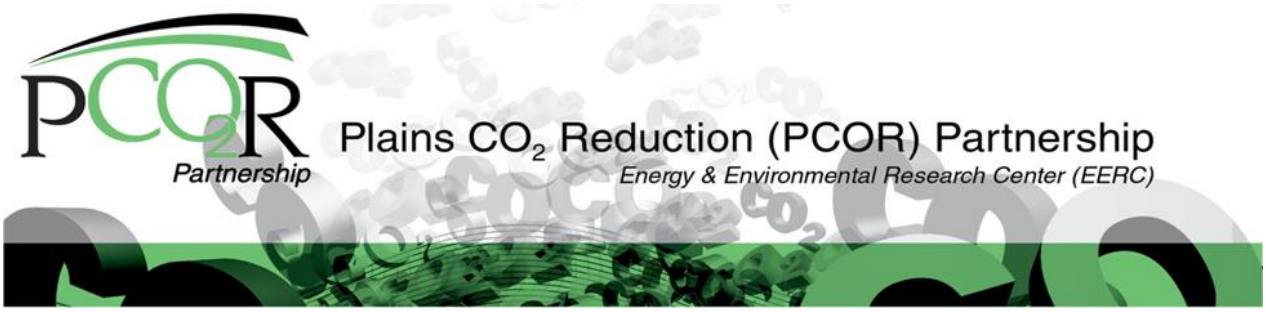

GEOLOGIC MODELING AND SIMULATION REPORT FOR THE AQUISTORE PROJECT

Plains CO_2 Reduction (PCOR) Partnership Phase III
Task 1 – Deliverable D93, Update

Originally Submitted: March 2014

Prepared for:

Andrea M. Dunn

National Energy Technology Laboratory
U.S. Department of Energy
626 Cochrans Mill Road
PO Box 10940
Pittsburgh, PA 15236-0940

DOE Cooperative Agreement No. DE-FC26-05NT42592

Prepared by:

Guoxiang Liu
Charles D. Gorecki
Terry P. Bailey
Wesley D. Peck
Edward N. Steadman

Energy & Environmental Research Center
University of North Dakota
15 North 23rd Street, Stop 9018
Grand Forks, ND 58202-9018

September 2014
2014-EERC-11-03 Approved

EERC DISCLAIMER

LEGAL NOTICE This research report was prepared by the Energy & Environmental Research Center (EERC), an agency of the University of North Dakota, as an account of work sponsored by the U.S. Department of Energy (DOE) National Energy Technology Laboratory (NETL). Because of the research nature of the work performed, neither the EERC nor any of its employees makes any warranty, express or implied, or assumes any legal liability or responsibility for the accuracy, completeness, or usefulness of any information, apparatus, product, or process disclosed or represents that its use would not infringe privately owned rights. Reference herein to any specific commercial product, process, or service by trade name, trademark, manufacturer, or otherwise does not necessarily constitute or imply its endorsement or recommendation by the EERC.

ACKNOWLEDGMENT

This material is based upon work supported by DOE NETL under Award No. DE-FC26-05NT42592.

DOE DISCLAIMER

This report was prepared as an account of work sponsored by an agency of the United States Government. Neither the United States Government, nor any agency thereof, nor any of their employees, makes any warranty, express or implied, or assumes any legal liability or responsibility for the accuracy, completeness, or usefulness of any information, apparatus, product, or process disclosed, or represents that its use would not infringe privately owned rights. Reference herein to any specific commercial product, process, or service by trade name, trademark, manufacturer, or otherwise does not necessarily constitute or imply its endorsement, recommendation, or favoring by the United States Government or any agency thereof. The views and opinions of authors expressed herein do not necessarily state or reflect those of the United States Government or any agency thereof.

NDIC DISCLAIMER

This report was prepared by the EERC pursuant to an agreement partially funded by the Industrial Commission of North Dakota, and neither the EERC nor any of its subcontractors nor the North Dakota Industrial Commission (NDIC) nor any person acting on behalf of either:

(A) Makes any warranty or representation, express or implied, with respect to the accuracy, completeness, or usefulness of the information contained in this report or that the use of any information, apparatus, method, or process disclosed in this report may not infringe privately owned rights; or

(B) Assumes any liabilities with respect to the use of, or for damages resulting from the use of, any information, apparatus, method, or process disclosed in this report.

Reference herein to any specific commercial product, process, or service by trade name, trademark, manufacturer, or otherwise does not necessarily constitute or imply its endorsement, recommendation, or favoring by the North Dakota Industrial Commission. The views and opinions of authors expressed herein do not necessarily state or reflect those of the North Dakota Industrial Commission.

TABLE OF CONTENTS

LIST OF FIGURES ii

LIST OF TABLES iii

EXECUTIVE SUMMARY iv

INTRODUCTION 1

BACKGROUND 4

APPROACH 5

GEOLOGIC UNCERTAINTY ANALYSIS 5

DYNAMIC SIMULATION AND MODEL SETTINGS 11

DYNAMIC SIMULATION RESULTS AND DISCUSSION 12
- Case 1 16
- Case 2 16
- Case 3 16
- Comparisons Between Cases 2 and 3 16

CONCLUSIONS AND FUTURE WORK 17

REFERENCES 18

GEOLOGIC REALIZATIONS MODELED ..... Appendix A

LIST OF FIGURES

1 Regional model that includes portions of North Dakota and Saskatchewan, with an area of 9740 square kilometers and a refined model of 34 square kilometers around the observation and injection wells 2

2 Simulation model with local grid refinement created to keep the grid resolution around the observation and injection wells 3

3 Magnification of the local grid refinement around the observation and injection wells in Figure 2 4

4 Distributed NTG in the P_{10} volume case near the Aquistore injection well 9

5 Distributed NTG in the P_{90} volume case near the Aquistore injection well 9

6 Distributed horizontal permeability in the P_{10} volume case near the Aquistore injection well 10

7 Distributed horizontal permeability in the P_{90} volume case near the Aquistore injection well 10

8 Relative permeability curves used for the simulation 12

9 Perforations along the injection well 13

10 Cumulative CO_2 injection histories for all cases 14

11 CO_2 injection rate histories for all cases 14

LIST OF TABLES

1 Pore Volume for the Black Island and Deadwood Sands in the Fine-Scale Model Area 6

2 PHIE, NTG, and Permeability of P_{10}, Base Case, P_{50}, and P_{90} for the Black Island and Deadwood Sands in the Model 8

3 Simulation Results Summary for All Cases 15

GEOLOGIC MODELING AND SIMULATION REPORT FOR THE AQUISTORE PROJECT

EXECUTIVE SUMMARY

The Plains CO_2 Reduction (PCOR) Partnership, through the Energy & Environmental Research Center (EERC), has been supporting, and continues to support, the Petroleum Technology Research Centre (PTRC) Aquistore project. This support has been in the form of geologic characterization, involvement in the Science and Engineering Research Committee (SERC), involvement in public outreach, developing geologic models and running predictive simulations on the expected injection program at the site. The Aquistore project is part of the world's first commercial postcombustion carbon capture, utilization, and storage project from a coal-fired power-generating facility, the SaskPower Boundary Dam, located in Saskatchewan, Canada, and will be acting as a storage site for a portion of the captured CO_2 from the Boundary Dam power plant. The Aquistore site includes one injection well and a 152-meter offset observation well. Both wells were drilled and completed in the Deadwood and Black Island Formations. At the time of this report, injection at the Aquistore site is anticipated to begin in late 2014.

To better understand the storage implications of injecting carbon dioxide (CO_2) at the Aquistore site, the EERC has constructed P_{10}, P_{50}, and P_{90} geologic model realizations and run three new predictive simulation scenarios on each realization. These models and simulations were constructed to better understand both operational and geologic uncertainties that may exist at the Aquistore site. The geologic model realizations and simulations are an update to those completed in the original report entitled "Geologic Modeling and Simulation Report for the Aquistore Project," Deliverable D93, approved in March 2014.

In this update, the same fine-scale model extent of the 34-square-kilometer PTRC 3-D seismic survey area, with higher structural resolution, was continually used for the uncertainty analysis. A low (P_{10}), mid (P_{50}), and high volumetric (P_{90}) case for the amount of pore volume accessible to store the potential injected CO_2 was ranked based on certain deviation variations of model-building parameters, including effective porosity and net-to-gross reservoir, in six sand units of the study area. Three cases with various injection rate and period schemes were simulated based on uncertainty models P_{10}, P_{50}, and P_{90}.

The first CO_2 breakthrough time, pressure change, CO_2 plume extent, and CO_2 movement probability distribution for three cases over all uncertainty realizations were monitored and calculated. The first CO_2 breakthrough for the high injection rate cases (Cases 1 and 3, 1000-tonne/day injection rate) most likely happened within the first injection month. With the various heterogeneities of the realizations, the breakthrough time may be earlier, between 14 to 19 days (Table ES-1). For the low injection rate Case 2 (1000-tonne/day injection rate), the first CO_2 breakthrough may be postponed to the end of the second month (~ 59 days) of when the injection started. This time was even extended to the middle of the third month, which is about 73 days for the first breakthrough (Table ES-1).

The pressure monitoring on the observation well was always lower than 37,250 kPa based on the injection bottomhole pressure constraint, 42,750 kPa, imposed on the injection well. The maximum reservoir pressure increasing due to CO_2 injection is around 4800 kPa within the first breakthrough time, as compared to the initial pressure of the reservoir.

The times of CO_2 breakthrough, pressure change, CO_2 movement, plume extent, and probability distribution were changed in Cases 2 and 3 because of the different injection rates and periods, especially in the individual time intervals. The differences may decrease after the same total amount of CO_2 is injected in Cases 2 and 3.

Uncertainty over geologic realizations is significant to influence CO_2 injection behavior and CO_2 movement underground. The first breakthrough time, pressure front, reservoir pressure buildup, CO_2 plume, and CO_2 probability distribution were significantly varied over such geologic realizations. Uncertainty analysis on the results by calculating the probability distribution could provide insights of CO_2 movement that ultimately helps on the decision of leakage monitoring, risk assessment, and the monitoring, verification, and accounting plan.

Table ES-1. Simulation Results Summary for All Cases

	Injection Rate, tonnes/day	Injection Period, days	Injection Pattern	First Breakthrough Time, days		
				P_{10}	P_{50}	P_{90}
Case 1	1000	30	Continuous	~19	~19	~30
Case 2	301	1095	Continuous	~59	~59	~73
Case 3	1000	933	Start–stop–start	~19	~19	~30

GEOLOGIC MODELING AND SIMULATION REPORT FOR THE AQUISTORE PROJECT

INTRODUCTION

The Plains CO_2 Reduction (PCOR) Partnership, through the Energy & Environmental Research Center (EERC), is collaborating with the Petroleum Technology Research Centre (PTRC) on site characterization; modeling and simulation; risk assessment; public outreach; and monitoring, verification, and accounting (MVA) activities for the Aquistore project. The Aquistore project is a carbon capture, utilization, and storage (CCUS) project situated near the town of Estevan, Saskatchewan, Canada, and the U.S.–Canada border. This project is managed by PTRC and will serve as buffer storage of carbon dioxide (CO_2) from the SaskPower Boundary Dam CCUS project, the world's first commercial-scale postcombustion CCUS project from a coal-fired electric generating facility. To date, an injection well and an observation research well (~152 meters apart) have been drilled and completed at the Aquistore site, with injection anticipated to begin in 2014. Using a combination of site characterization data provided by PTRC and independently acquired information, the PCOR Partnership has constructed a static geologic model to assess the potential storage capacity of the Aquistore site and provide the foundation for dynamic simulation. The geologic model and the results of the predictive simulations will be used in the risk assessment process to help define an overall monitoring plan for the project and to ensure stakeholders that the injected CO_2 will remain safely stored.

The deep saline system targeted for storage comprises the Deadwood and Black Island Formations, the deepest sedimentary units in the Williston Basin. At nearly 3500 meters below the surface, this saline system is situated below the oil production and potash-bearing formations in the region and provides a secure location for the storage of CO_2. Characterization data acquired from the Aquistore site for these formations include a 3-D seismic survey, petrophysical core data, and a comprehensive logging suite. All such available data were incorporated into model development and dynamic simulations that were reported in the previous deliverable D93 (Peck and others, 2014). This report updates the studies included in the previous deliverable D93 that focused on fine-tuning the first CO_2 breakthrough timing and pressure changes observed at the monitoring well with the various injection rates and injection periods. The model area is the same as the previous version's fine-scale 34-square-kilometer PTRC 3-D seismic survey area (Figures 1–3). The results from this study will be used in the risk assessment process for CO_2 monitoring and, ultimately, an MVA plan.

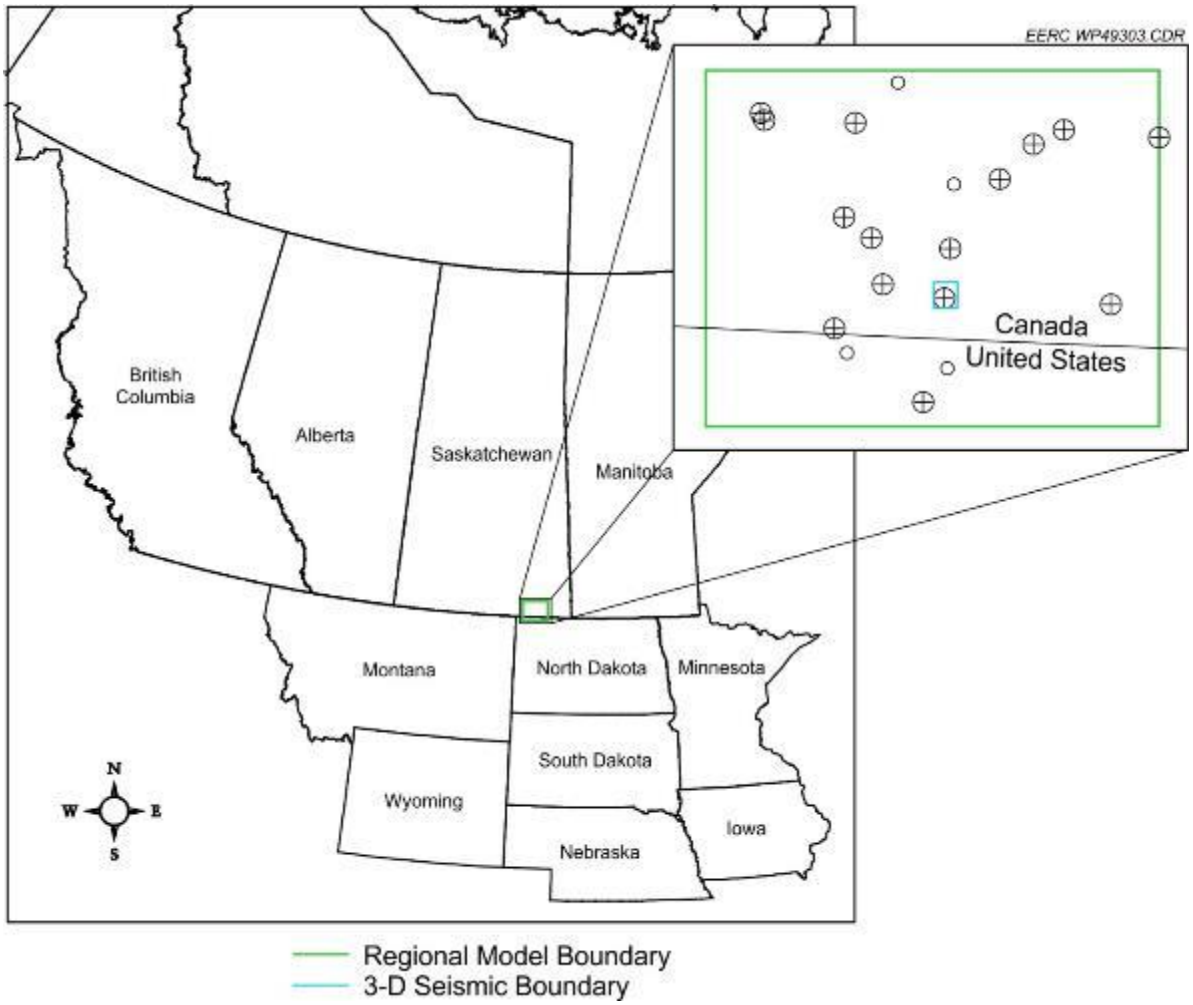

Figure 1. Regional model that includes portions of North Dakota and Saskatchewan, with an area of 9740 square kilometers and a refined model of 34 square kilometers around the observation and injection wells.

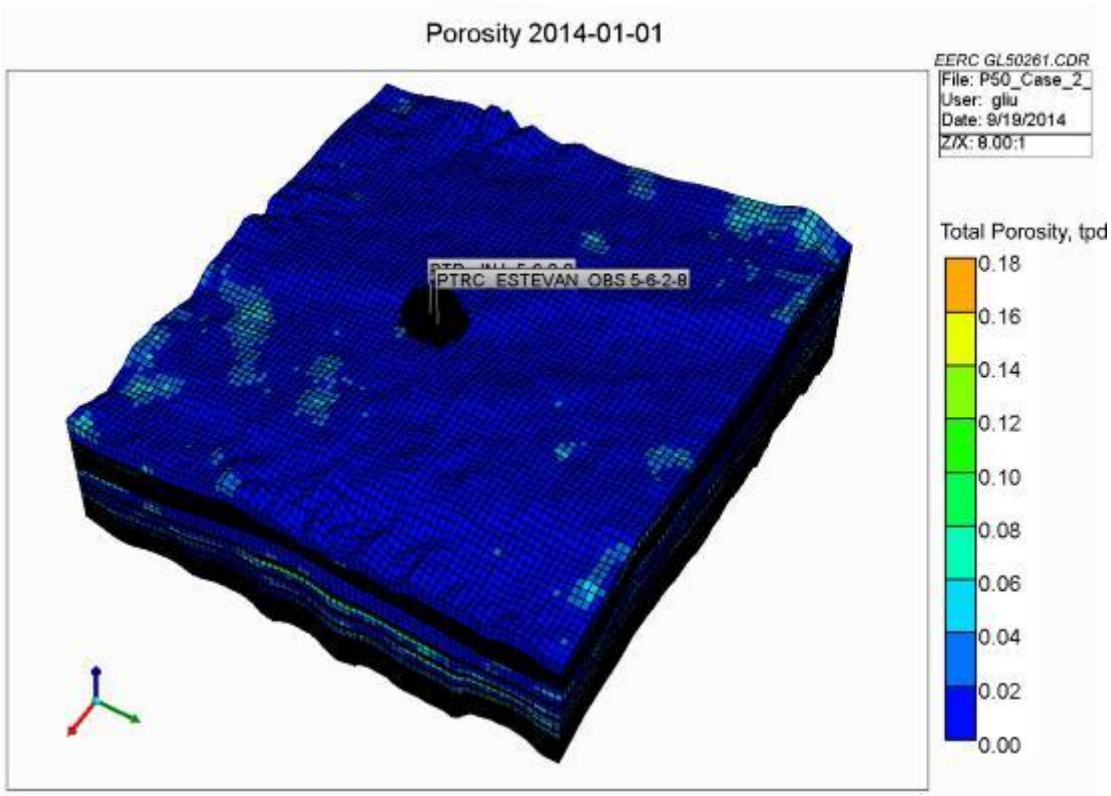

Figure 2. Simulation model with local grid refinement created to keep the grid resolution around the observation and injection wells (will be magnified in Figure 3).

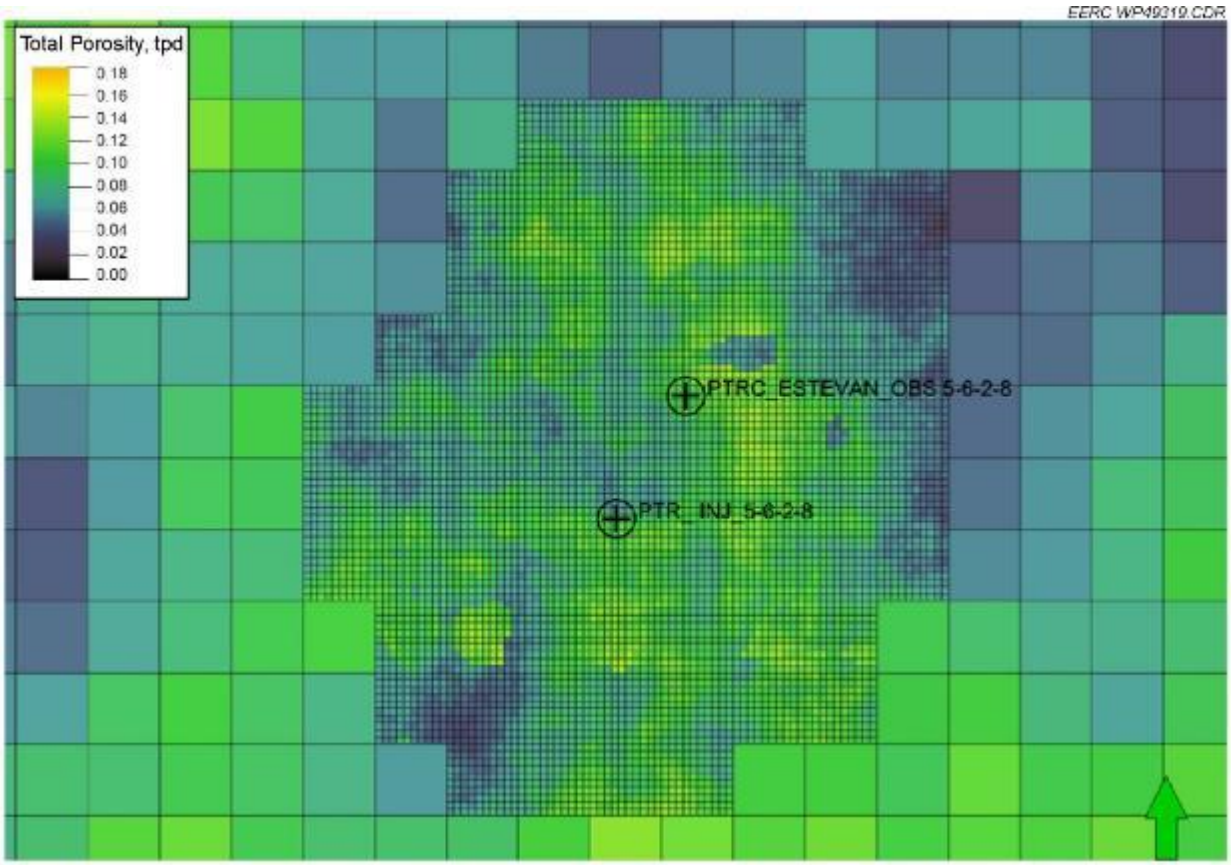

Figure 3. Magnification of the local grid refinement around the observation and injection wells in Figure 2. Large cells are 76 × 76, meters and small cells are 7.6 × 7.6 meters (Peck and others, 2014).

BACKGROUND

This project updated the modeling and simulation results of the first CO_2 breakthrough time, pressure change, and CO_2 plume extent for three different geologic realizations and three different operating scenarios. These simulation results can be used to assist in the risk assessment process and MVA planning for the Aquistore project. The geologic model used in this report was based on the work detailed in the original report entitled "Geologic Modeling and Simulation Report for the Aquistore Project" (Peck and others, 2014). The main content of the original report included the following:

- A regional-scale model was first constructed to determine the regional stratigraphic reservoir and nonreservoir zones. From this regional model, a fine-scale model was constructed with an extent of the 34-square-kilometer PTRC 3-D seismic survey area and incorporated higher structural resolution. Integration of the data derived from the regional model and the data from the 3-D seismic survey resulted in a robust and heterogeneous model around the Aquistore injection well and the observation well.

- The volumetric CO_2 storage capacities with P_{10}, P_{50}, and P_{90} cases of the fine-scale model were assessed based on the approach described in the U.S. Department of Energy (DOE) Atlas III (U.S. Department of Energy Office of Fossil Energy, 2010) which builds on the IEAGHG work of Gorecki and others (2009).

- Nine simulation cases were designed to verify the volumetric CO_2 storage capacities by considering pressure changes and other operational factors such as boundary conditions, injection rates, relative permeabilities, and time lengths.

- CO_2 plume extent and pressure responses during injection and postinjection periods were also assessed.

APPROACH

The approach used in this update is to assess the effect that geologic uncertainty and different operational parameters play in the breakthrough time at the monitoring well, pressure perturbation and dissipation, and CO_2 plume evolution. This approach first started with the construction of multiple geologic realizations of the fine-scale area. Modeling building parameters varied in these models include shale volume, porosity, variogram range, structural interpretation, and net-to-gross reservoir in all 12 traceable zones, including six sand units and six shale units throughout the regional study area. The results of the uncertainty analysis were then ranked accordingly by calculated pore volume, resulting in a low (P_{10}), mid (P_{50}), and high volumetric (P_{90}) case for the amount of pore volume accessible to store the potential injected CO_2.

Three operational cases were selected to cover a range of possible injection scenarios that may be experienced at the Aquistore site. Case 1 was set up to run for 30 days of injection (and 35 months of postinjection) at an injection rate of 1000 metric tons of CO_2/day for a total of 30,000 metric tons of CO_2 injected. Case 2 was designed to inject 301 metric tons of CO_2/day for 3 years or a total of 300,000 metric tons of CO_2. Case 3 was designed to inject 1000 metric tons of CO_2/day for 30 days, shut in for 2 months, return to injection at the original rate of 1000 metric tons of CO_2/day for a month, then repeat the cycle of injection and shut in until 300,000 metric tons of CO_2 had been injected (about 3 years). Case 1 was designed to evaluate first CO_2 breakthrough times, the accompanying pressures at the observation well, and the CO_2 plume extents. Cases 2 and 3 were designed to evaluate the effects of operational considerations (rate and timing of injection) on pressure evolution, CO_2 plume extent, and to evaluate for any other resultant differences. The simulation results of each injection scenario were incorporated back to the uncertainty-based geologic models to calculate the probability distributions of each monitored parameter and are reported in this update.

GEOLOGIC UNCERTAINTY ANALYSIS

Schlumberger's Uncertainty and Optimization process within its Petrel software was used to create P_{10}, P_{50}, and P_{90} volumetric cases based on the same fine-scale model extent of the 34-square-kilometer PTRC 3-D seismic survey area, with higher structural resolution as reported

by Peck and others (2014). These cases were created from the base case simulation model by model-building parameters, including shale volume, porosity, variogram range, structural interpretation, and reservoir net-to-gross cutoff criteria in all 12 traceable zones, including six sand units and six shale units throughout the regional study area. However, since the earlier study showed that the most significant parameters were effective porosity (PHIE) and reservoir net-to-gross (NTG) cutoff criteria, the uncertainty variation in this report only focused on these two key parameters (Peck and others, 2014).

To develop low (P_{10}), mid (P_{50}), and high (P_{90}) volumetric cases, 250 realizations were run in which two reservoir properties, PHIE and NTG, were varied. The base case PHIE from the Aquistore geologic model documented in the previous study was varied by three standard deviations. The resulting PHIE was then used in determining NTG with the PHIE cutoff ranging from 3% to 5%. NTG was set equal to 1 if PHIE equaled or exceeded the cutoff and 0 if the cutoff criterion were not met. Normal distributions of both PHIE and NTG were assumed, and a Monte Carlo sampling method was used. The 250 resulting cases were ranked by pore volume from lowest to highest, and P_{10}, P_{50}, and P_{90} volume cases were selected for simulation that were not only close to their volume percentile rankings but also near their respective rankings in effective porosity and NTG cutoff criterion. This was done to avoid a volumes case having extremely pessimistic criterion for one of the variables and an extremely optimistic criterion for the second variable. The base case model's volume, effective porosity, and NTG discussed in the previous report were also validated by comparison with the P_{50} case from the uncertainty analysis. For simulation of the uncertainty volumetric cases, P_{10}, P_{50}, and P_{90} permeability cases were then created from the porosity property found in the P_{10}, P_{50}, and P_{90} volumetric cases using the same methodology as used in populating the base case model with permeability (bivariate relationship determined from the porosity and permeability analysis from the core data). The details of uncertainty results are listed in Tables 1 and 2.

The closeness in the ranges and mean values of effective porosity in the various volume cases makes it difficult to distinguish variances in this property visually. The distribution of the NTG property in the P_{10} and P_{90} volume cases at the location of the injector well are shown in Figures 4 and 5, respectively, while horizontal permeability is displayed in Figures 6 and 7. Table 2 reveals that in the Black Island and Deadwood sands, the permeability value of the base case is closer to the P_{10} than to the P_{50} case. The table also shows that the P_{90} permeability is lower than the P_{50} permeability in the Upper Black Island and Deadwood C sands. These results are a result of populating the models with permeability using a bivariate distribution method (derived from core permeability and porosity data) which has a large range in permeability over a small range of porosity.

Although subtle, the differences can be seen between the permeability in the P_{10} case (Figure 6) and in the P_{90} permeability case (Figure 7). For example, east of the injector well in the Deadwood D sand zone (above 2682 feet subsea depth), a greater number of cells have permeability above 100 millidarcies (orange color) in the P_{90} case than in the P_{10} case.

Table 1. Pore Volume for the Black Island and Deadwood Sands in the Fine-Scale Model Area

Pore Volume, 10^6 cubic meters							
Case	U BI Sand	L BI Sand	Deadwood D	Deadwood C	Deadwood B	Deadwood A	Total
P_{10}	6.4	36.7	19.9	8.6	3.3	62.5	137.4
Base	7.2	40.1	20.8	9.7	4.0	68.2	149.9
P_{50}	7.2	40.1	20.8	9.7	4.0	68.0	149.8
P_{90}	8.1	43.2	21.6	10.8	4.6	73.8	162.2

Table 2. PHIE, NTG, and Permeability of P_{10}, Base Case, P_{50}, and P_{90} for the Black Island and Deadwood Sands in the Model

Zone	Property	Case											
		P_{10}			Base Case			P_{50} Case			P_{90}		
		Range			Range			Range			Range		
		Min.	Max.	Mean	Min.	Max.	Mean	Min.	Max.	Mean	Min.	Max.	Mean
U Blk Island Sand	PHIE	0	0.126	0.039	0	0.131	0.040	0	0.131	0.040	0	0.135	0.041
L Blk Island Sand		0	0.145	0.047	0	0.151	0.049	0	0.151	0.049	0	0.155	0.050
Deadwood D Sd.		0	0.142	0.070	0	0.147	0.073	0	0.147	0.073	0	0.151	0.075
Deadwood C Sd.		0	0.120	0.045	0	0.125	0.047	0	0.125	0.047	0	0.128	0.048
Deadwood B Sd.		0	0.113	0.032	0	0.117	0.033	0	0.117	0.034	0	0.120	0.034
Deadwood A Sd.		0	0.160	0.049	0	0.166	0.050	0	0.166	0.051	0	0.171	0.052
All Sands		0	0.160	0.048	0	0.166	0.050	0	0.166	0.050	0	0.171	0.051
		P_{10}			Base Case			P_{50} Case			P_{90}		
		Range			Range			Range			Range		
		Min.	Max.	Mean	Min.	Max.	Mean	Min.	Max.	Mean	Min.	Max.	Mean
U Blk Island Sand	NTG	0	1.000	0.395	0	1.000	0.451	0	1.000	0.446	0	1.000	0.521
L Blk Island Sand		0	1.000	0.552	0	1.000	0.599	0	1.000	0.596	0	1.000	0.654
Deadwood D Sd.		0	1.000	0.902	0	1.000	0.925	0	1.000	0.923	0	1.000	0.944
Deadwood C Sd.		0	1.000	0.570	0	1.000	0.649	0	1.000	0.641	0	1.000	0.723
Deadwood B Sd.		0	1.000	0.300	0	1.000	0.353	0	1.000	0.349	0	1.000	0.420
Deadwood A Sd.		0	1.000	0.562	0	1.000	0.612	0	1.000	0.608	0	1.000	0.668
All Sands		0	1.000	0.562	0	1.000	0.612	0	1.000	0.608	0	1.000	0.667
		P_{10}			Base Case			P_{50} Case			P_{90}		
		Range			Range			Range			Range		
		Min.	Max.	Mean	Min.	Max.	Mean	Min.	Max.	Mean	Min.	Max.	Mean
U Blk Island Sand	k_h	0.026	97.0	1.8	0.040	97.0	1.7	0.040	97.0	3.6	0.040	97.0	3.4
L Blk Island Sand		0.028	97.0	3.3	0.040	97.0	2.5	0.040	97.0	4.0	0.040	97.0	4.4
Deadwood D Sd.		0.004	312.3	25.5	0.005	312.3	23.8	0.005	312.3	30.9	0.005	312.3	34.1
Deadwood C Sd.		0.004	312.3	11.7	0.005	312.3	10.2	0.005	312.3	18.4	0.005	312.3	17.6
Deadwood B Sd.		0.002	312.3	9.1	0.005	312.3	6.0	0.005	312.3	12.3	0.005	312.3	13.4
Deadwood A Sd.		0.040	312.3	12.8	0.005	312.3	10.6	0.005	312.3	15.8	0.005	312.3	18.7
All Sands		0.005	312.3	10.2	0.005	312.3	8.5	0.005	312.3	12.9	0.005	312.3	14.6

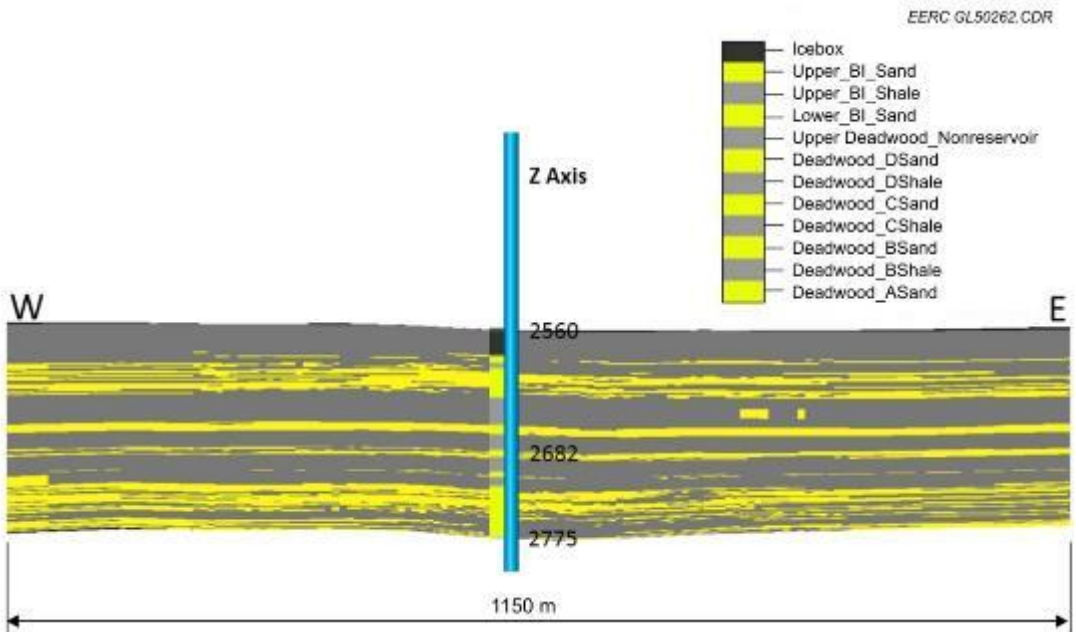

Figure 4. Distributed NTG in the P_{10} volume case near the Aquistore injection well. A zonation log is displayed along the wellbore to show the reservoir (yellow) and nonreservoir zones (gray). Z axis is in subsea depth (meters).

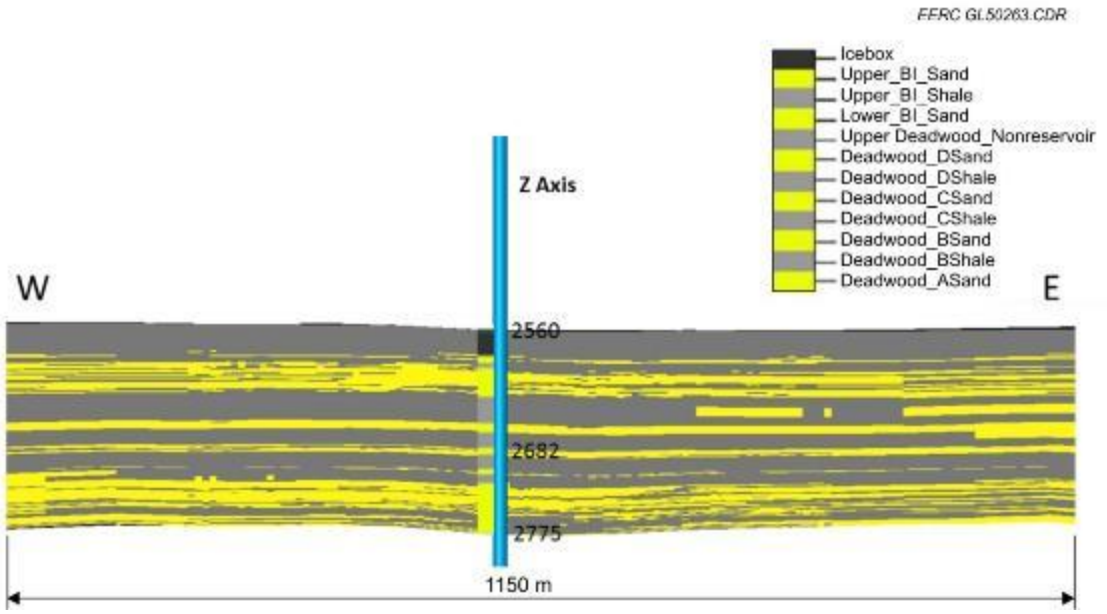

Figure 5. Distributed NTG in the P_{90} volume case near the Aquistore injection well. A zonation log is displayed along the wellbore to show the reservoir (yellow) and nonreservoir zones (gray). Z axis is in subsea depth (meters). Note the greater number of cells meeting the NTG cutoff criteria (yellow color) in the P_{90} volume case (this figure) when compared to the P_{10} volume case (Figure 4).

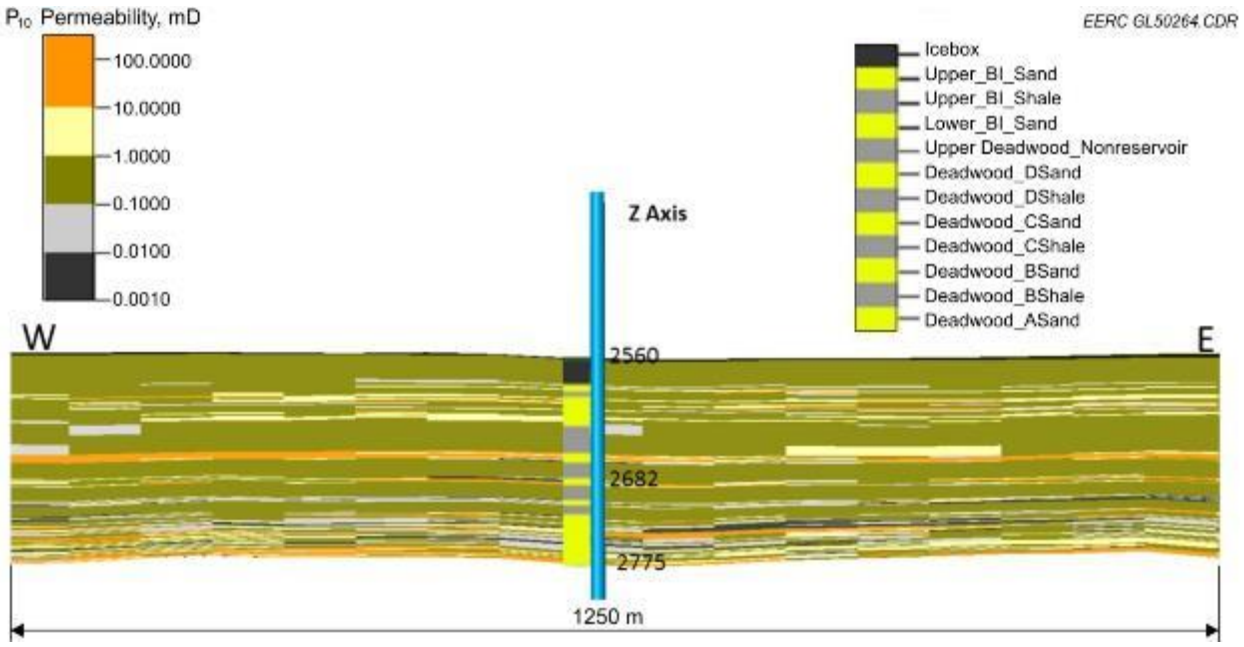

Figure 6. Distributed horizontal permeability in the P_{10} volume case near the Aquistore injection well. A zonation log is displayed along the wellbore to show the reservoir (yellow) and nonreservoir zones (gray). Z axis is in subsea depth (meters).

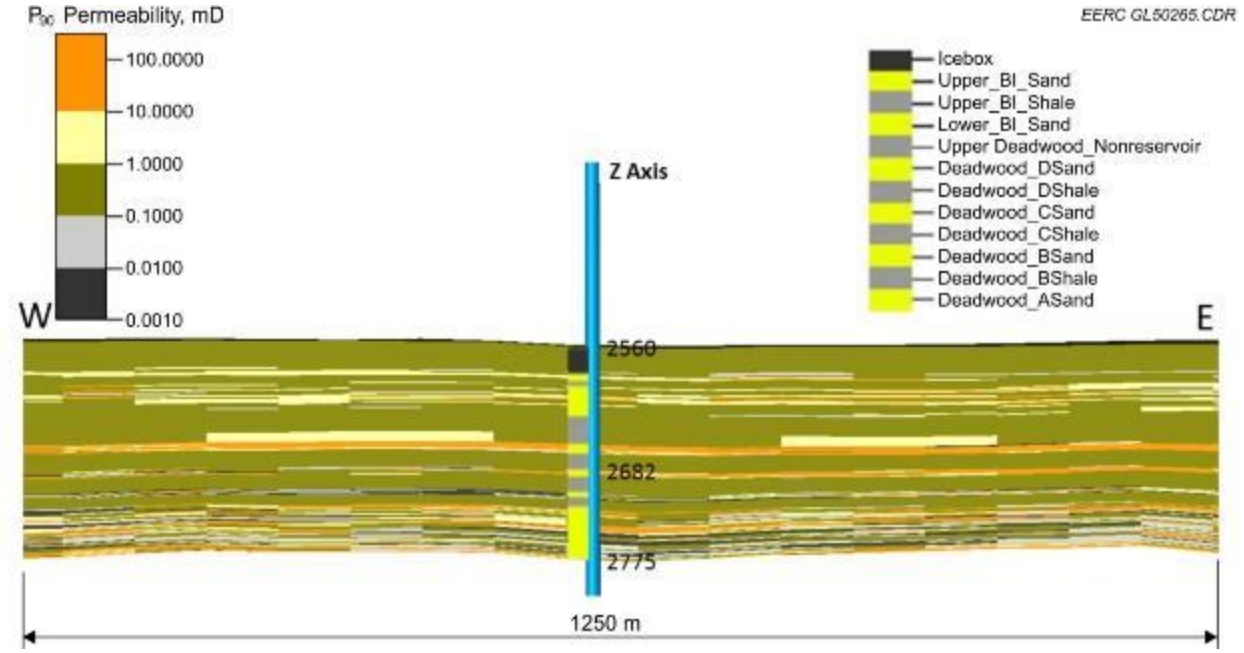

Figure 7. Distributed horizontal permeability in the P_{90} volume case near the Aquistore injection well. A zonation log is displayed along the wellbore to show the reservoir (yellow) and nonreservoir zones (gray). Z axis is in subsea depth (meters).

DYNAMIC SIMULATION AND MODEL SETTINGS

To further tune the CO_2 movement and pressure change over the injection and postinjection period of the previous work (Peck and others, 2014), three cases with various injection rates and periods were simulated. Moreover, based on the uncertainty of the geology, three more realizations along with the base case (Peck and others, 2014) were simulated to assess the uncertainty effects on CO_2 breakthrough time, pressure propagation, and CO_2 movement underground. Three simulation cases were run on each of the three geologic realizations for a total of nine simulation runs.

The dynamic simulation workflow reported in the previous report was repeated in this effort. The fluid system, CO_2 dissolution option, and aqueous density and viscosity correlations over the varying pressure and temperature kept the same settings. The relative permeabilities (Figure 8) for the rock–fluid system were the second set of curves referenced from Bachu and Adams (2003) and Bachu and others (2011). All of the dynamic simulations were performed using Computer Modelling Group Ltd.'s (CMG's) general equation-of-state modeling (GEM) software package (www.cmgl.ca/) on a 184-core, high-performance parallel computing cluster.

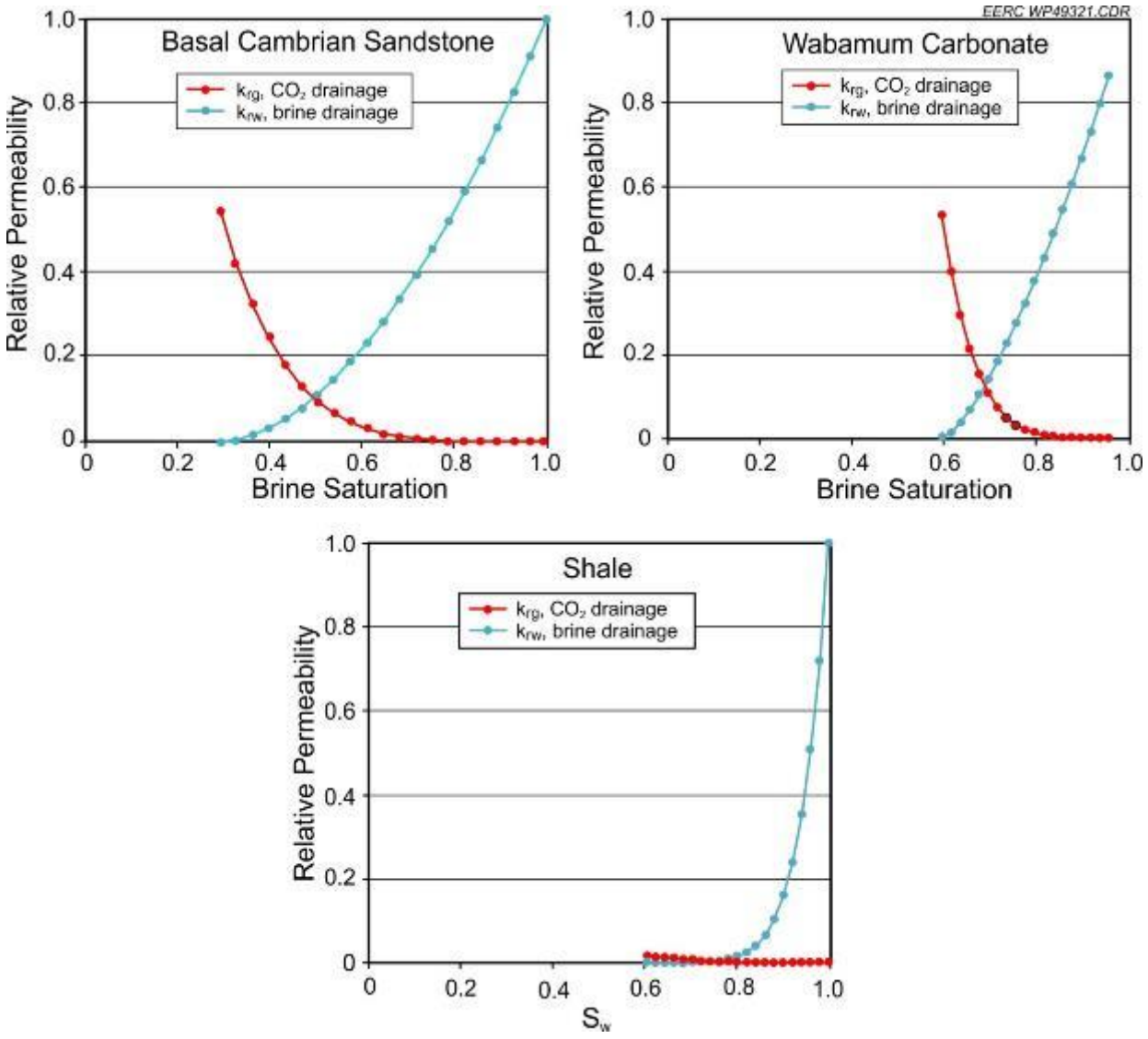

Figure 8. Relative permeability curves used for the simulation (Bachu and Adams, 2003; Bachu and others, 2011).

DYNAMIC SIMULATION RESULTS AND DISCUSSION

Nine cases were designed to address CO_2 breakthrough, CO_2 movement, pressure change, and CO_2 probability distributions over the various injection rates, periods, and geologic realizations. Case 1 is based on an injection rate of 1000 tonnes/day for only 30 days (a total of 30,000 tonnes of CO_2) followed by a 2-year postinjection observation. Case 2 focused on a cumulative 330,000 tonnes of CO_2 injected in 3 years. The injection rate for this case was approximately 301 tonnes/day. Case 3 also kept the same cumulative 330,000 tonnes of CO_2 injection, but with an injection rate of 1000 tonnes/day for 30 days, followed by 60 days of noninjection, then another 1000 tonnes/day for 30 days. This start–stop–start pattern was

repeated until 330,000 tonnes was injected (933 days or about 3 years). The perforation of the injection well was updated in the model by referencing PTRC data (Figure 9). All three cases were analyzed based on the three uncertainty realizations P_{10}, P_{50}, and P_{90}. Because of the small amount of expected CO_2 injection compared to the total potential storage capacity of the study area (1.5 Mt, Peck and others, 2014), all expected CO_2 could be injected, as shown in Figures 10 and 11.

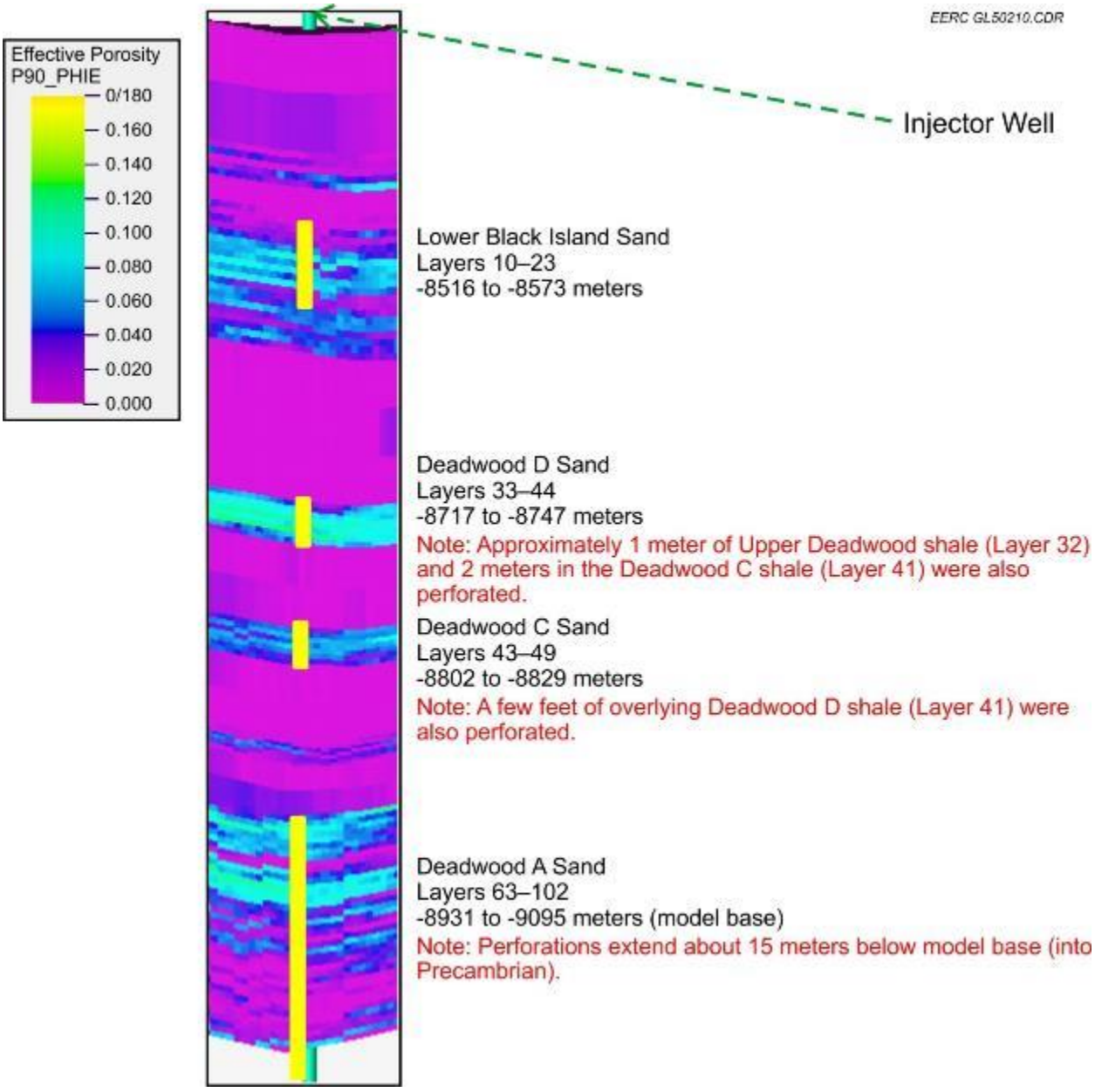

Figure 9. Perforations along the injection well.

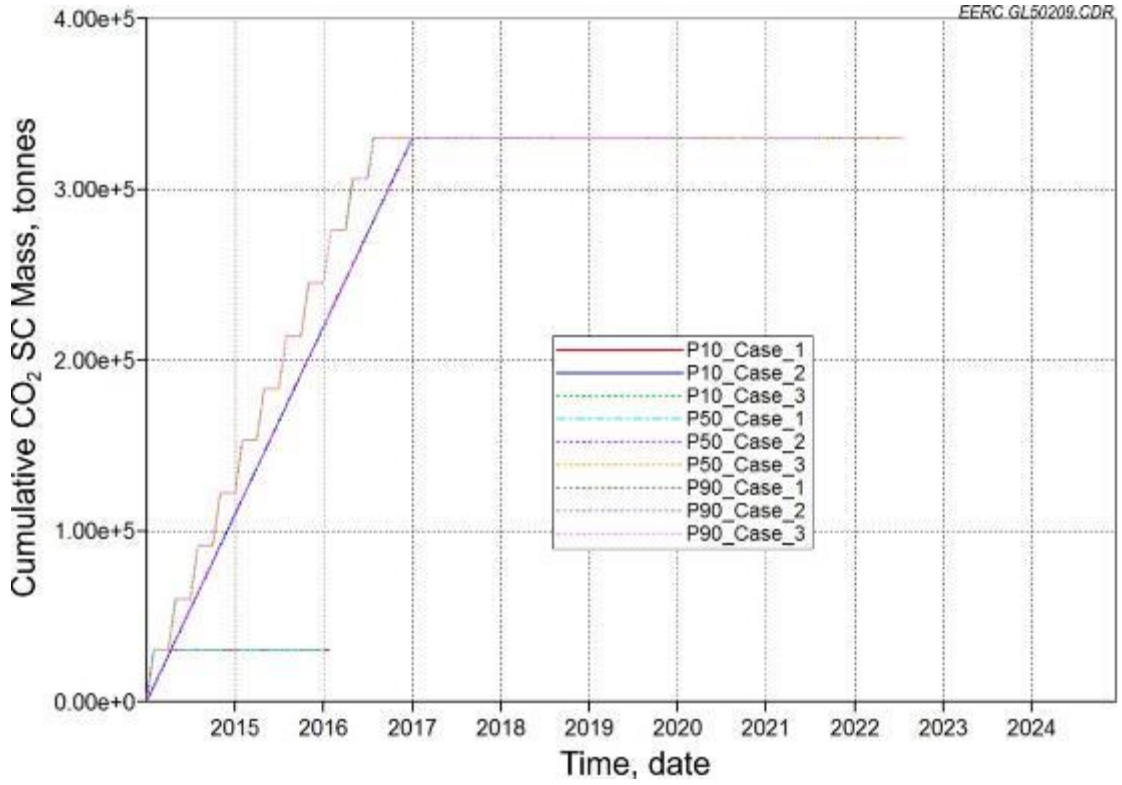

Figure 10. Cumulative CO_2 injection histories for all cases.

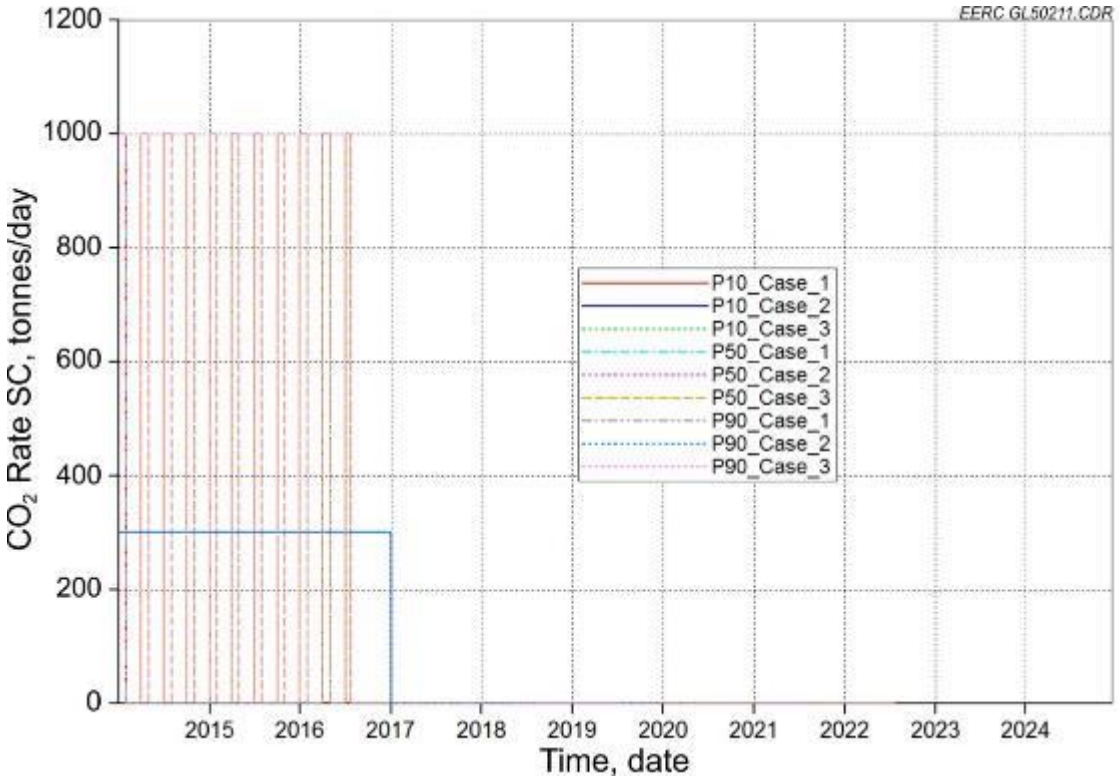

Figure 11. CO_2 injection rate histories for all cases.

Times of the first CO_2 breakthrough on the observation well were monitored by measuring the CO_2 saturation during the injection period for all cases. The cross-sectional images of the CO_2 saturation included in the report were cut along the plane of the injection well and the observation well from top to bottom of the study area. Details of the CO_2 movement for each zone were demonstrated in each of the monitoring time periods. CO_2 saturations along the observation well from top to bottom were measured to detect CO_2 movement over time (Figure 9). Such plots provided a profile of the CO_2 breakthrough from individual zones and indicated how much the CO_2 saturation would be at the specific time frame. The first CO_2 breakthroughs for all cases are summarized in Table 3. Based on the properties of geologic realizations, the first breakthrough of P_{10} happened in the base reservoir zone (Deadwood A Sand Unit), while P_{50} was in the Deadwood C Sand Unit, and P_{90} was in the Deadwood D Sand Unit. These trends were also true for all cases regardless of the injection scheme. Detailed results will be demonstrated by case in the next sections.

The pressure change resulting from the injection of CO_2 was also tracked by plotting the comparisons of the time periods for cases and realizations along the observation well from top to bottom (Figure 9). Such plots provide some idea of the reservoir's response due to CO_2 injection for risk assessment and monitoring even before actual CO_2 breakthrough happens at the observation well. Overall, pressure monitoring on the observation well showed that the pressure changes for all cases were lower than 37,250 kPa which is notably lower than the 42,750 kPa bottomhole pressure (BHP) constraint placed on the injection well. The maximum reservoir pressure increase because of CO_2 injection was lower than 4800 kPa within the first breakthrough time, compared to the initial pressure (Cases 1 and 3). The main reason is the designed injection rate for the three cases is lower than the possible maximum potential based on the available injectivity (0.7 Mt/yr, Peck and others (2014)).

The plan views of the CO_2 plume extent over time were created to provide insight into CO_2 movement in the study area. Variation in heterogeneitity across the various geologic realizations resulted in differences in CO_2 plume extents and shapes. To comprehensively understand the uncertainty of the simulation results, the probability distributions for each of the cases were calculated based on the realizations. These distributions indicted some high, mid, and low estimations of the CO_2 extents over the injection and postinjection periods. All results will be discussed by case in the following.

Table 3. Simulation Results Summary for All Cases

	Injection Rate, tonnes/day	Injection Period, days	Injection Pattern	First Breakthrough Time, days		
				P_{10}	P_{50}	P_{90}
Case 1	1000	30	Continuous	~19	~19	~30
Case 2	301	1095	Continuous	~59	~59	~73
Case 3	1000	933	Start–stop–start	~19	~19	~30

Case 1

The cumulative CO_2 injection in this case is 30,000 tonnes at a rate of 1000 tonnes/day for 30 days (Figures A-1 and A-2). During the injection period, the first CO_2 breakthrough was monitored for three geologic realizations by cross-section imaging and observation well plotting (Figures A-3 to A-5). Overall, the CO_2 movement in realization P_{10} and P_{50} was faster than the one in P_{90}. This is the reason why the time of the first breakthrough for P_{10} and P_{50} is earlier (19 days) than P_{90}'s (30 days). Pressure change plotting along the observation well, CO_2 plume extent, and CO_2 movement probabilities over geologic uncertainties were also monitored over a 2-year postinjection period (Figures A-6 to A-10).

Case 2

The cumulative CO_2 injection for this case is 330,000 tonnes at a rate of 301 tonnes/day for 3 years (1095 days, Figures A-11 and A-12). During the injection period, the first CO_2 breakthrough was monitored for three geologic realizations by cross-section imaging and observation well plotting (Figures A-13 to A-15). Overall, the time of the first breakthrough for both P_{10} and P_{50} was about 59 days, while the P_{90} was around 90 days. Pressure change plotting along the observation well, CO_2 plume extent, and CO_2 movement probabilities over geologic uncertainties were also monitored over the injection period (Figures A-16 to A-20).

Case 3

The cumulative CO_2 injection in this case is 330,000 tonnes at a rate of 1000 tonnes/day for 30 days, followed by 60 days of noninjection, then another 1000 tonnes/day for 30 days. This start–stop–start pattern was repeated until 330,000 tonnes was injected (Figures A-21 and A-22). The injection process lasted about 933 days for a total of 330,000 tonnes of injected CO_2. During the injection period, the first CO_2 breakthrough was monitored for three geologic realizations by cross-section imaging and observation well plotting (Figures A-23 to A-25). Overall, the time of the first breakthrough was exactly the same as the results in Case 1 because the first breakthrough for the three realizations happened before injection was stopped for the next injection cycle. Pressure change plotting along the observation well, CO_2 plume extent, and CO_2 movement probabilities over geologic uncertainties were also monitored over the injection period (Figures A-26 to A-30).

Comparisons Between Cases 2 and 3

Both Cases 2 and 3 injected a total of 330,000 tonnes of CO_2 but at different injection rates and schemes. Case 2 is 301 tonnes/day for 3 years, and Case 3 is 1000 tonnes/day following a start–stop–start pattern: 30 days of injection, then stopping 60 days, then another 30 days of injection. This start–stop–start pattern was repeated until 330,000 tonnes was injected. This process took 933 days for the total amount of expected CO_2 injection. Because of the different injection rates and schemes, the breakthrough time, pressure change, CO_2 movement, plume extent, and probability distribution varied greatly. Because of the lower injection rate, the first breakthrough time of Case 2, 2 months or longer (about 59 to 73 days), is longer than Case 3's, within the first month (about 19 days to 30 days) (Figures A-31 and A-32). Correspondingly, the reservoir pressure buildup in Case 2 is much lower (about 2,750 kPa) than the one in Case 3 (Figure

A-33). Regarding CO_2 movement and plume extent, Case 3 with the higher injection rate was slightly larger than Case 2's right after the same amount of CO_2 injection (Figure A-34). This trend was also true for the comparisons of CO_2 movement probabilities in Cases 2 and 3 (Figure A-35).

CONCLUSIONS AND FUTURE WORK

Based on the simulation results, all expected amounts of CO_2 could be injected over all designed cases and geologic realizations. It means that there are no injectivity concerns for these scenarios with varied injection rates, periods, and schemes. The main reason is that the expected injection rate is only 50% of the maximum rate (0.73 Mt/yr, Peck and others, 2014).

The first breakthrough for Cases 1 and 3, with a CO_2 injection rate of 1000 tonnes/day, most likely happened around 19 days after injection started for realizations P_{10} and P_{50}. However, this time may be extended 30 days in realization P_{90} because of different geologic properties. Overall, the first breakthrough time in Case 1 was within the first month. Regarding Case 2, at a 301-tonne/day injection rate, the first breakthrough time happened at the end of the second month (about 59 days) after injection started. This time also may be extended to the third month (about 73 days) in realization P_{90}.

The pressure monitoring on the observation well is always lower than 37,250 kPa based on the injection BHP constraint of 42,750 kPa imposed on the injection well. The maximum reservoir pressure increase due to CO_2 injection is around 4800 kPa above the original reservoir pressure of approximately 36 MPa. The main reason for the small increase in reservoir pressure is that the target injection rate in these cases was less than half of the maximum injection rate as estimated from the previous investigations (Peck and others, 2014).

Regarding comparisons between Cases 2 and 3, the time of CO_2 breakthrough, pressure change, CO_2 movement, plume extent, and probability distribution were different because of the varied injection rates and periods, especially in the individual time intervals. The differences decrease after the same total amount of CO_2 is injected. When the resultant final CO_2 plumes in Cases 2 and 3 are compared, the results are nearly identical, with only a slightly larger plume extent in the simulations on Case 3.

Uncertainty over geologic realizations is certain to influence CO_2 injection behavior and CO_2 movement underground. The first breakthrough time, pressure front, reservoir pressure buildup, CO_2 plume, and CO_2 probability distribution were significantly varied over such geologic realizations. The results of uncertainty analysis in calculating the probability distribution could provide insight into CO_2 movement that ultimately helps with decisions involving leakage monitoring, risk assessment, and the MVA plan.

The studies covered in this report are limited to 3 years of simulation results. A longer period of investigation may be necessary to help with any long-term risk assessment and MVA plan. Moreover, the other phenomenon such as geomechanical behavior, relative permeability hysteresis, and rock compressibility variations over the study area may have an effect on the first

breakthrough time and overall CO_2 movement. These uncertainties will be addressed in the next phase of the work.

REFERENCES

Bachu, S., and Adams, J. J., 2003, Sequestration of CO_2 in geological media in response to climate change—capacity of deep saline aquifers to sequester CO_2 in solution: Energy Conversion and Management, v. 44, no. 20, p. 3151–3175.

Bachu, S., Faltinson, J., Hauck, T., Perkins, E., Peterson, J., Talman, S., and Jensen, G., 2011, The Basal Aquifer in the Prairie region of Canada—characterization for CO_2 storage: Preliminary report for Stage I (Phases 1 and 2), Alberta Innovates Technology Futures.

Gorecki, C.D., Sorensen, J.A., Bremer, J.M., Knudsen, D.J., Smith, S.A., Steadman, E.N., and Harju, J.A., 2009, Development of storage coefficients for determining the effective CO_2 storage resource in deep saline formations: SPE Paper 126444, SPE International Conference on CO_2 Capture, Storage, and Utilization, San Diego, November 2–4, 2009.

Peck, W., Klenner, R., Liu, G., Gorecki, C., and Steadman, E., 2014, Geologic modeling and simulation report for the Aquistore project: Plains CO_2 Reduction (PCOR) Partnership Phase III, Task 1 – Deliverable D93, Technical Report, March.

U.S. Department of Energy Office of Fossil Energy, 2010, Carbon sequestration atlas of the United States and Canada, 3rd edition.

APPENDIX A

GEOLOGIC REALIZATIONS MODELED

CASE 1

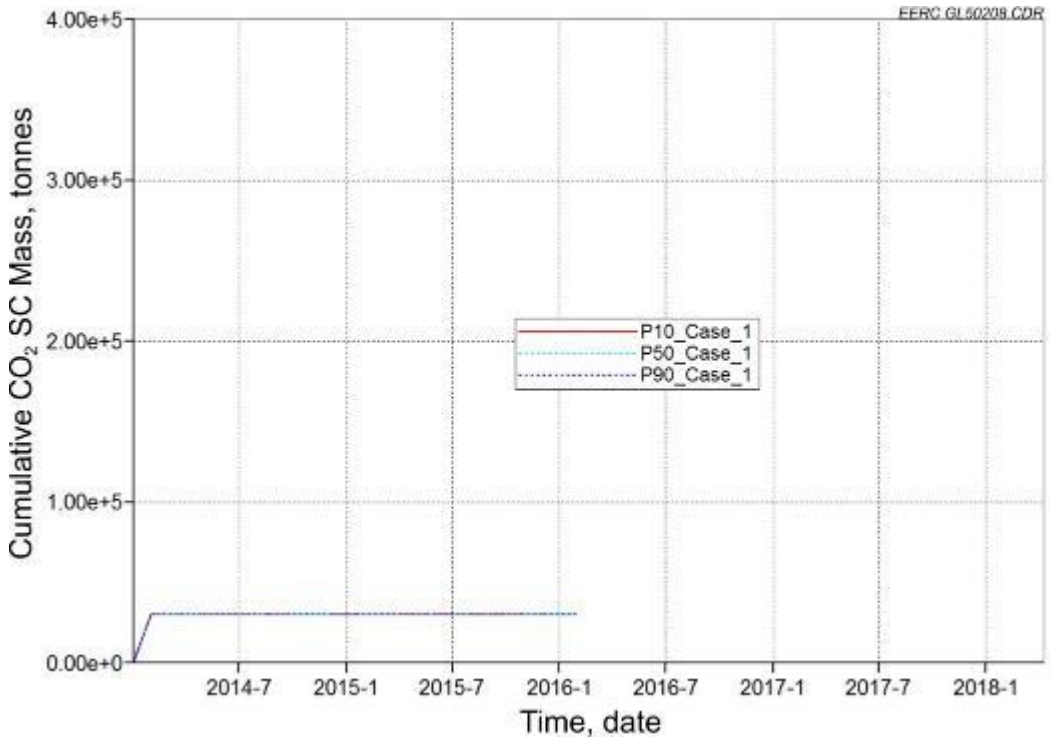

Figure A-1. Cumulative CO_2 injection histories for Case 1 over three realizations.

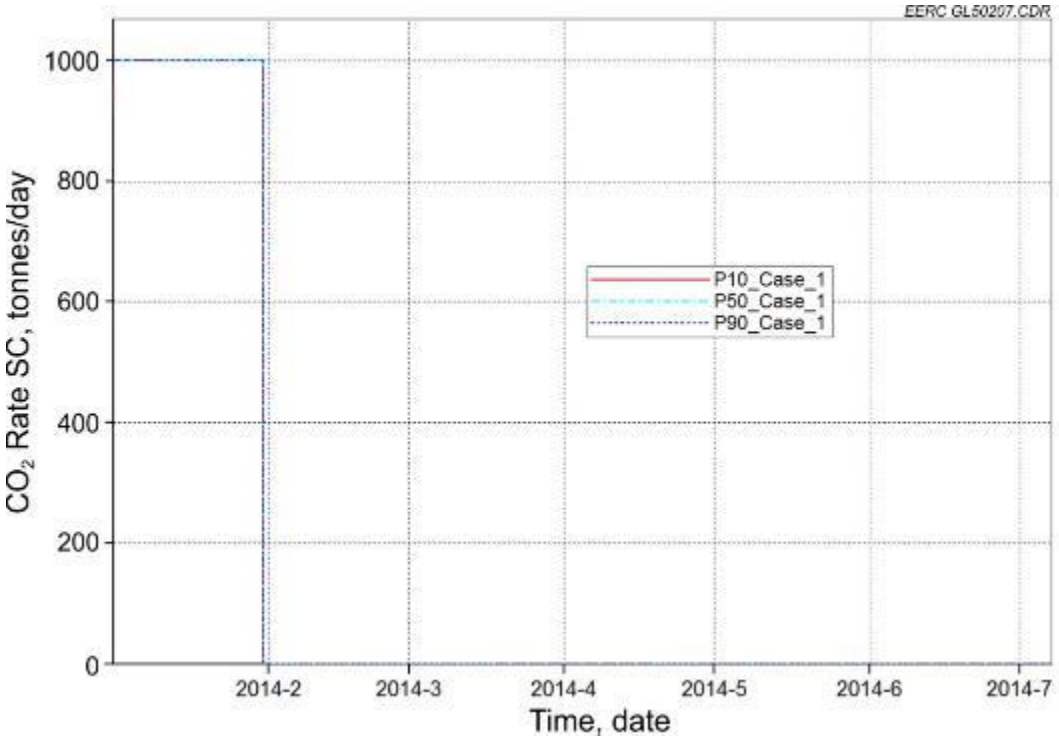

Figure A-2. CO_2 injection rate histories for Case 1 over three realizations.

Case 1 CO_2 Breakthrough Monitoring

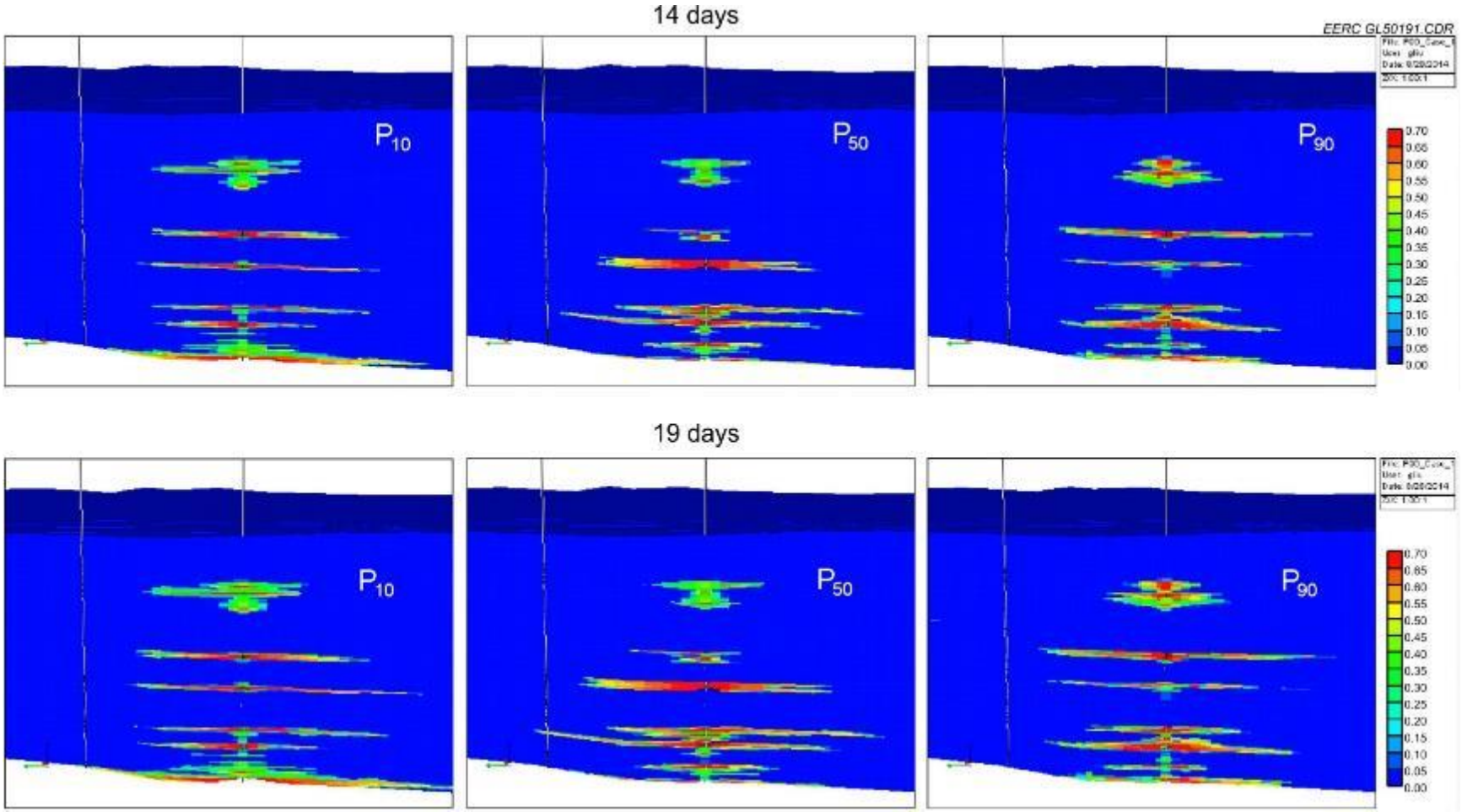

Figure A-3. Cross-section view of CO_2 saturation over time, starting from the injection beginning (continued).

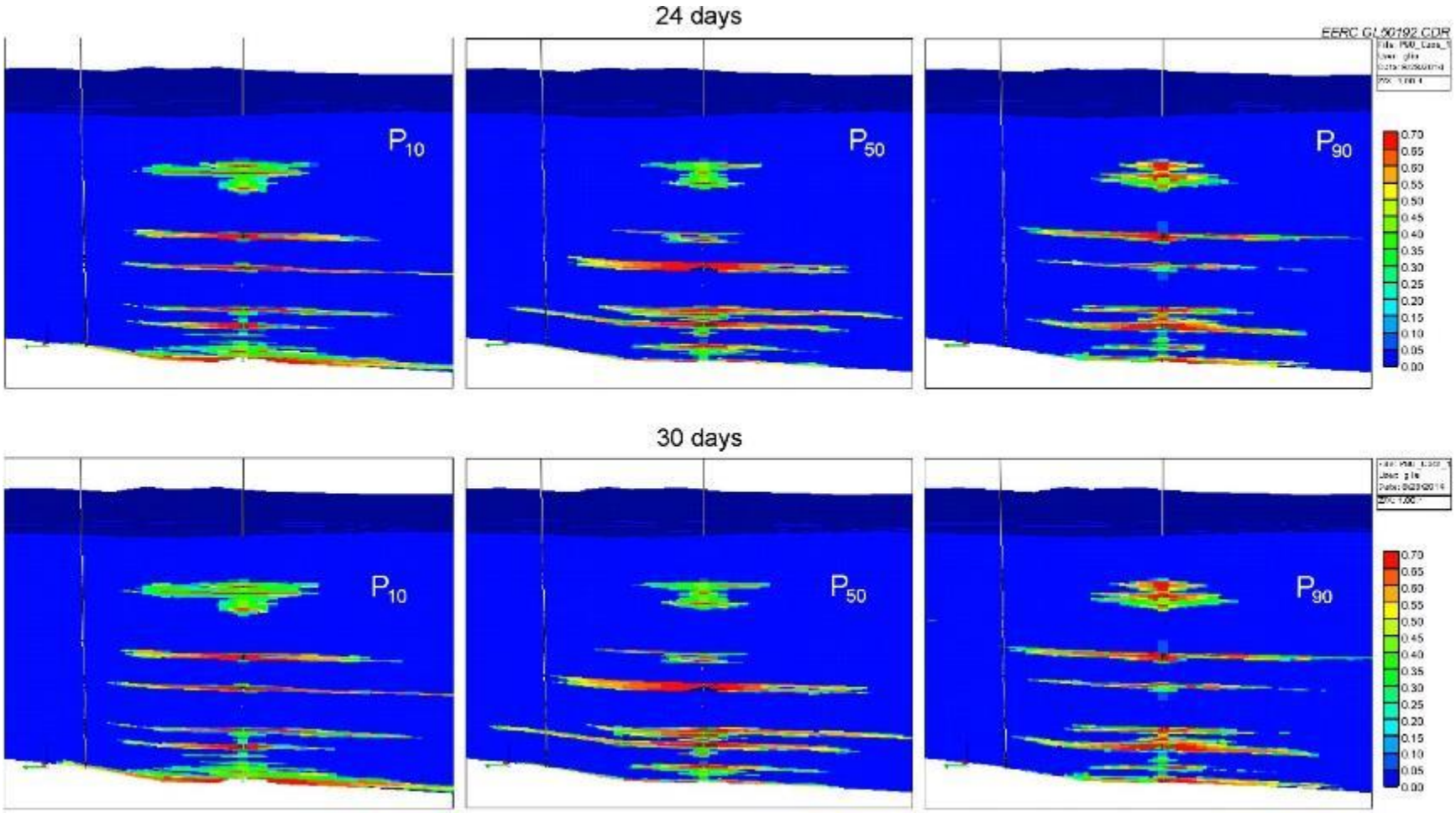

Figure A-3 (continued). Cross-section view of CO_2 saturation over time, starting from the injection beginning (continued).

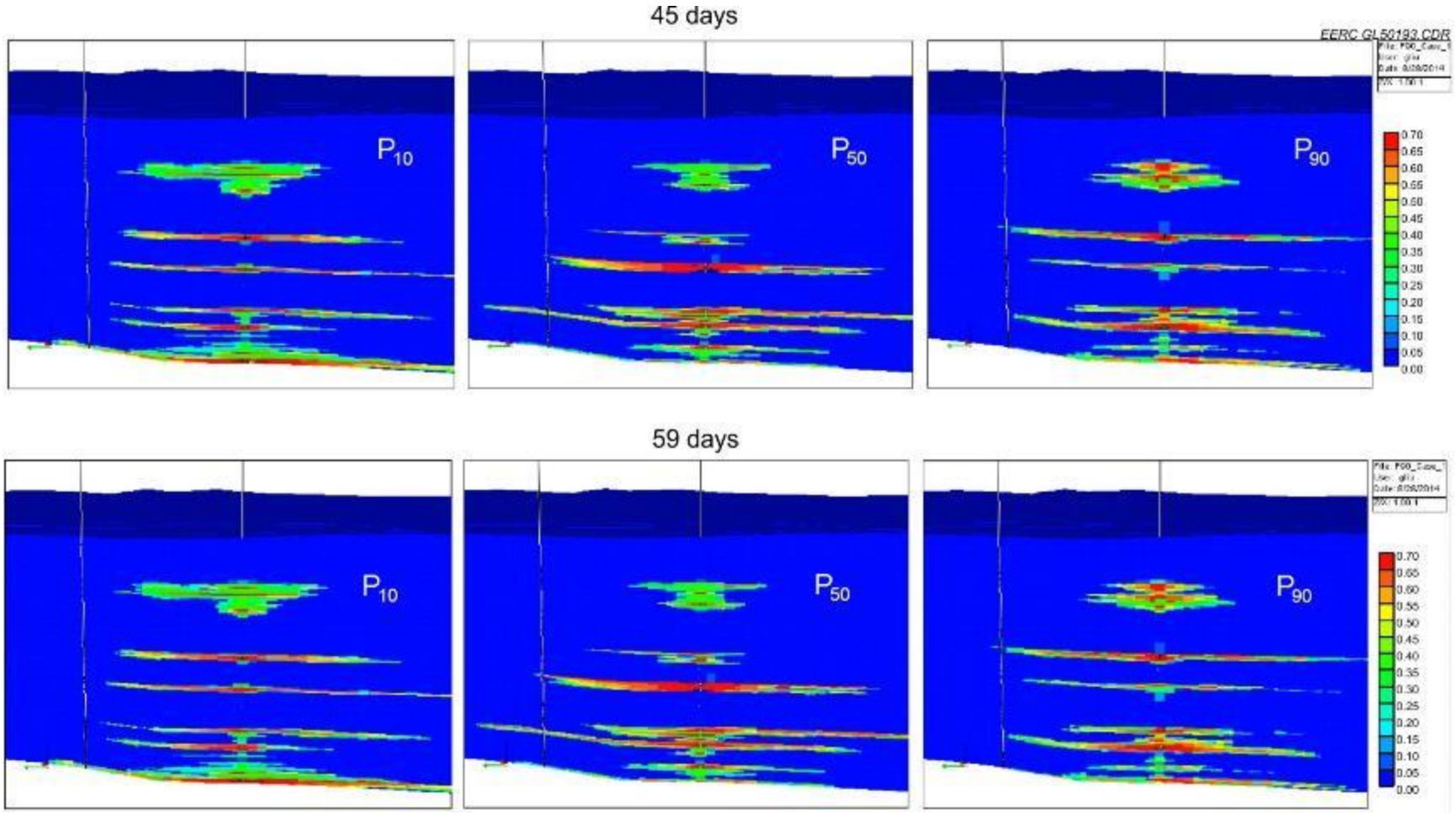

Figure A-3 (continued). Cross-section view of CO_2 saturation over time, starting from the injection beginning (continued).

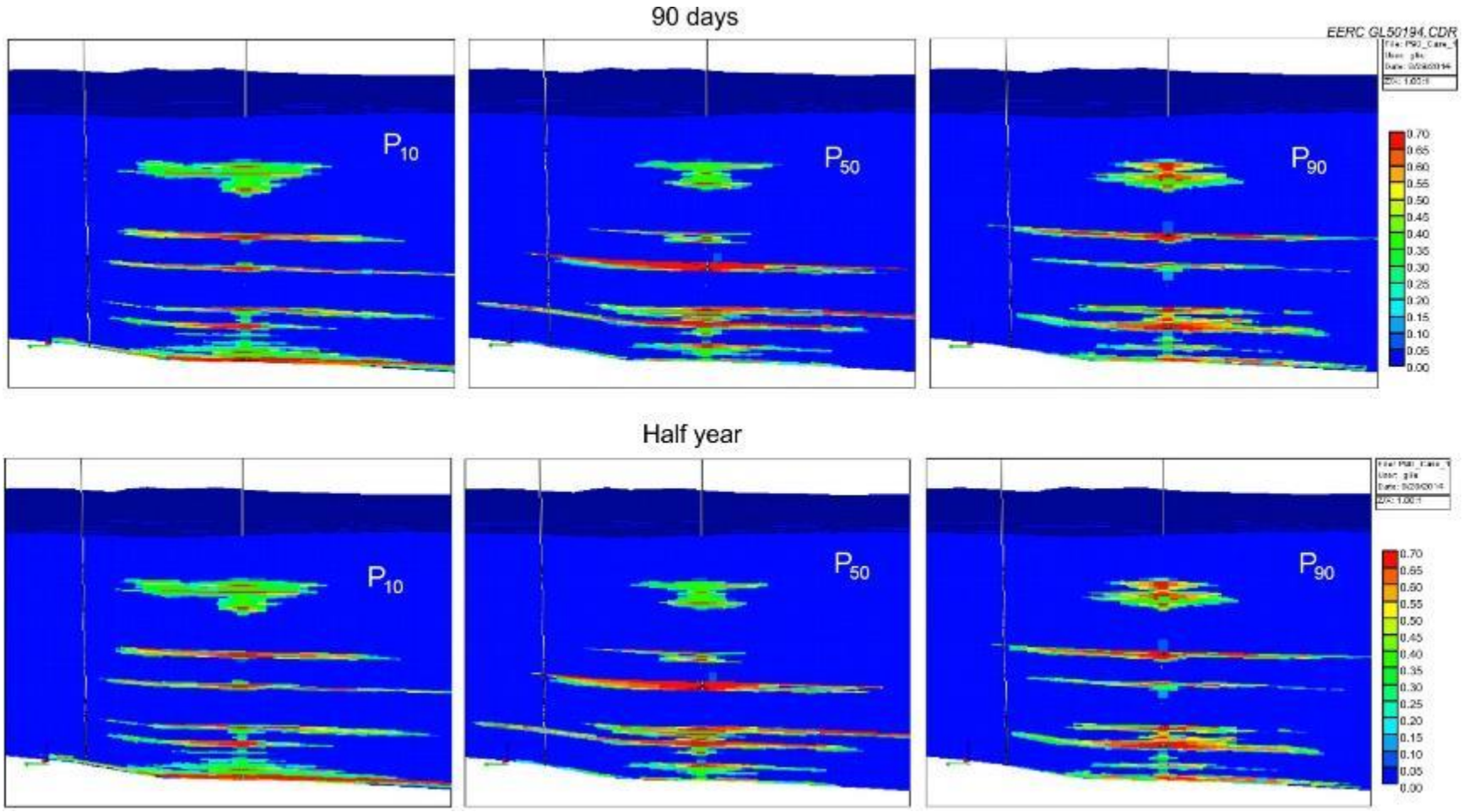

Figure A-3 (continued). Cross-section view of CO_2 saturation over time, starting from the injection beginning (continued).

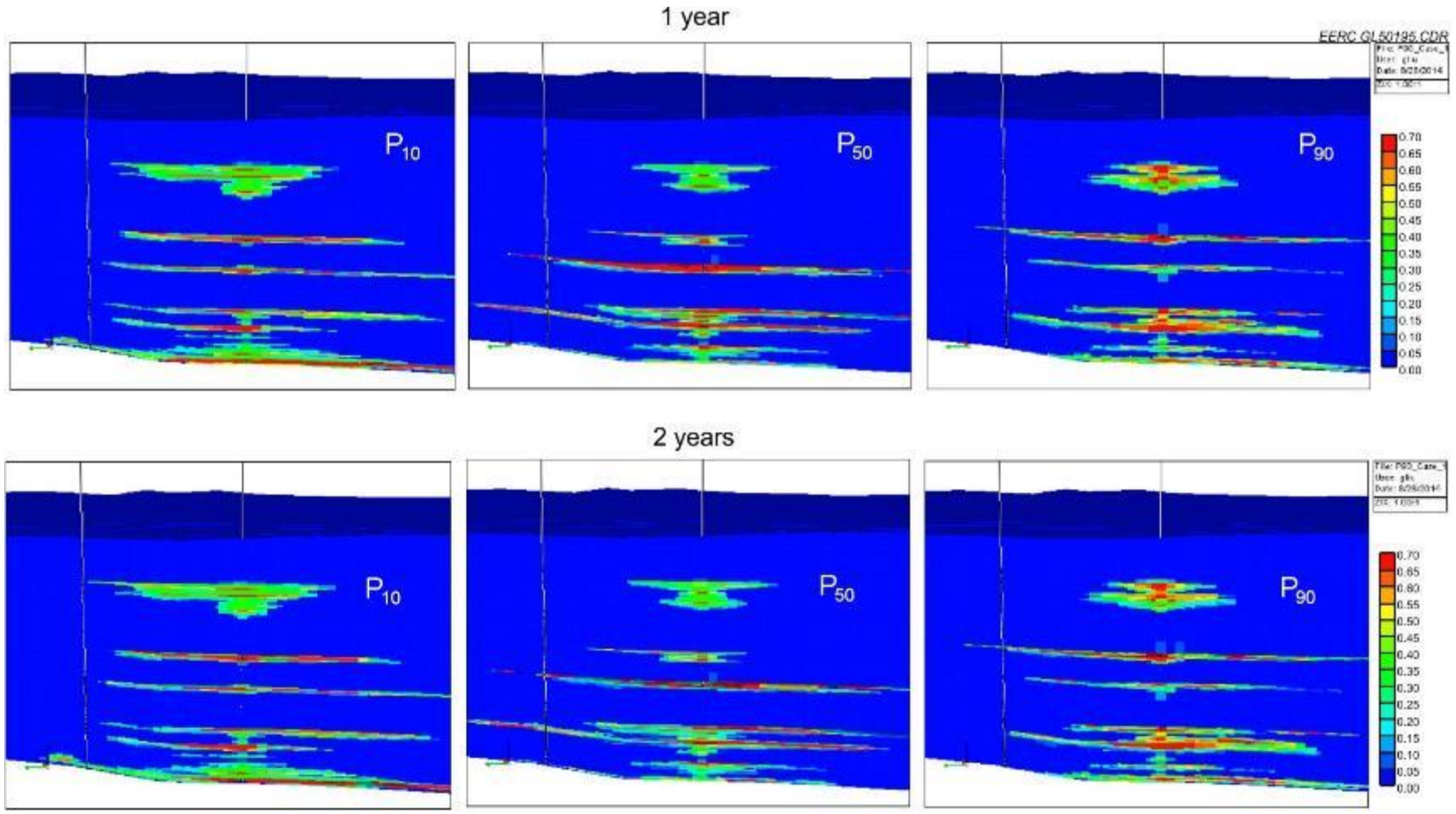

Figure A-3 (continued). Cross-section view of CO_2 saturation over time, starting from the injection beginning.

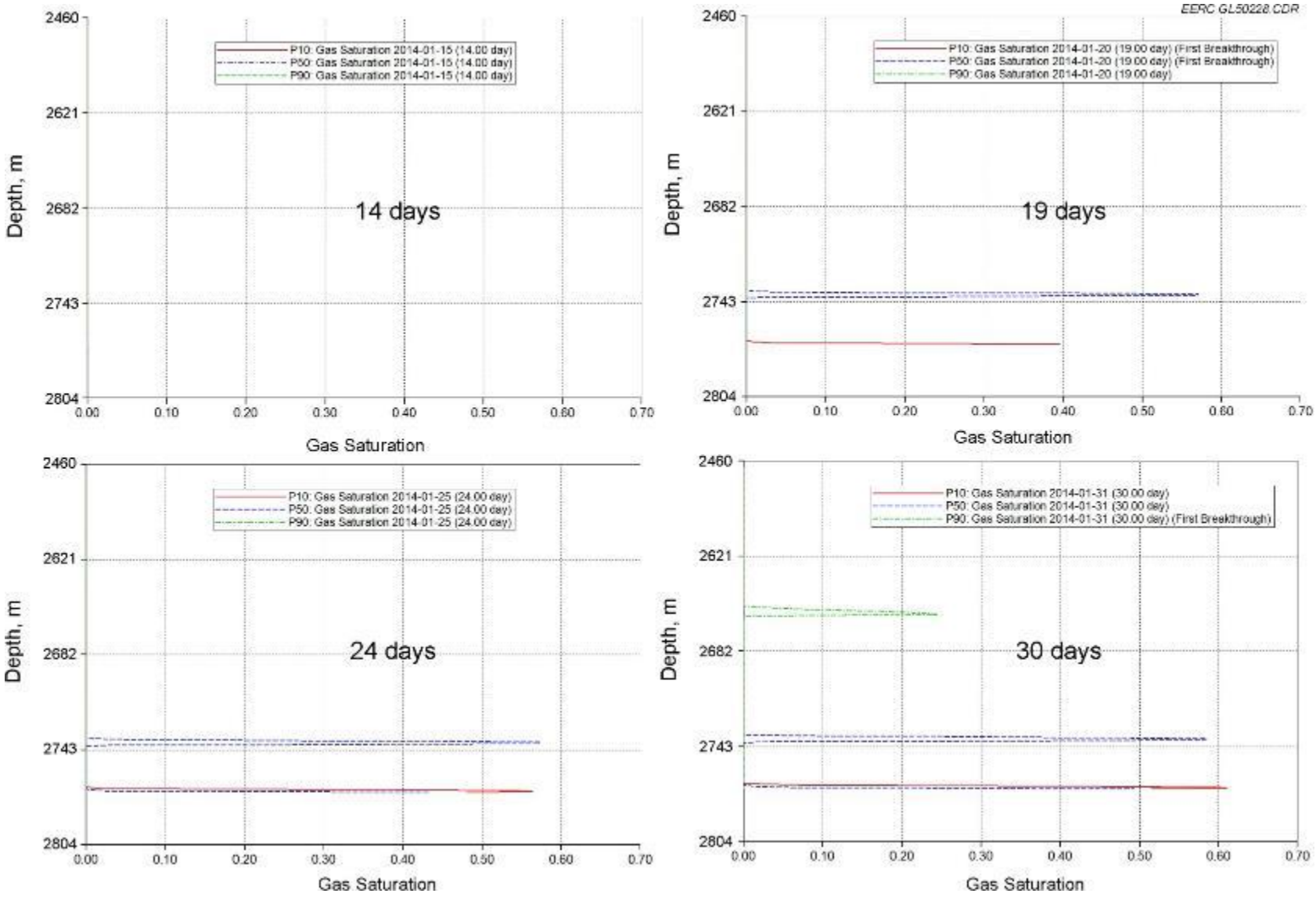

Figure A-4. CO_2 saturation plots along the observation well from top to bottom over time, starting from the injection beginning (continued).

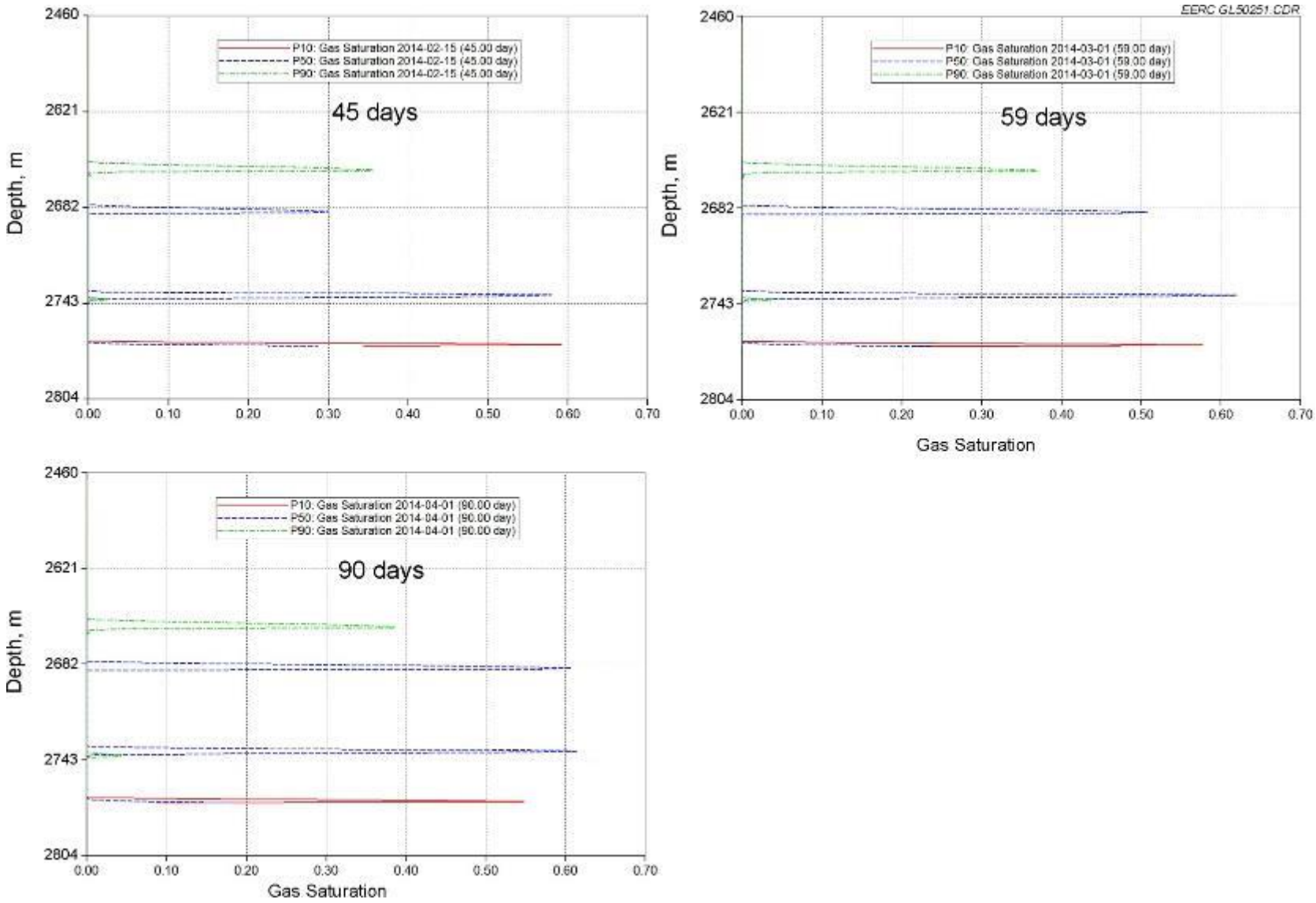

Figure A-4 (continued). CO_2 saturation plots along the observation well from top to bottom over time, starting from the injection beginning.

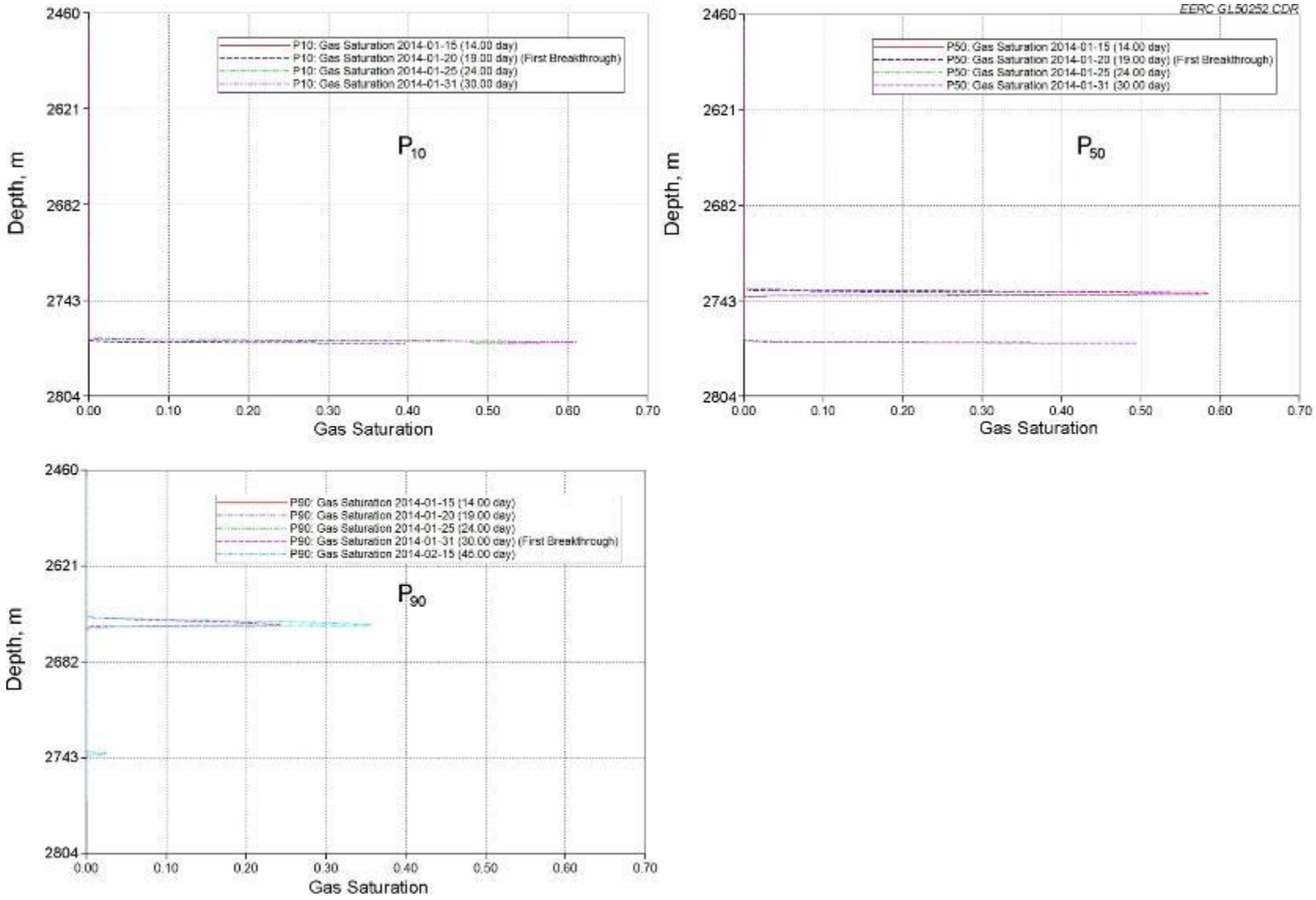

Figure A-5. CO_2 saturation plots along the observation well from top to bottom over time based on three geologic realizations.

Case 1 Pressure Change Monitoring

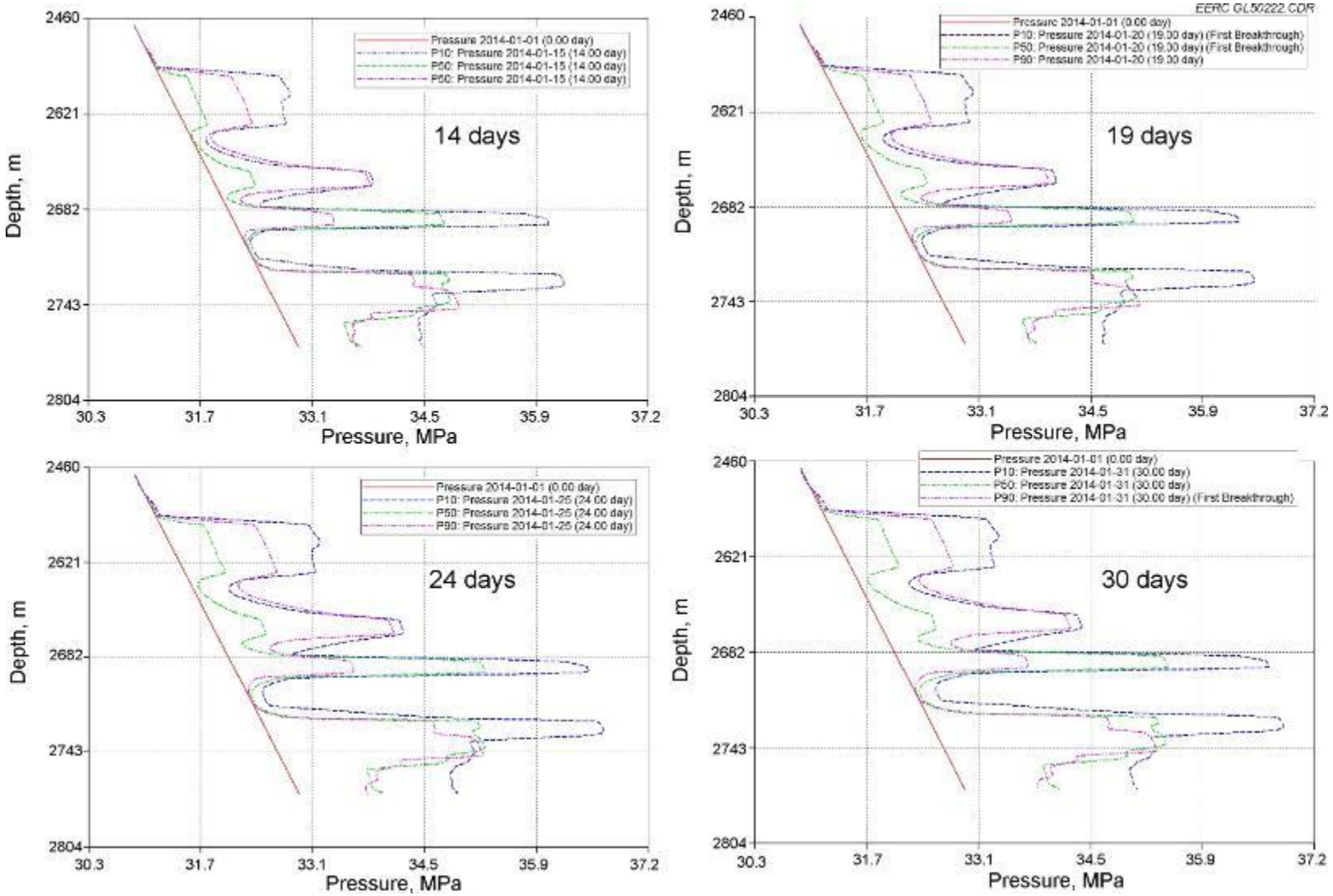

Figure A-6. Pressure plots along the observation well from top to bottom over time, starting from the injection beginning (continued).

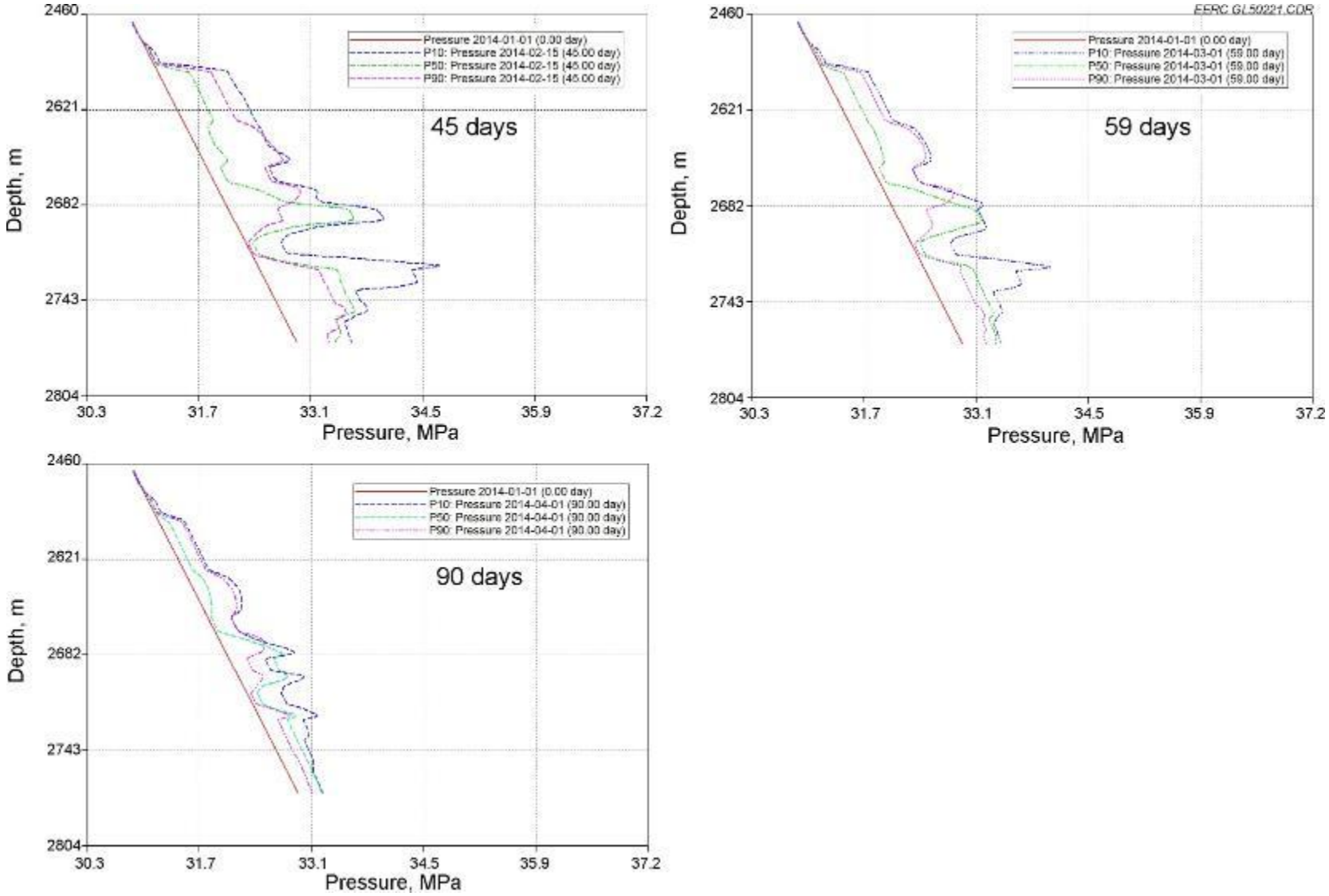

Figure A-6 (continued). Pressure plots along the observation well from top to bottom over time, starting from the injection beginning.

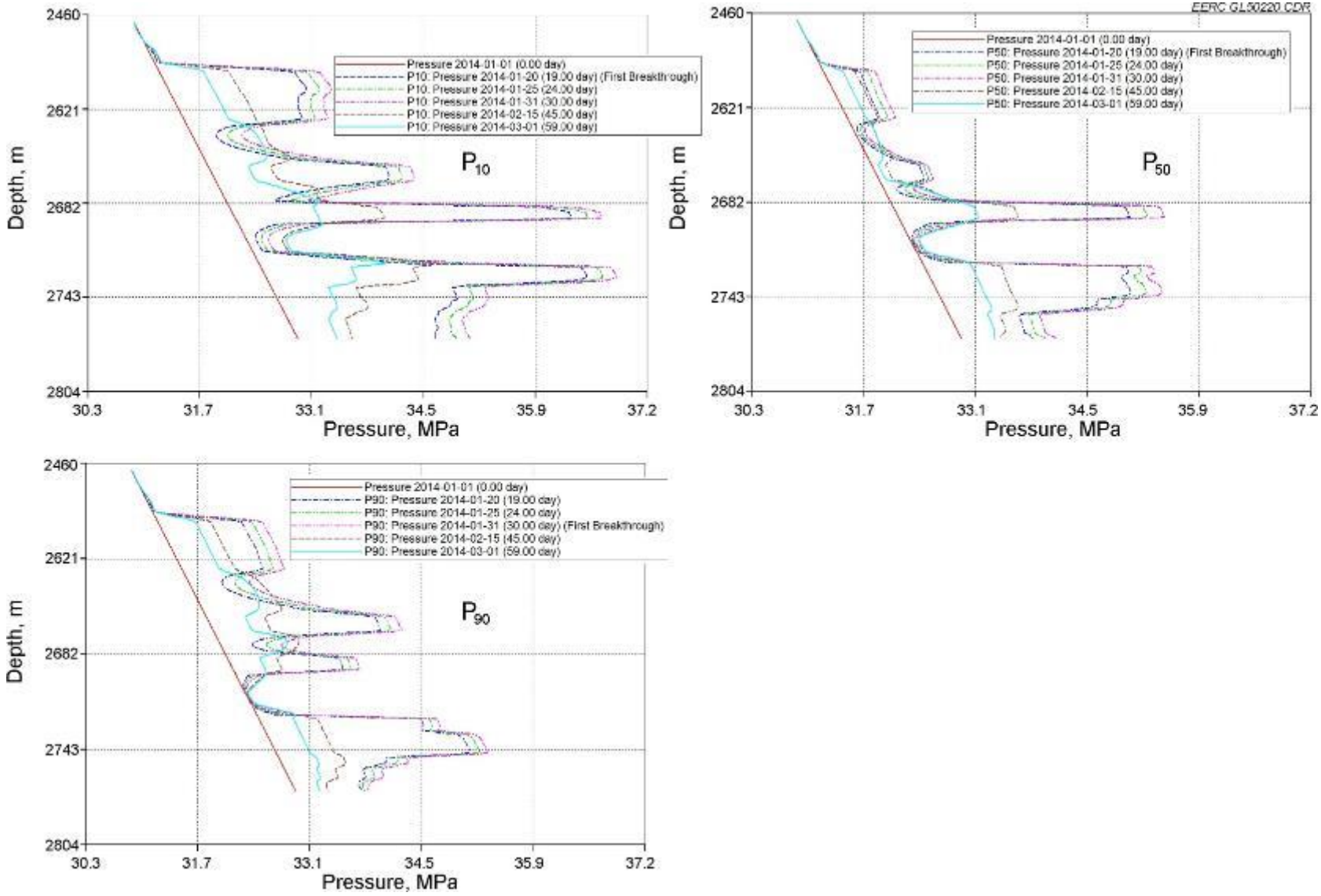

Figure A-7. CO_2 saturation plots along the observation well from top to bottom over time based on three geologic realizations.

Case 1 CO_2 Plume Movements

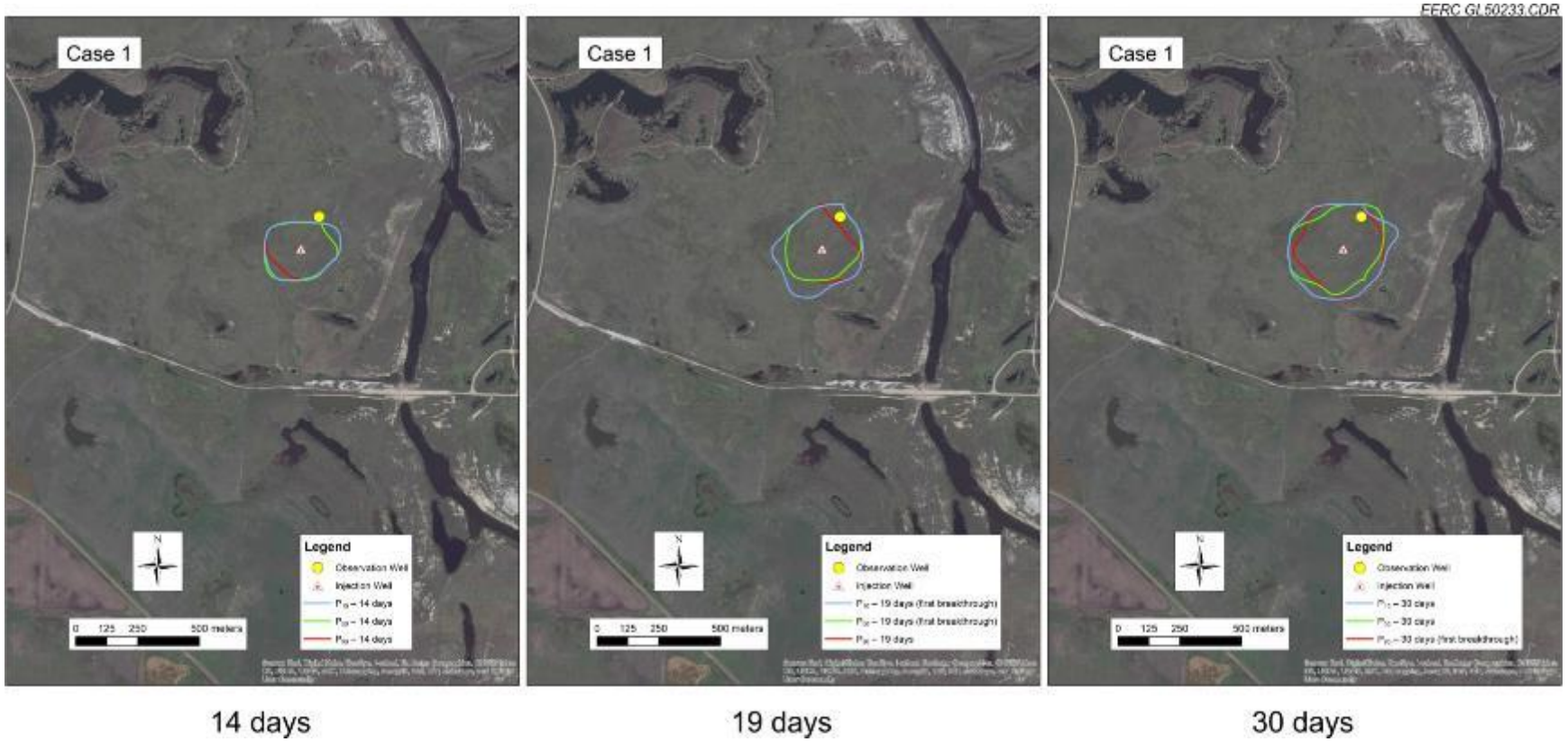

Figure A-8. CO_2 plume maps over time, starting from the injection beginning (continued).

Figure A-8 (continued). CO_2 plume maps over time, starting from the injection beginning (continued).

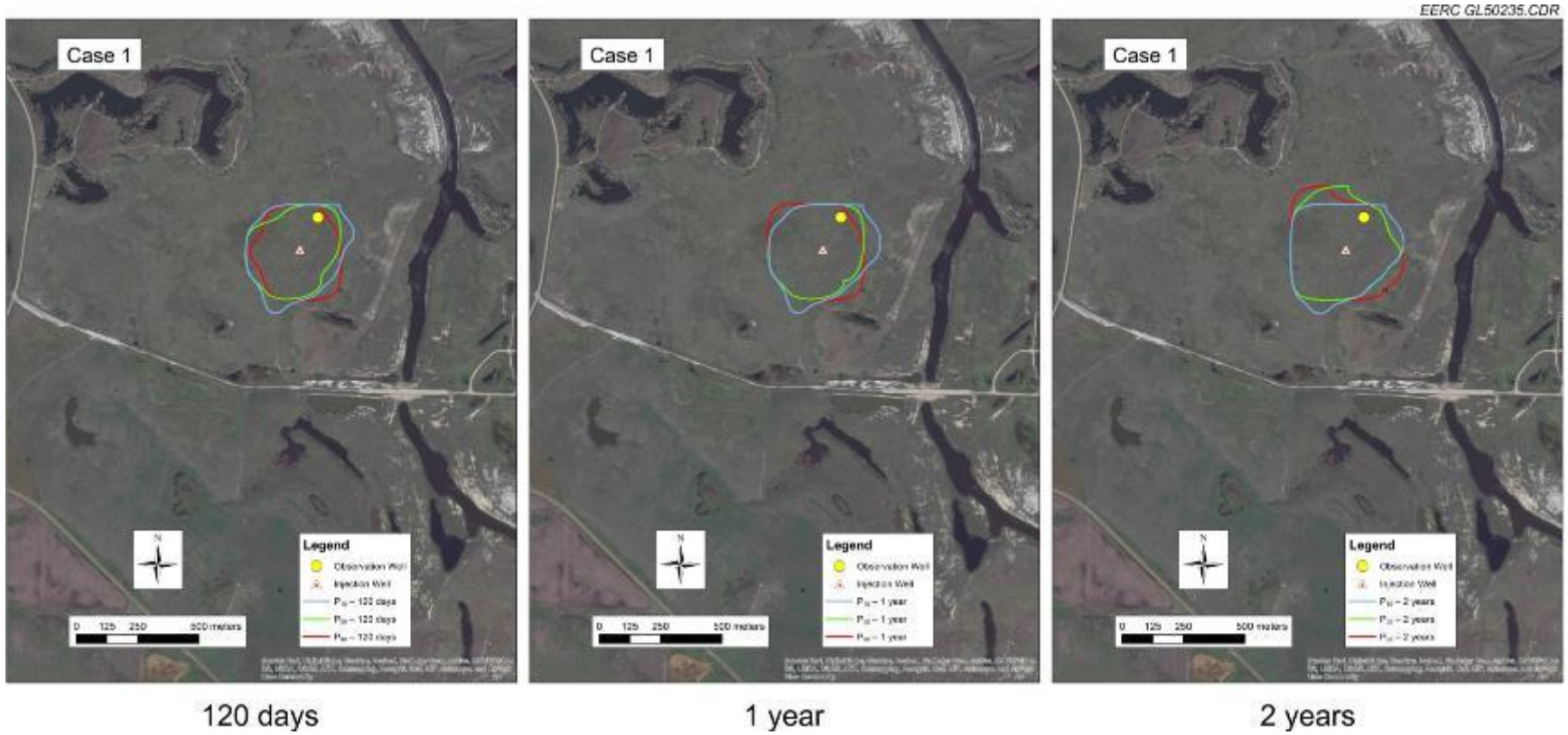

Figure A-8 (continued). CO_2 plume maps over time, starting from the injection beginning.

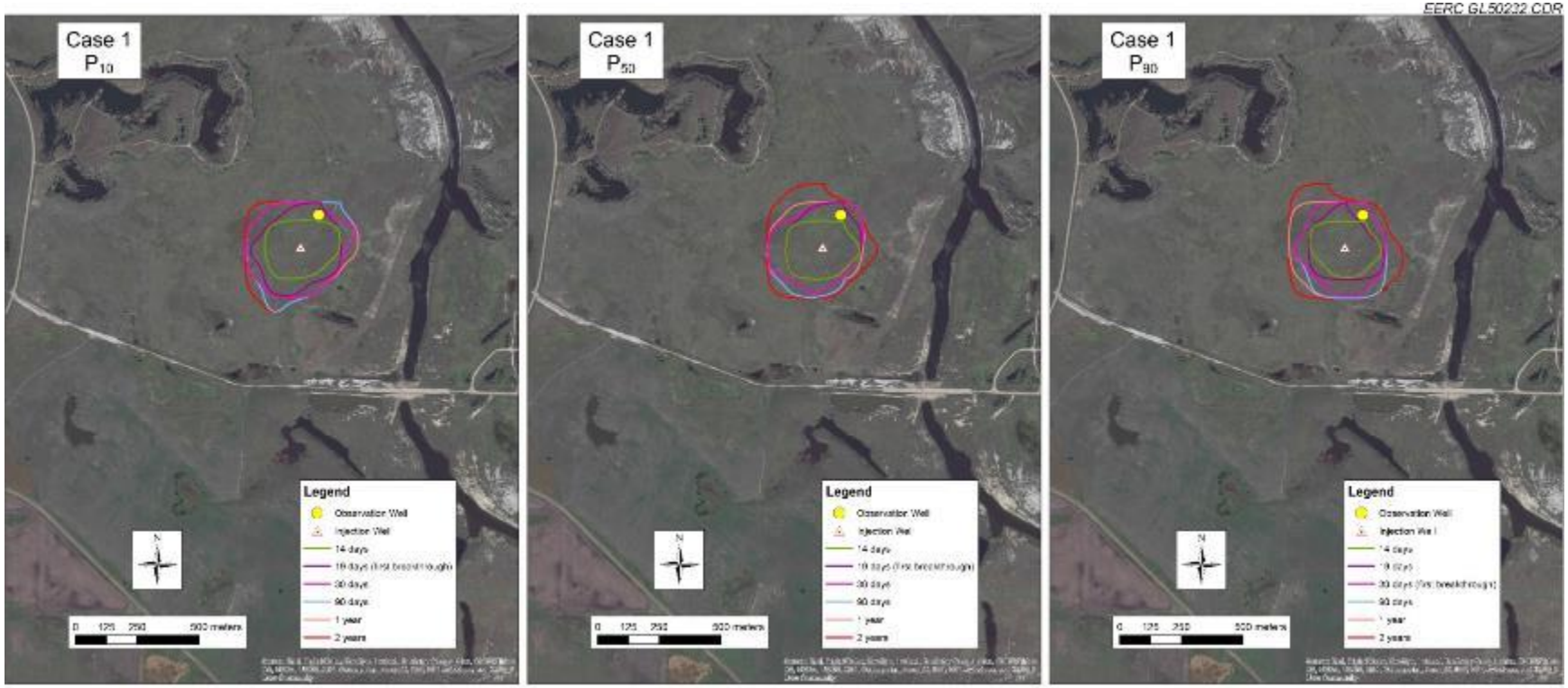

Figure A-9. CO_2 plume maps over three geologic realizations.

Case 1 Probability Distributions of CO_2 Movement

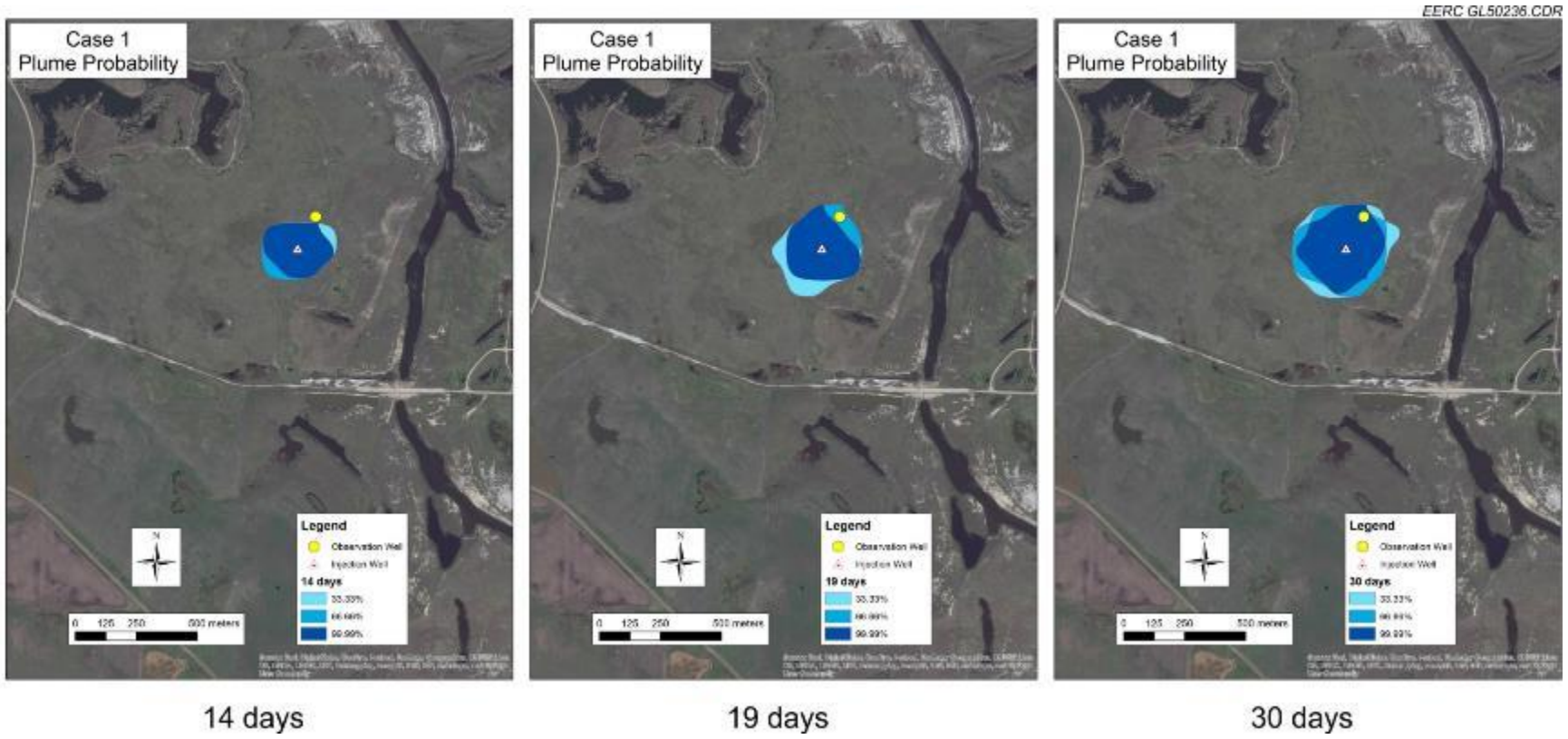

Figure A-10. Probability distributions of CO_2 movement over time (continued).

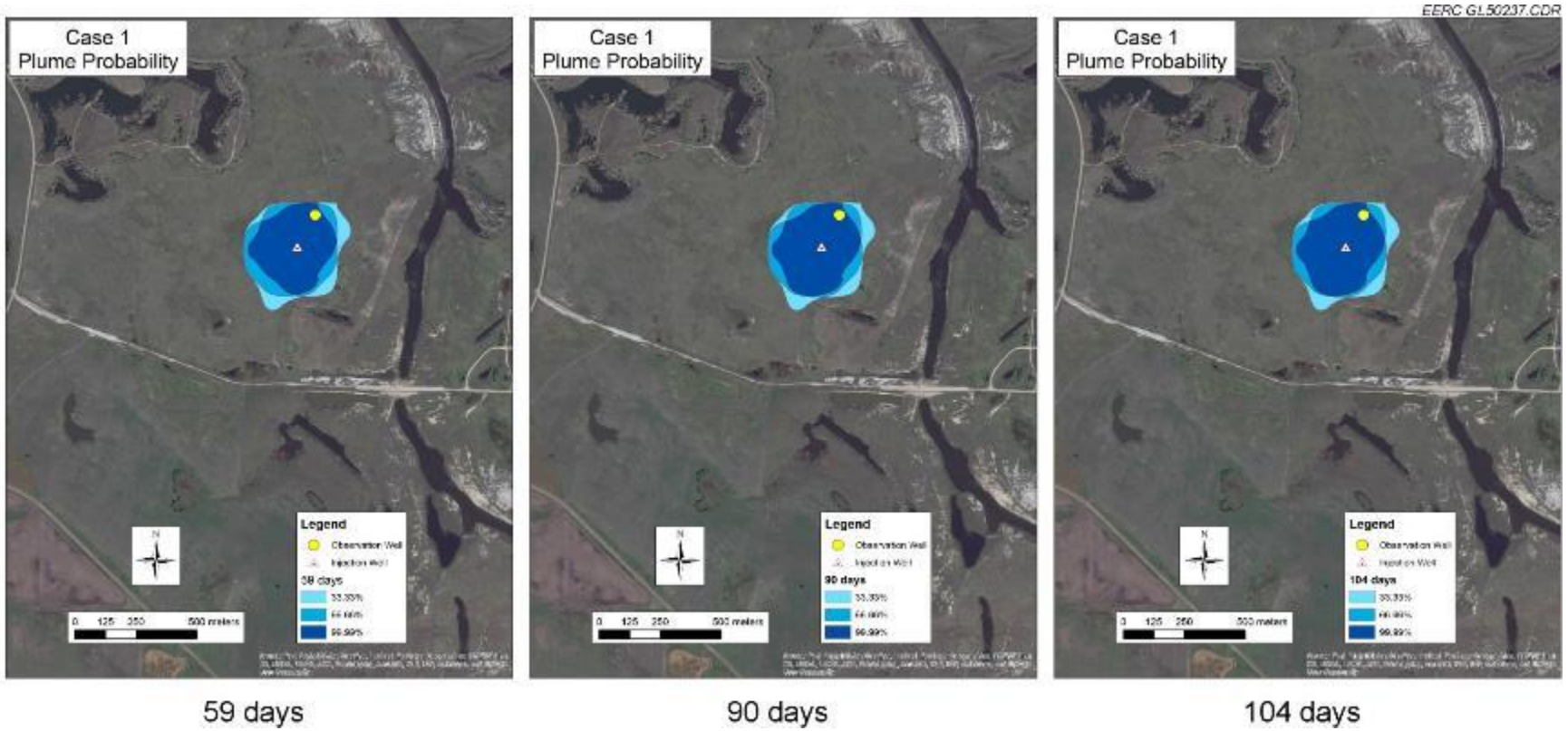

Figure A-10 (continued). Probability distributions of CO_2 movement over time (continued).

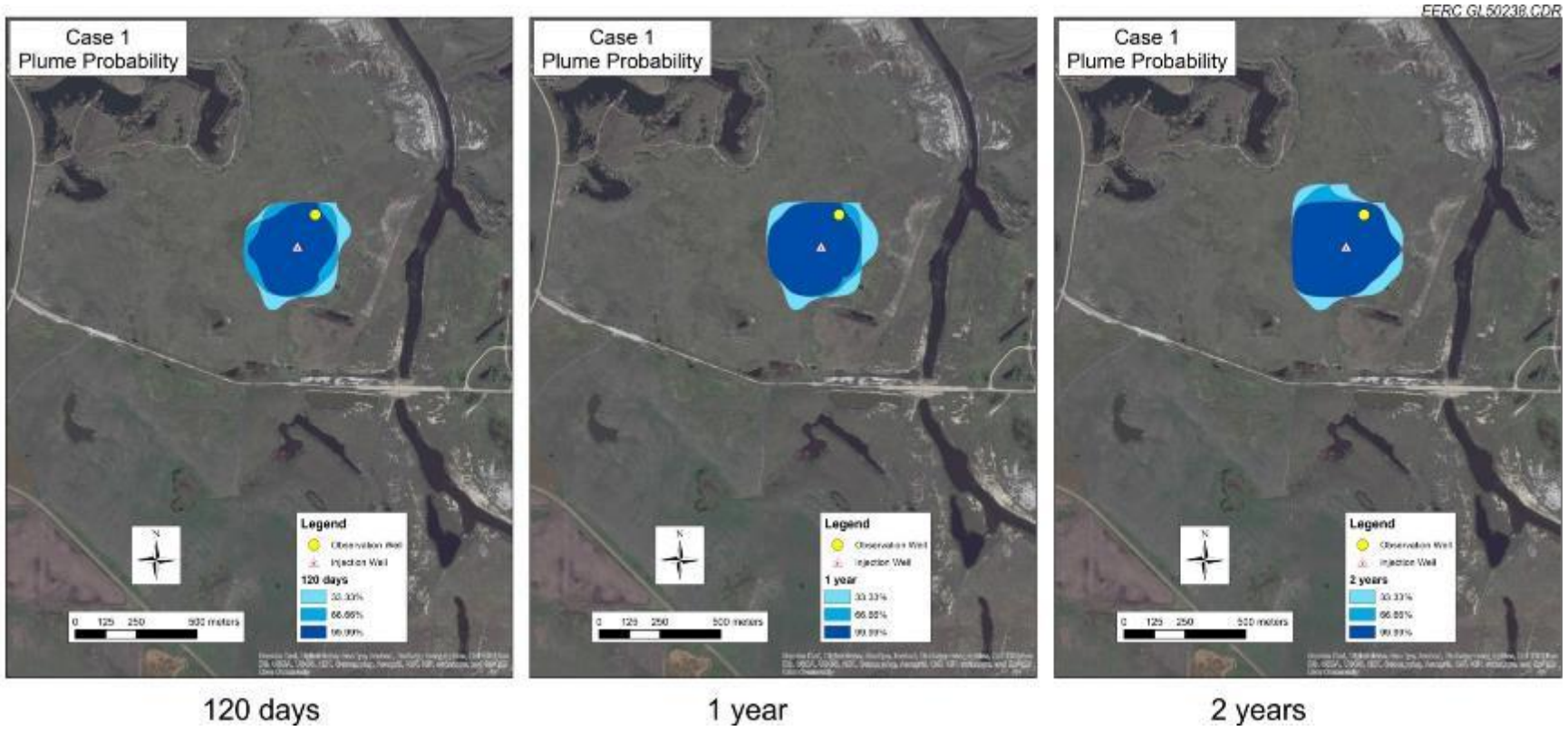

Figure A-10 (continued). Probability distributions of CO_2 movement over time.

CASE 2

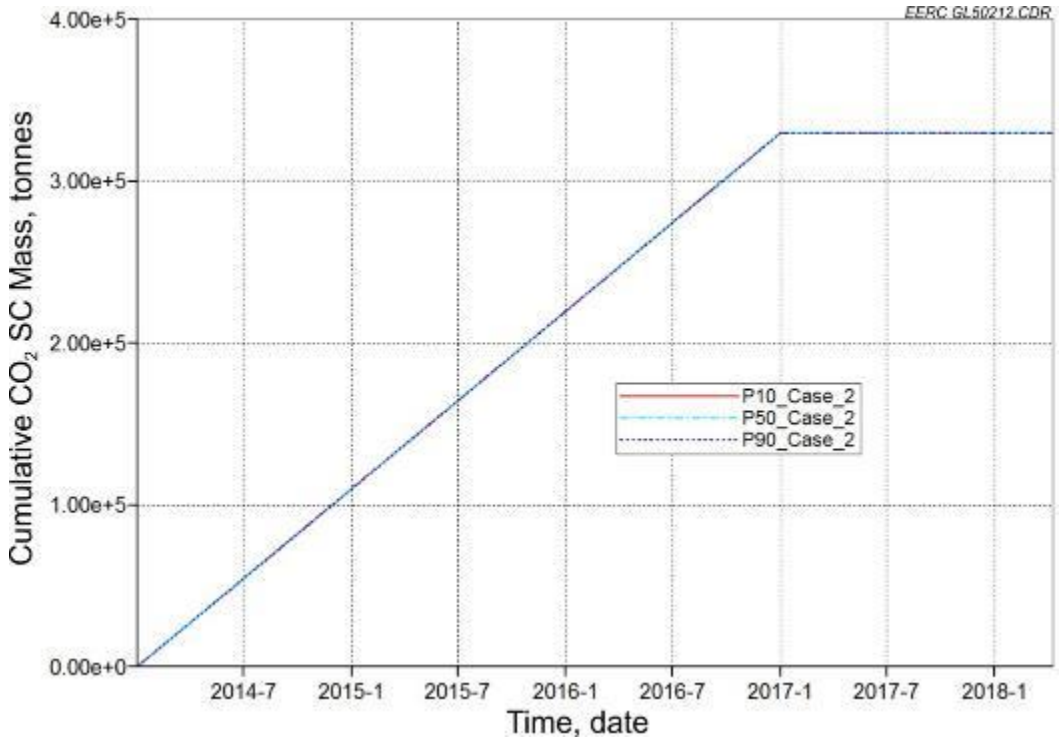

Figure A-11. Cumulative CO_2 injection histories for Case 2 over three realizations.

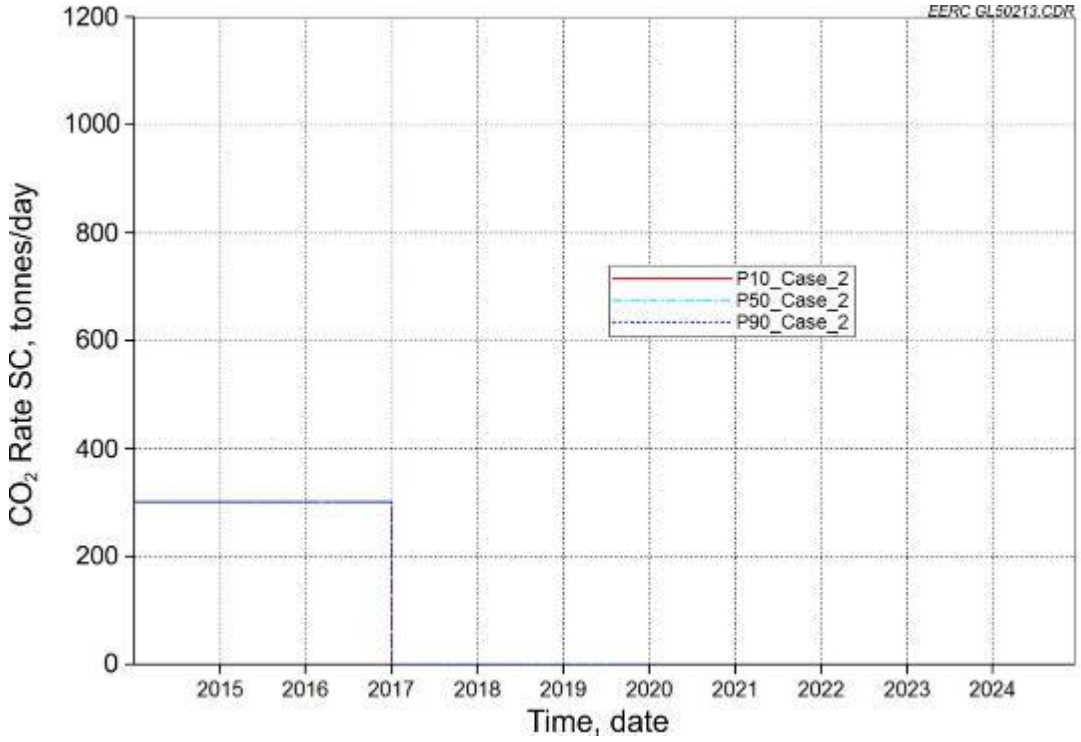

Figure A-12. CO_2 injection rate histories for Case 2 over three realizations.

Case 2 CO_2 Breakthrough Monitoring

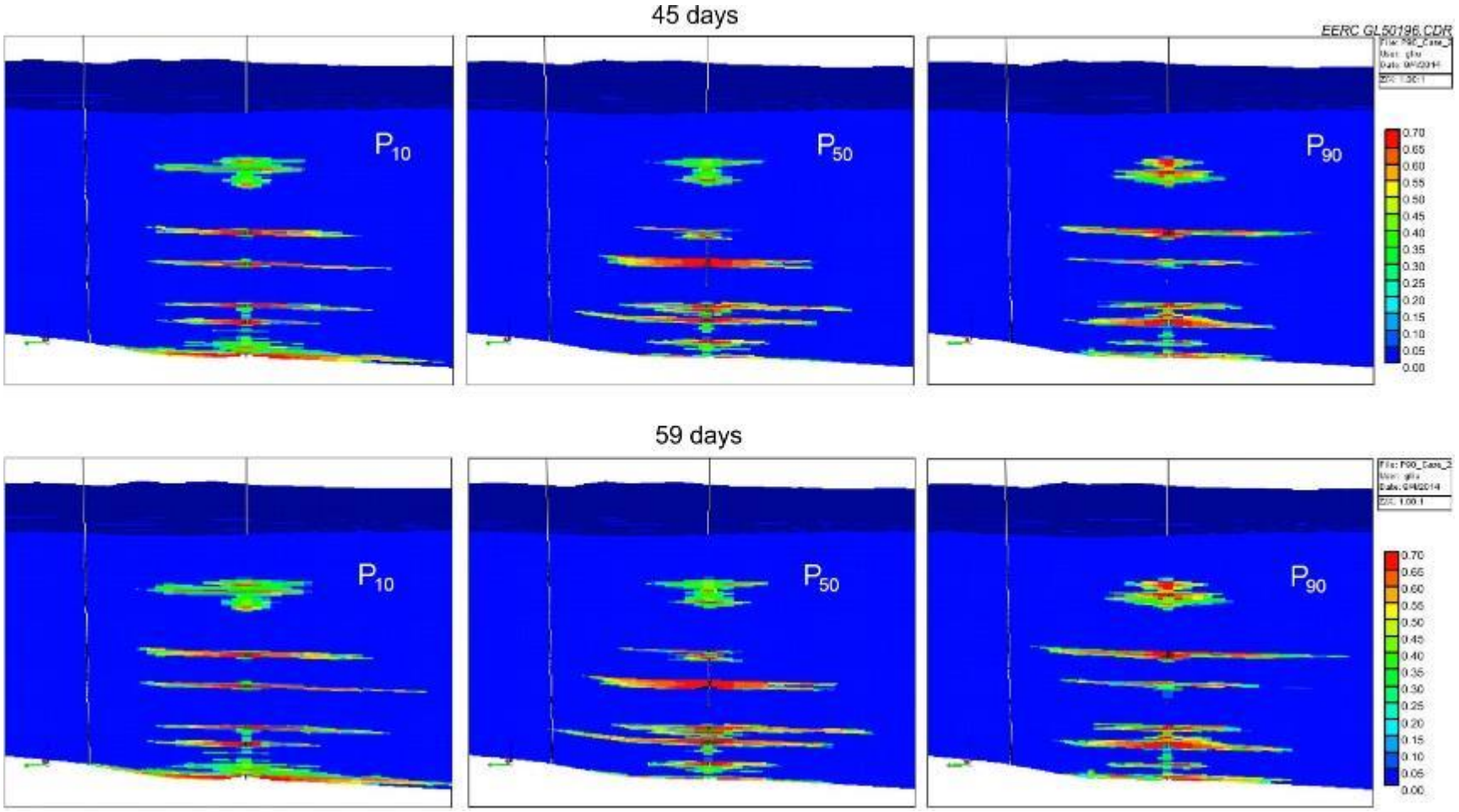

Figure A-13. Cross-section view of CO_2 saturation over time, starting from the injection beginning.

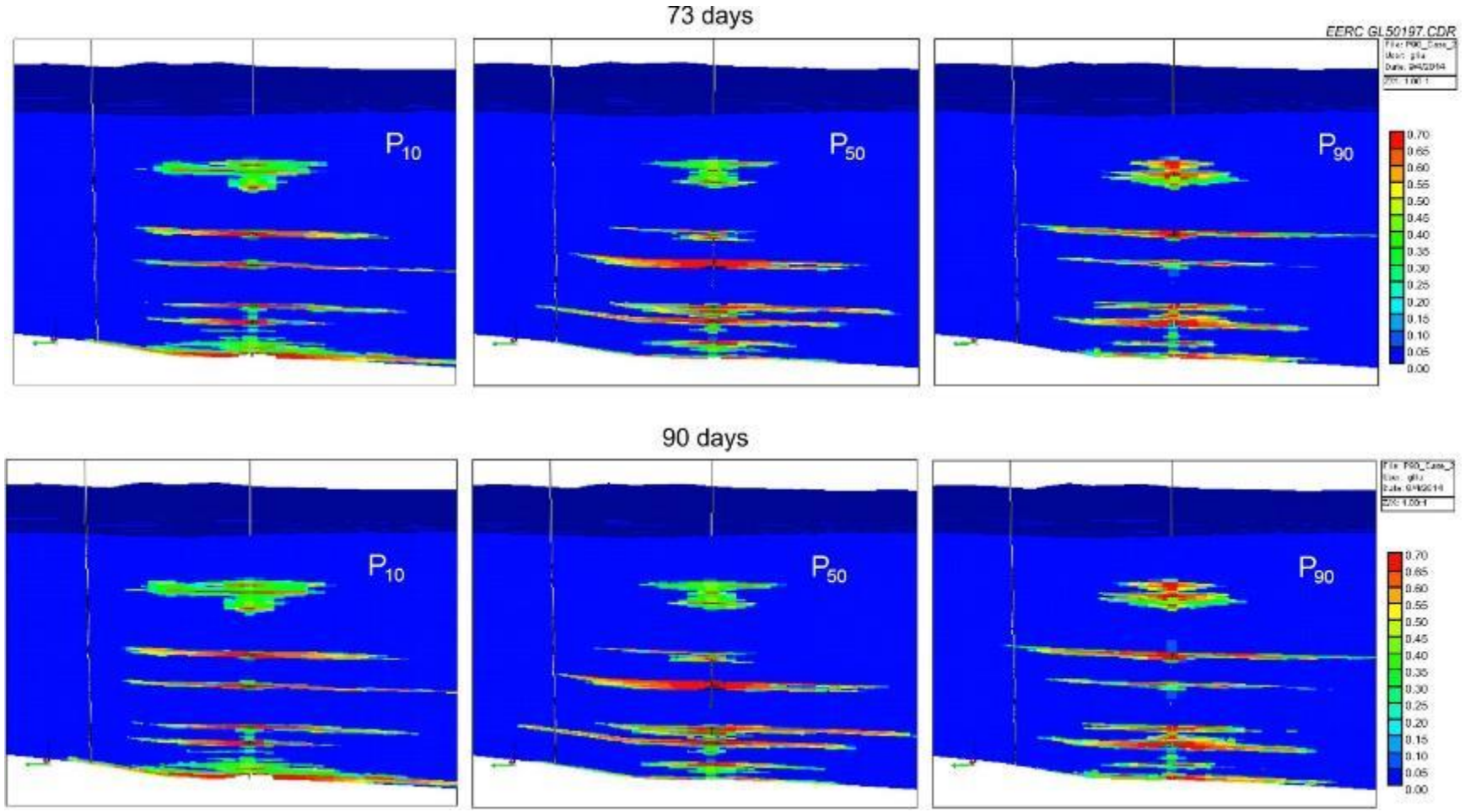

Figure A-13 (continued). Cross-section view of CO_2 saturation over time, starting from the injection beginning (continued).

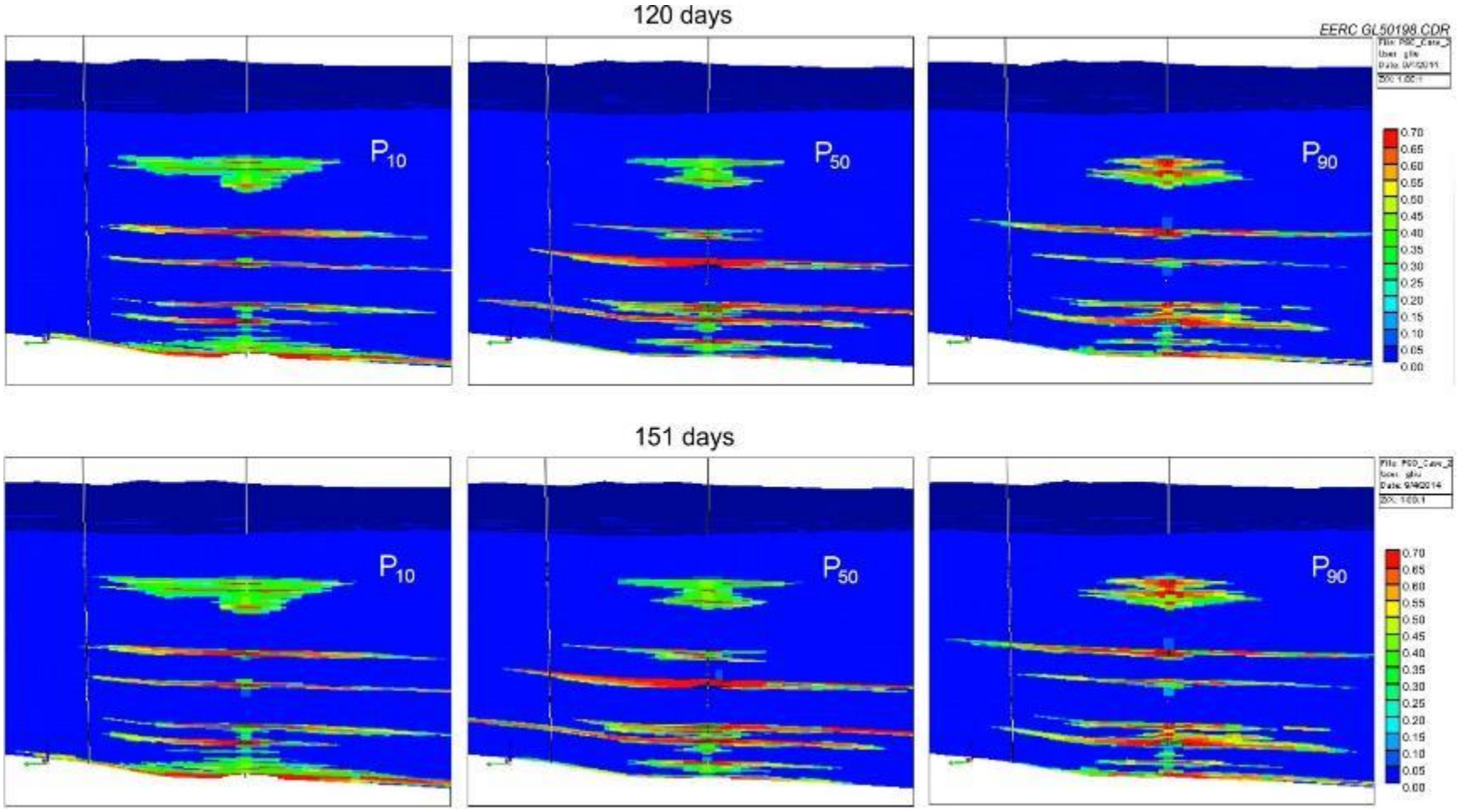

Figure A-13 (continued). Cross-section view of CO_2 saturation over time, starting from the injection beginning.

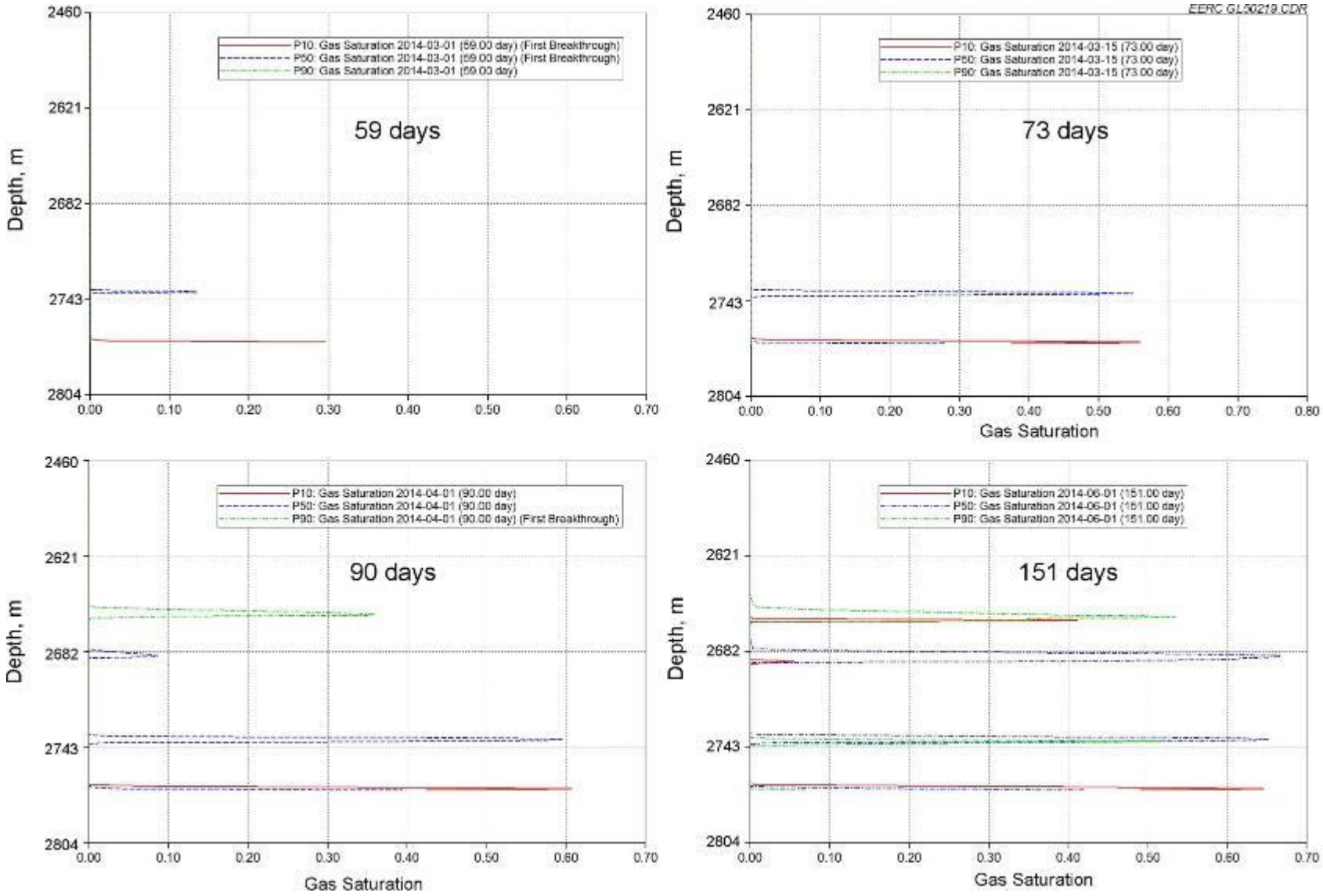

Figure A-14. CO_2 saturation plots along the observation well from top to bottom over time, starting from the injection beginning (continued).

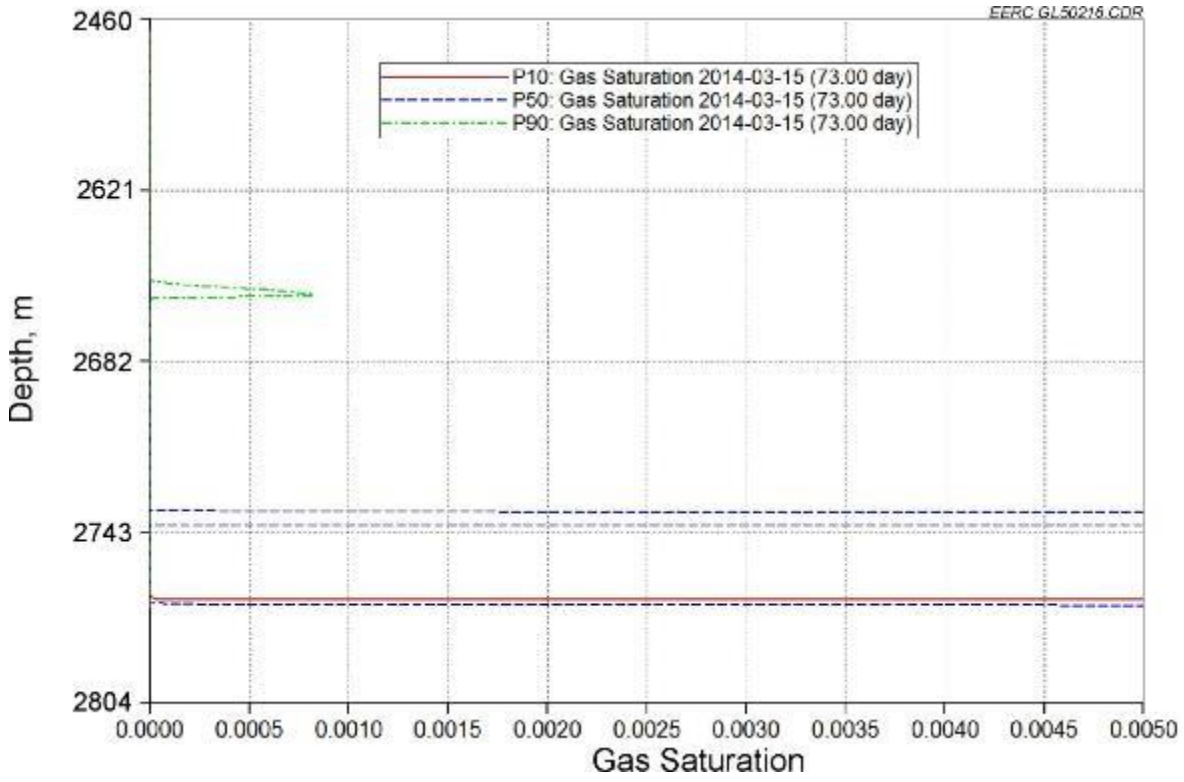

Figure A-14 (continued). Modification of CO_2 saturation on 73rd day.

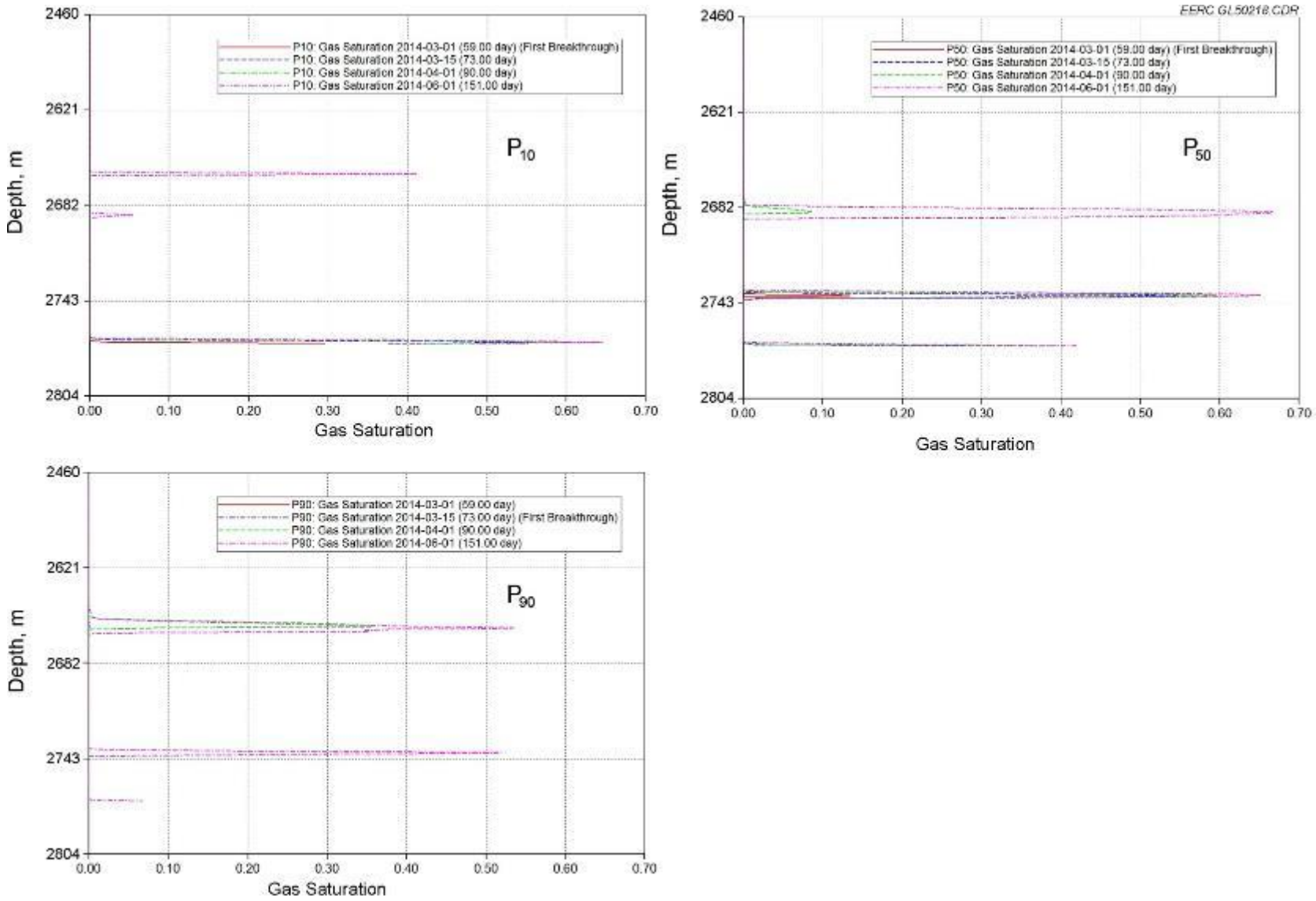

Figure A-15. CO_2 saturation plots along the observation well from top to bottom over time based on three geologic realizations.

Case 2 Pressure Change Monitoring

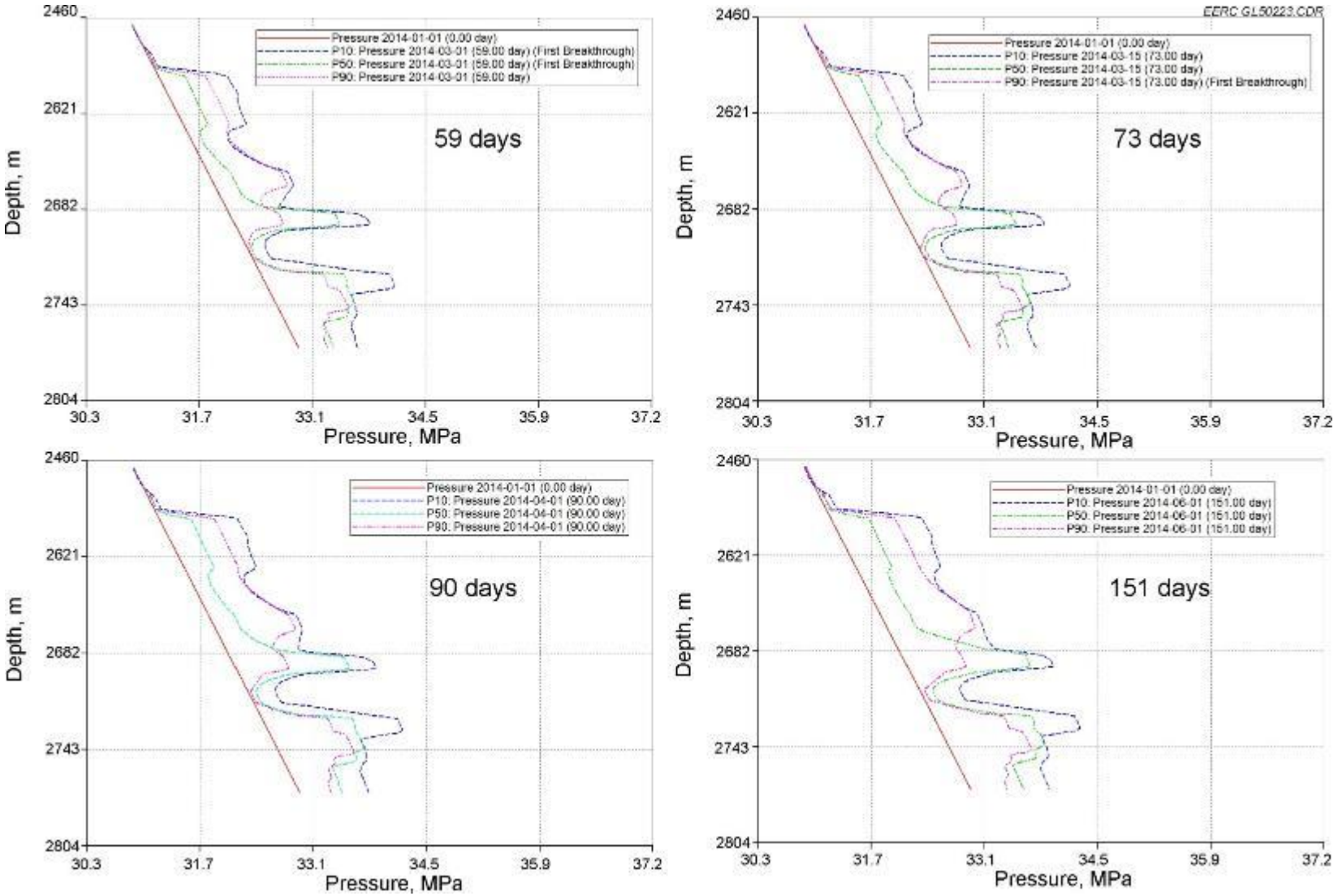

Figure A-16. Pressure plots along the observation well from top to bottom over time, starting from the injection beginning.

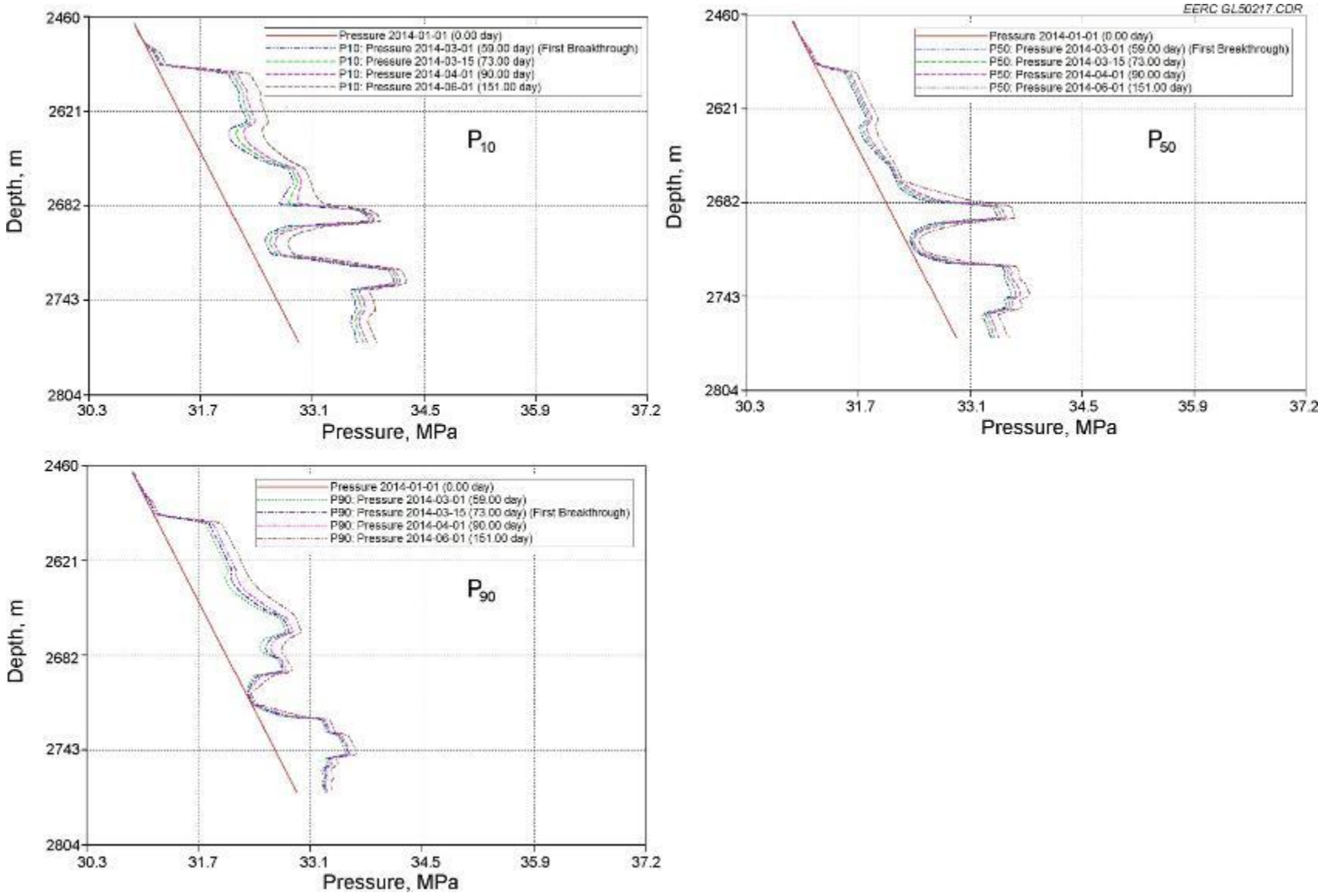

Figure A-17. CO_2 saturation plots along the observation well from top to bottom over time based on three geologic realizations.

Case 2 CO_2 Plume Movements

Figure A-18. CO_2 plume maps over time, starting from the injection beginning (continued).

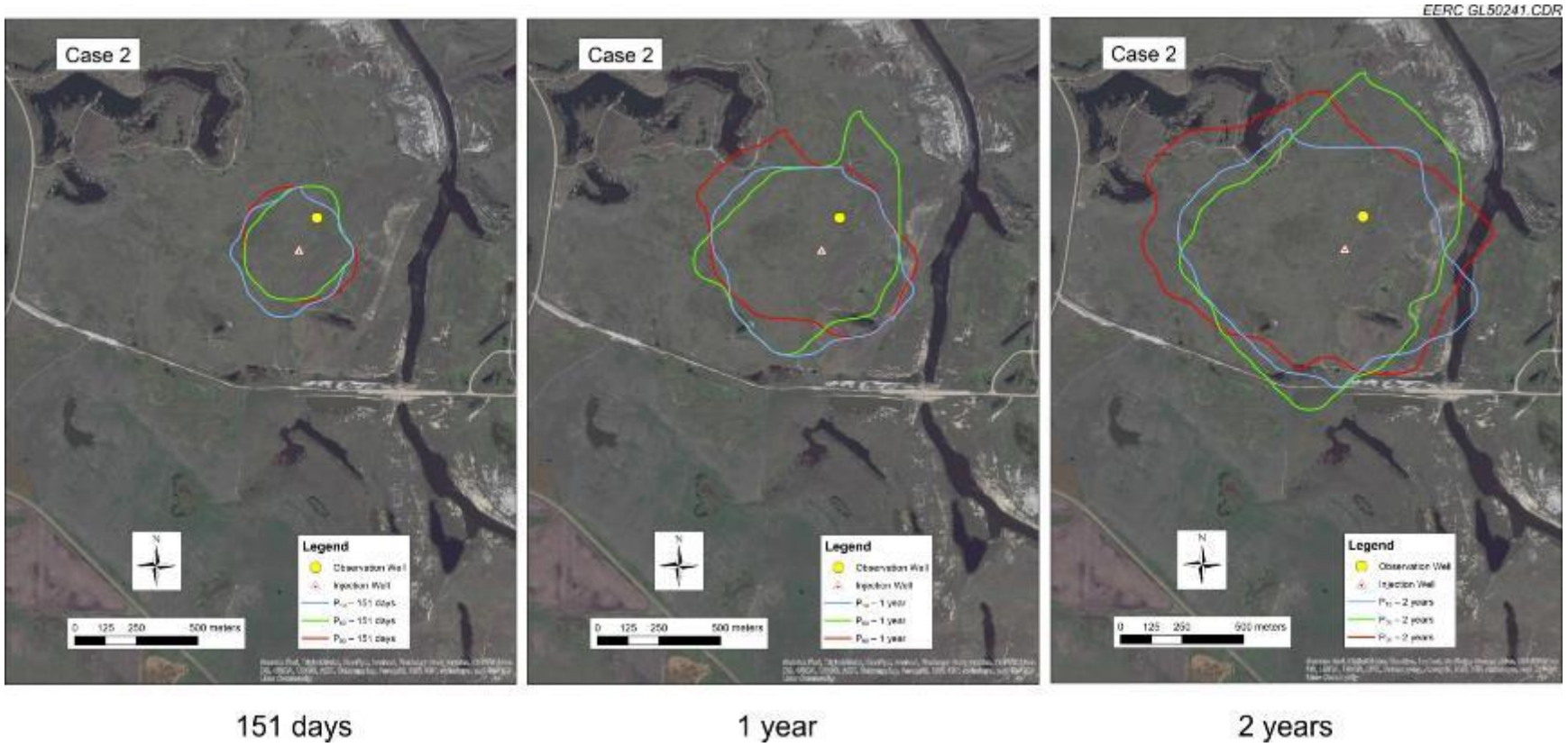

Figure A-18 (continued). CO_2 plume maps over time, starting from the injection beginning.

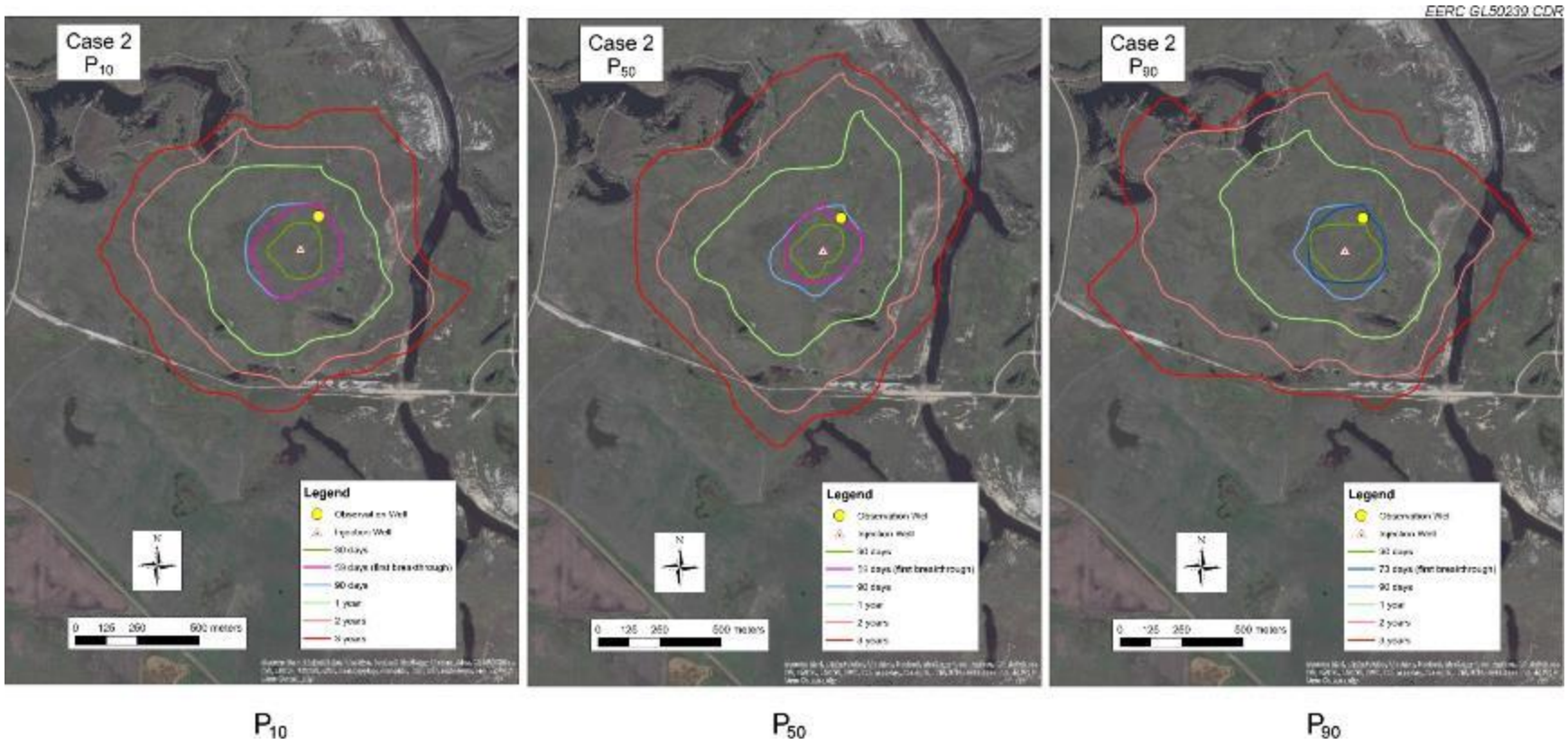

Figure A-19. CO_2 plume maps over three geologic realizations.

Case 2 Probability Distributions of CO_2 Movement

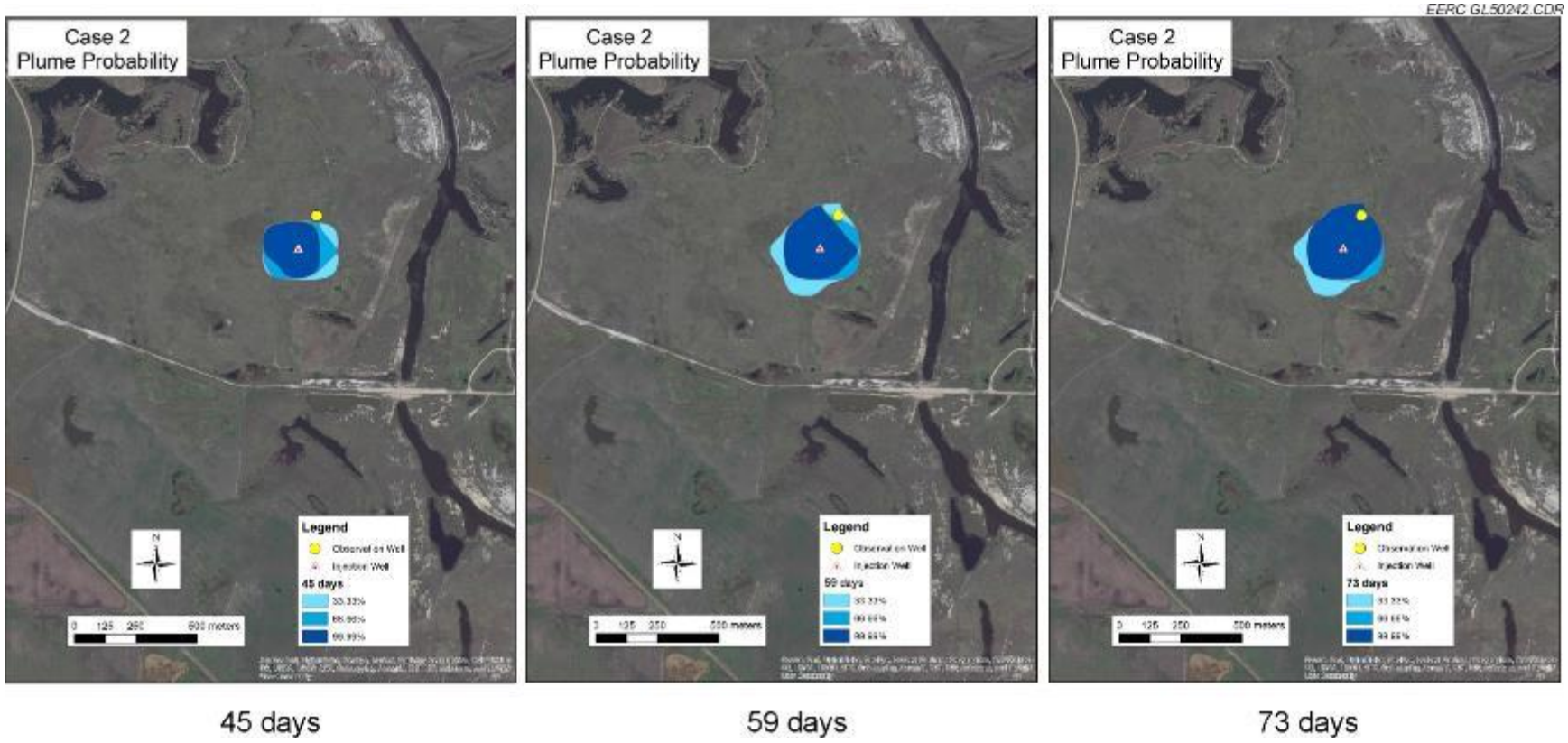

Figure A-20. Probability distributions of CO_2 movement over time (continued).

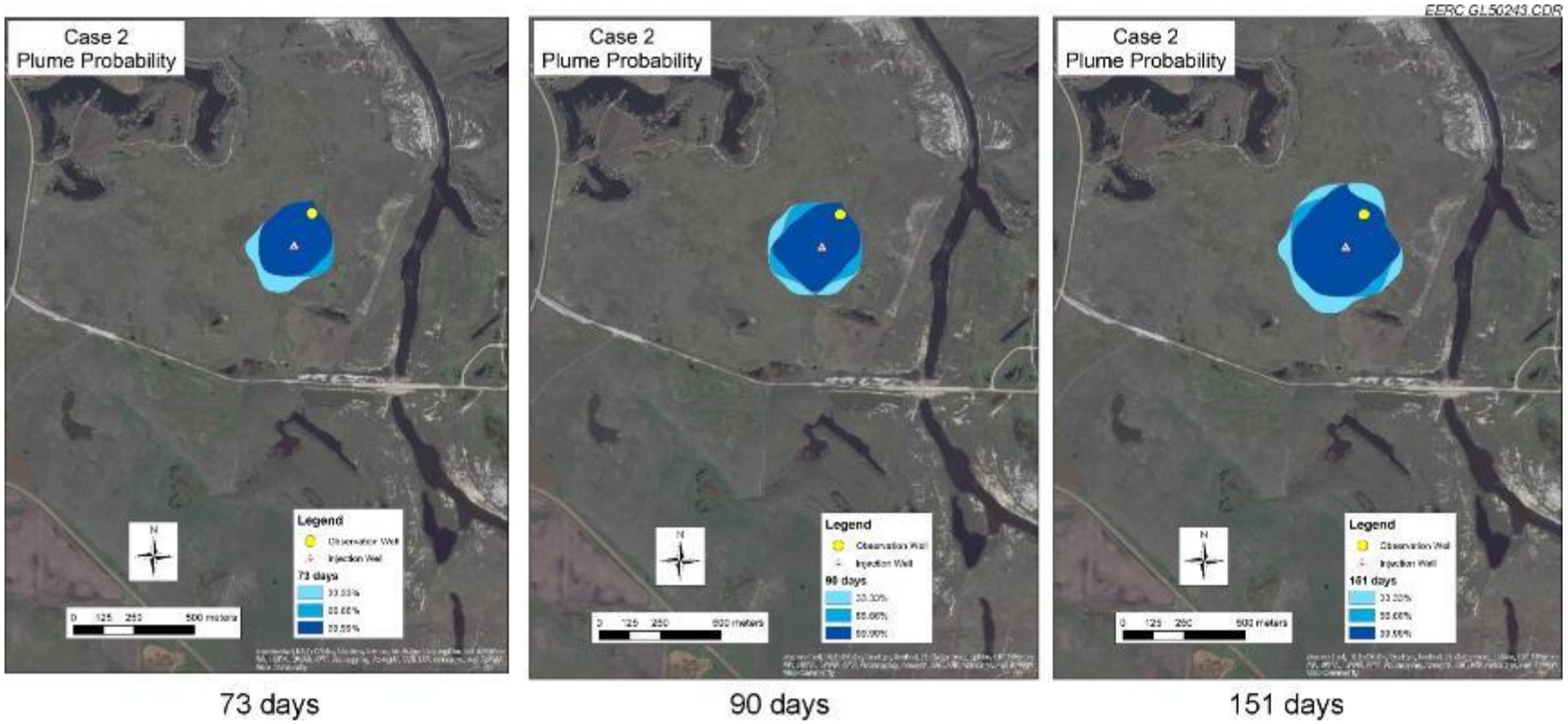

Figure A-20 (continued). Probability distributions of CO_2 movement over time (continued).

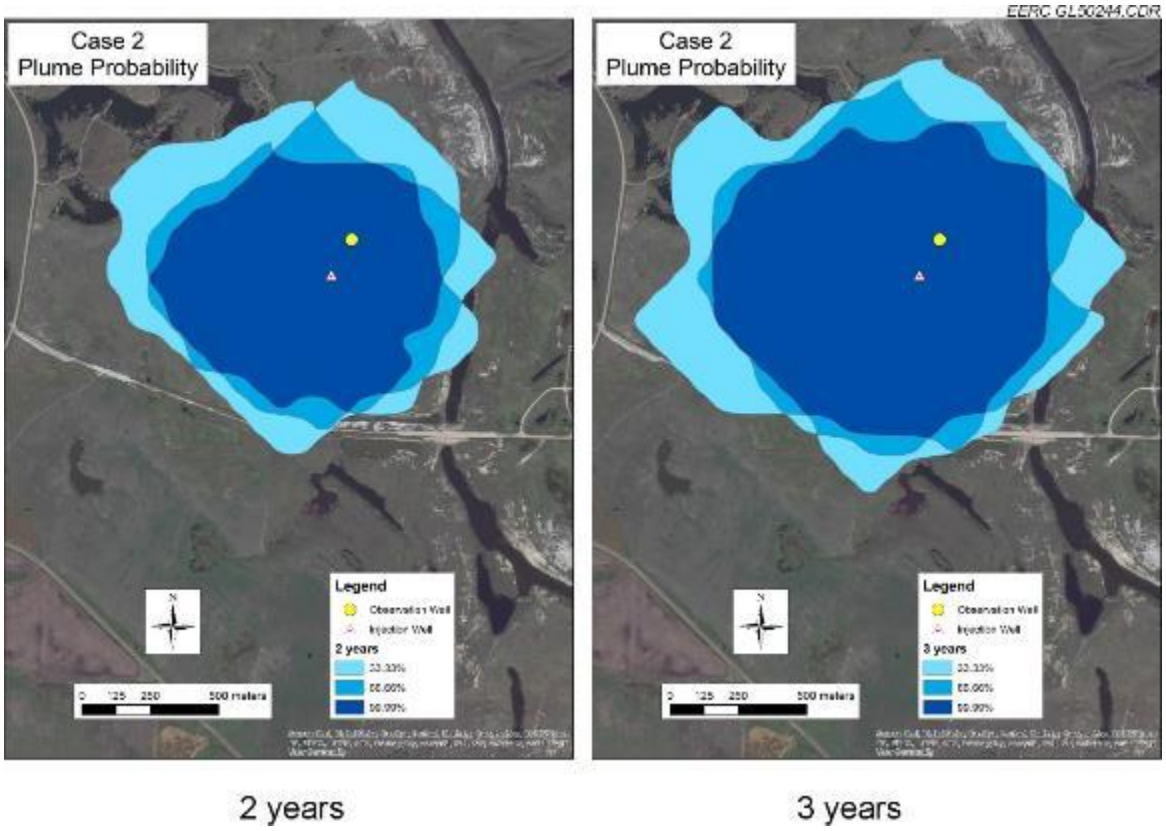

Figure A-20 (continued). Probability distributions of CO_2 movement over time.

CASE 3

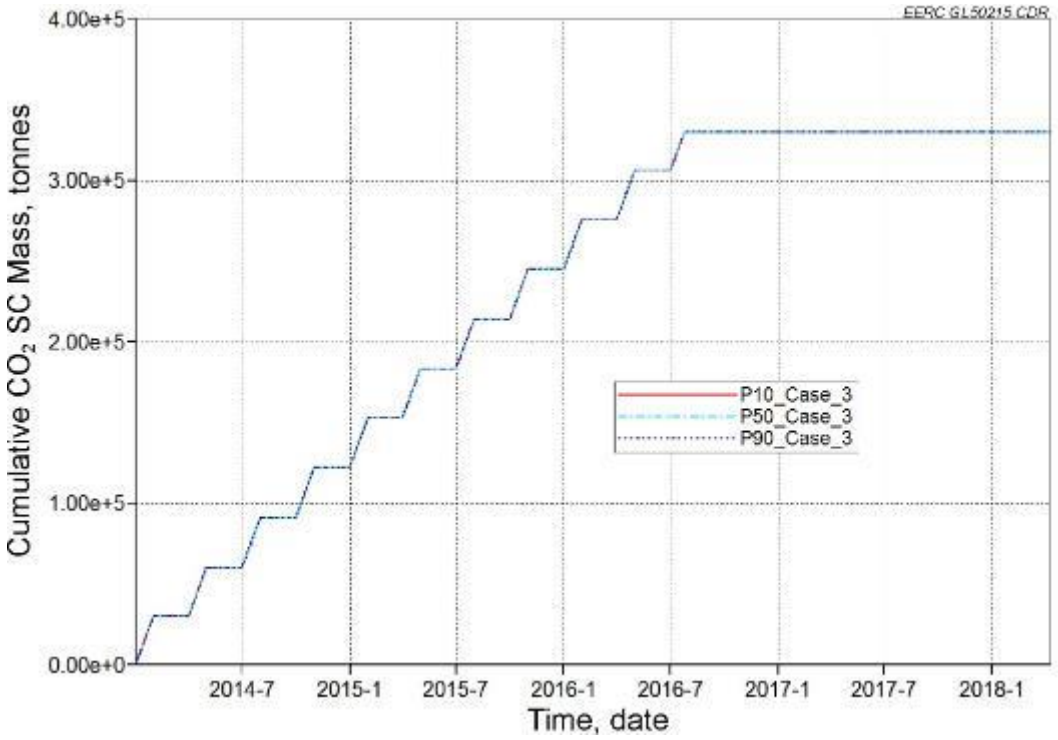

Figure A-21. Cumulative CO_2 injection histories for Case 3 over three realizations.

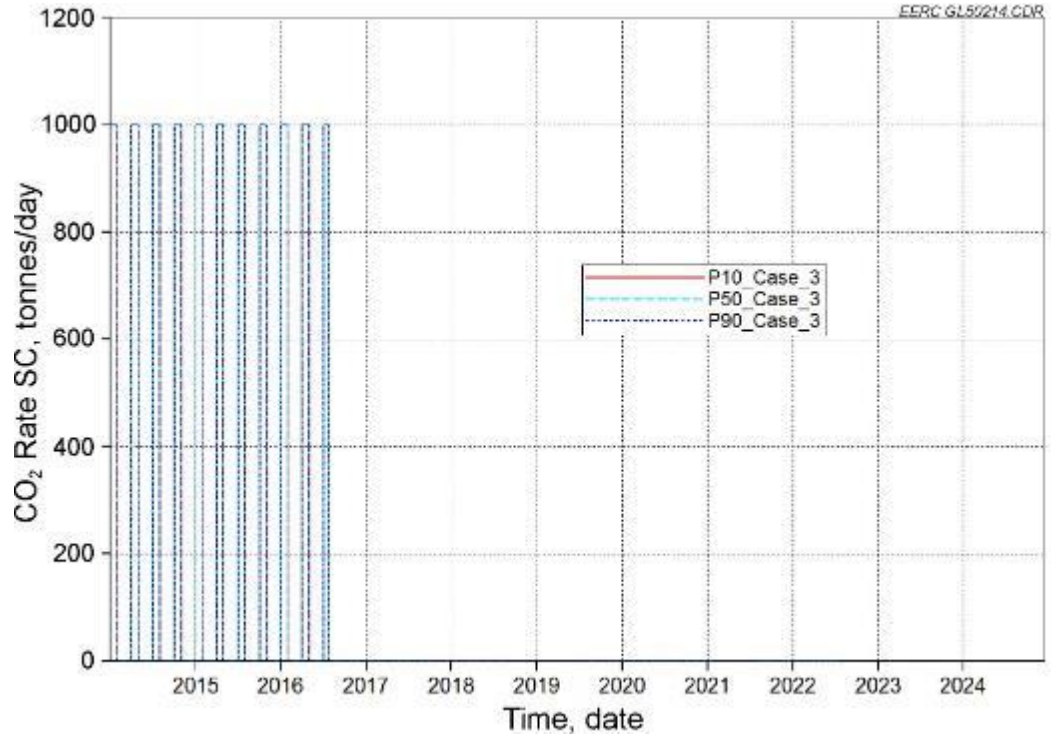

Figure A-22. CO_2 injection rate histories for Case 3 over three realizations.

Case 3 CO_2 Breakthrough Monitoring

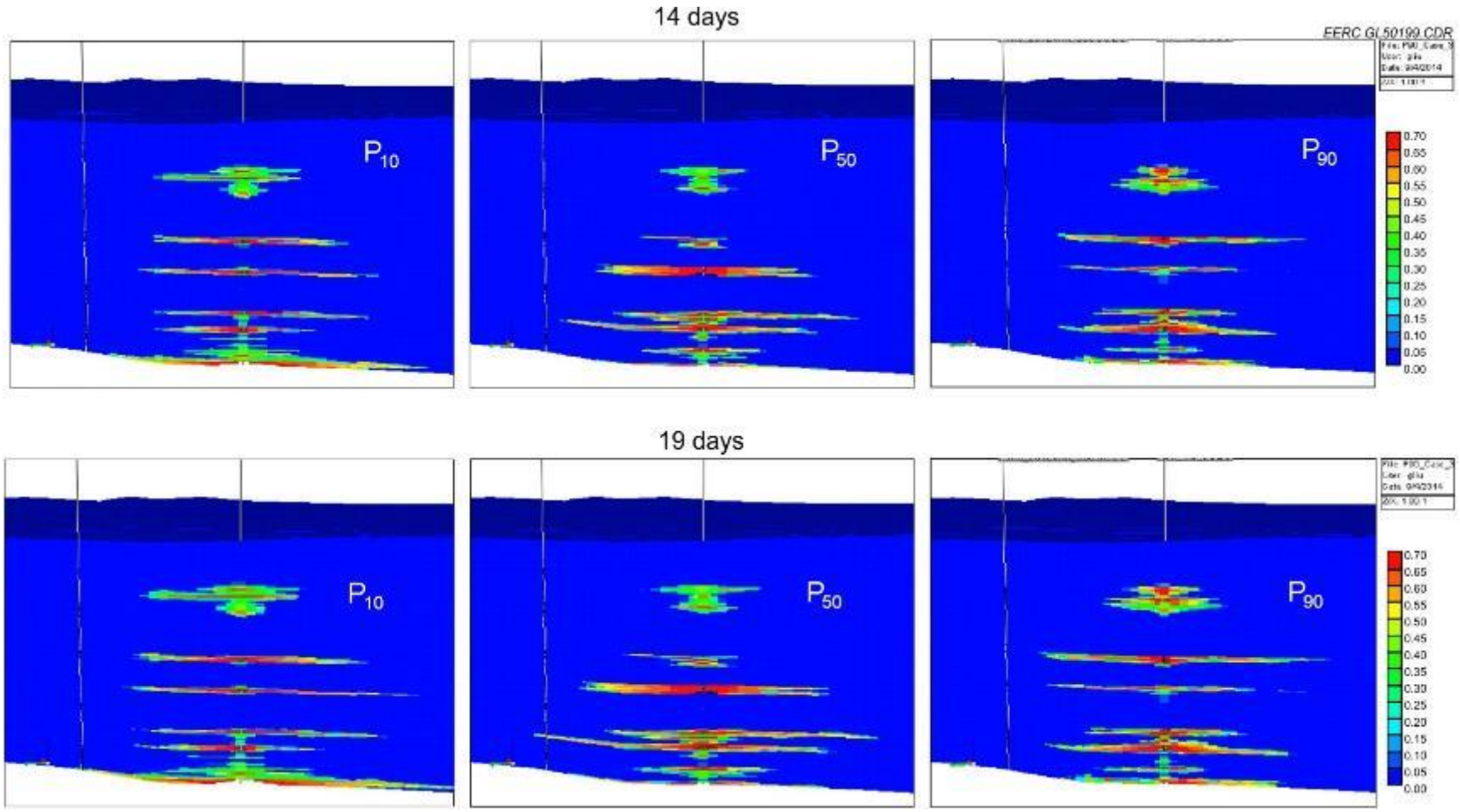

Figure A-23. Cross-section view of CO_2 saturation over time, starting from the injection beginning (continued).

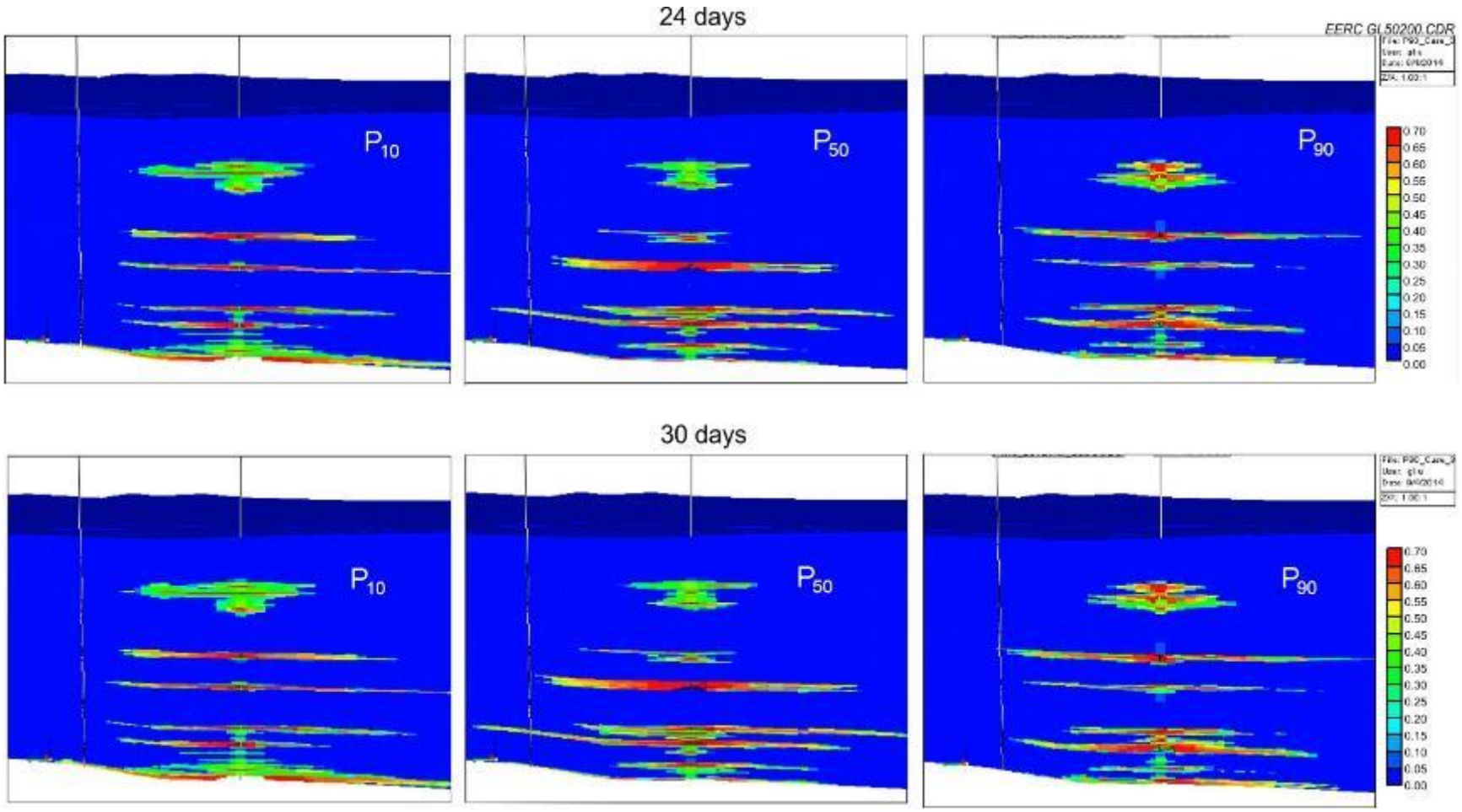

Figure A-23 (continued). Cross-section view of CO_2 saturation over time, starting from the injection beginning (continued).

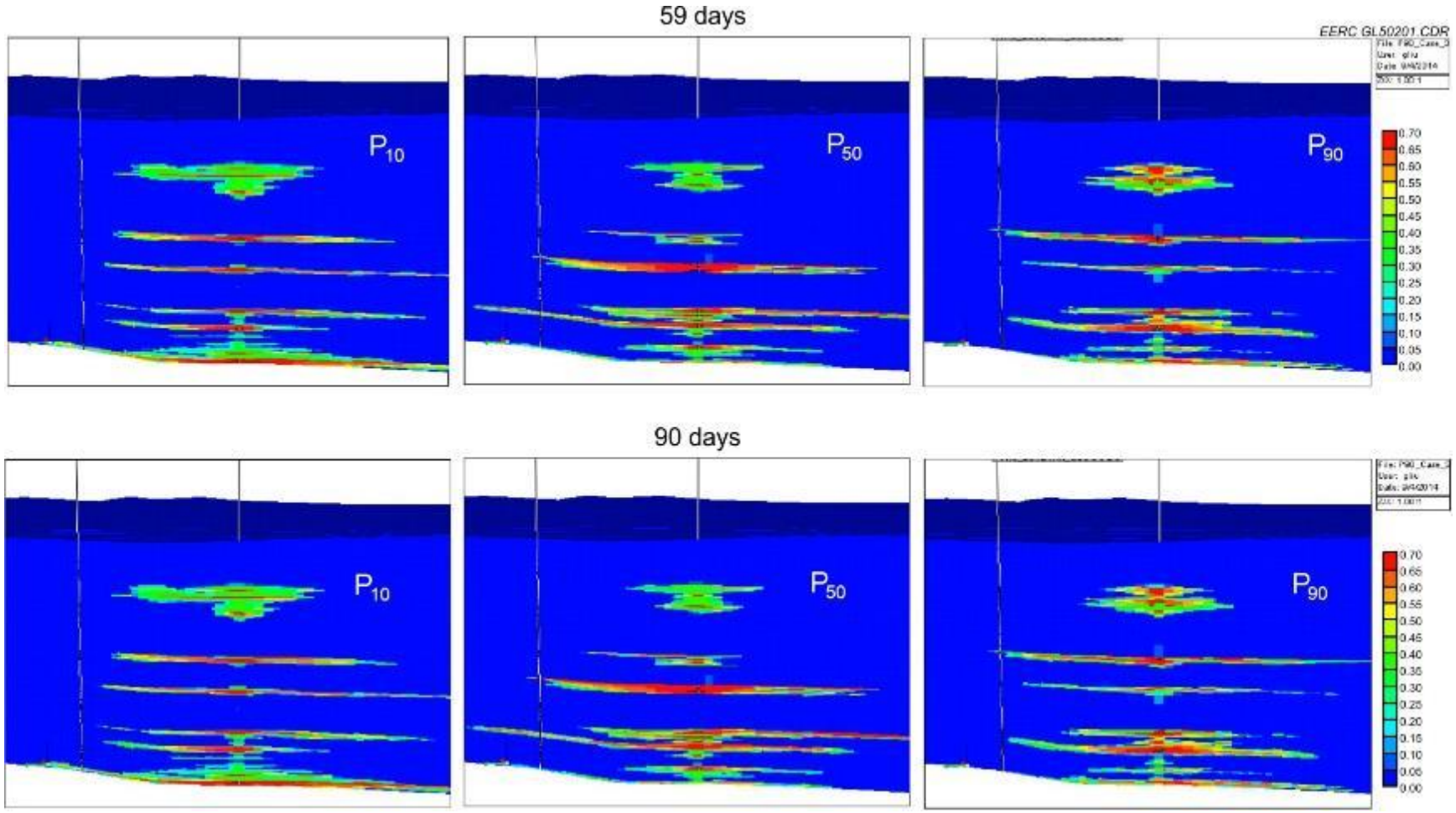

Figure A-23 (continued). Cross-section view of CO_2 saturation over time, starting from the injection beginning (continued).

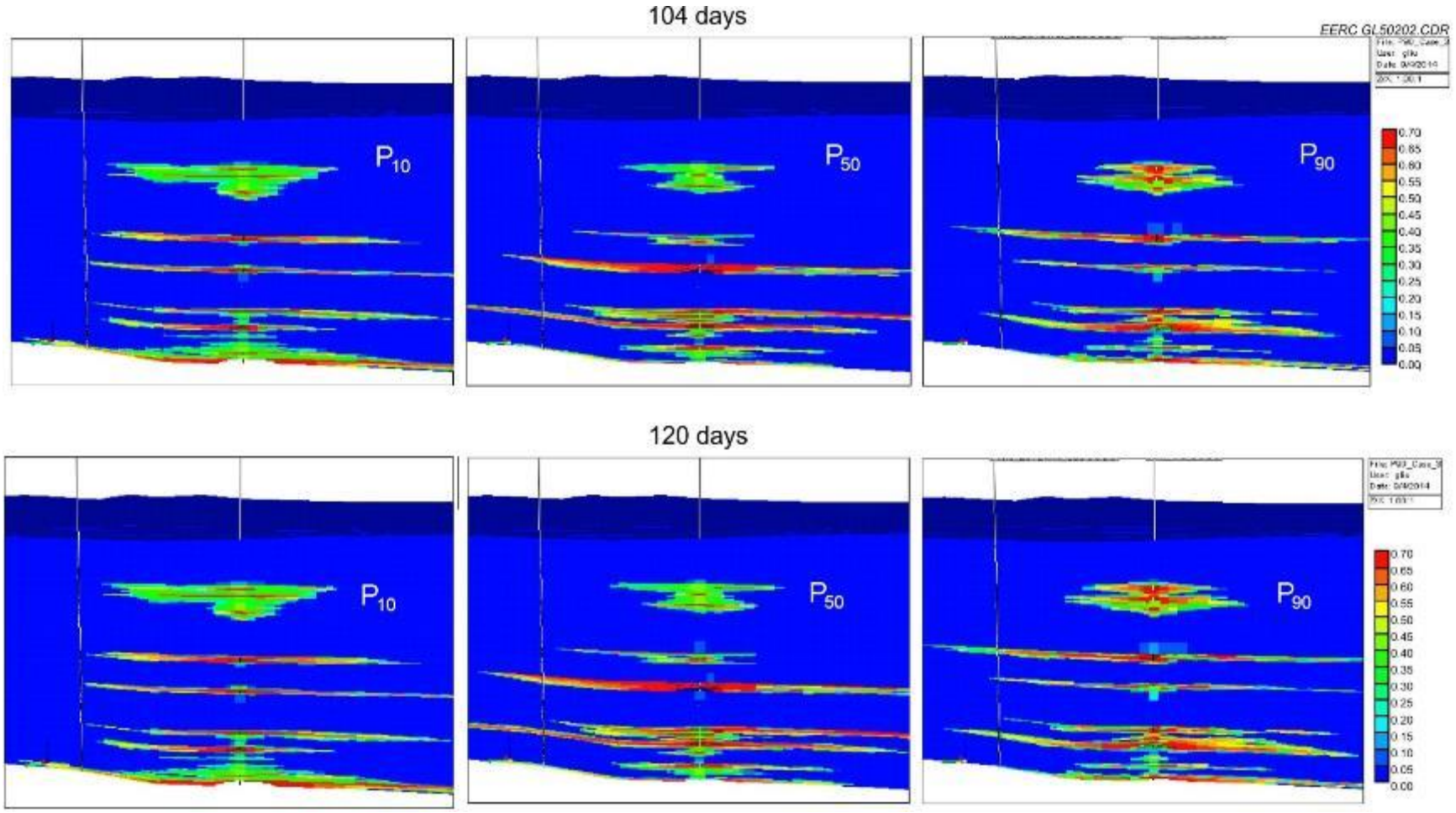

Figure A-23 (continued). Cross-section view of CO_2 saturation over time, starting from the injection beginning.

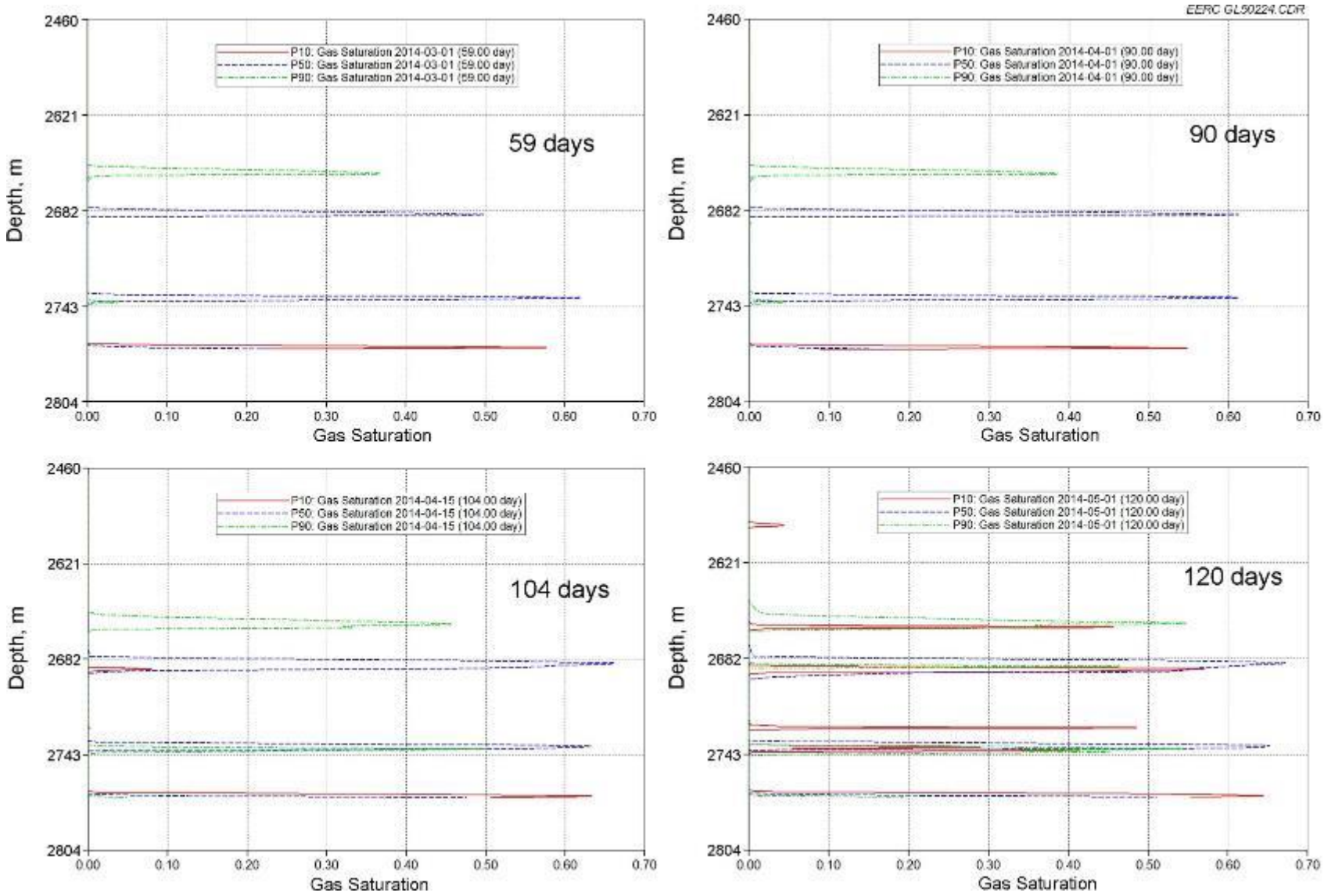

Figure A-24. CO_2 saturation plots along the observation well from top to bottom over time, starting from the injection beginning.

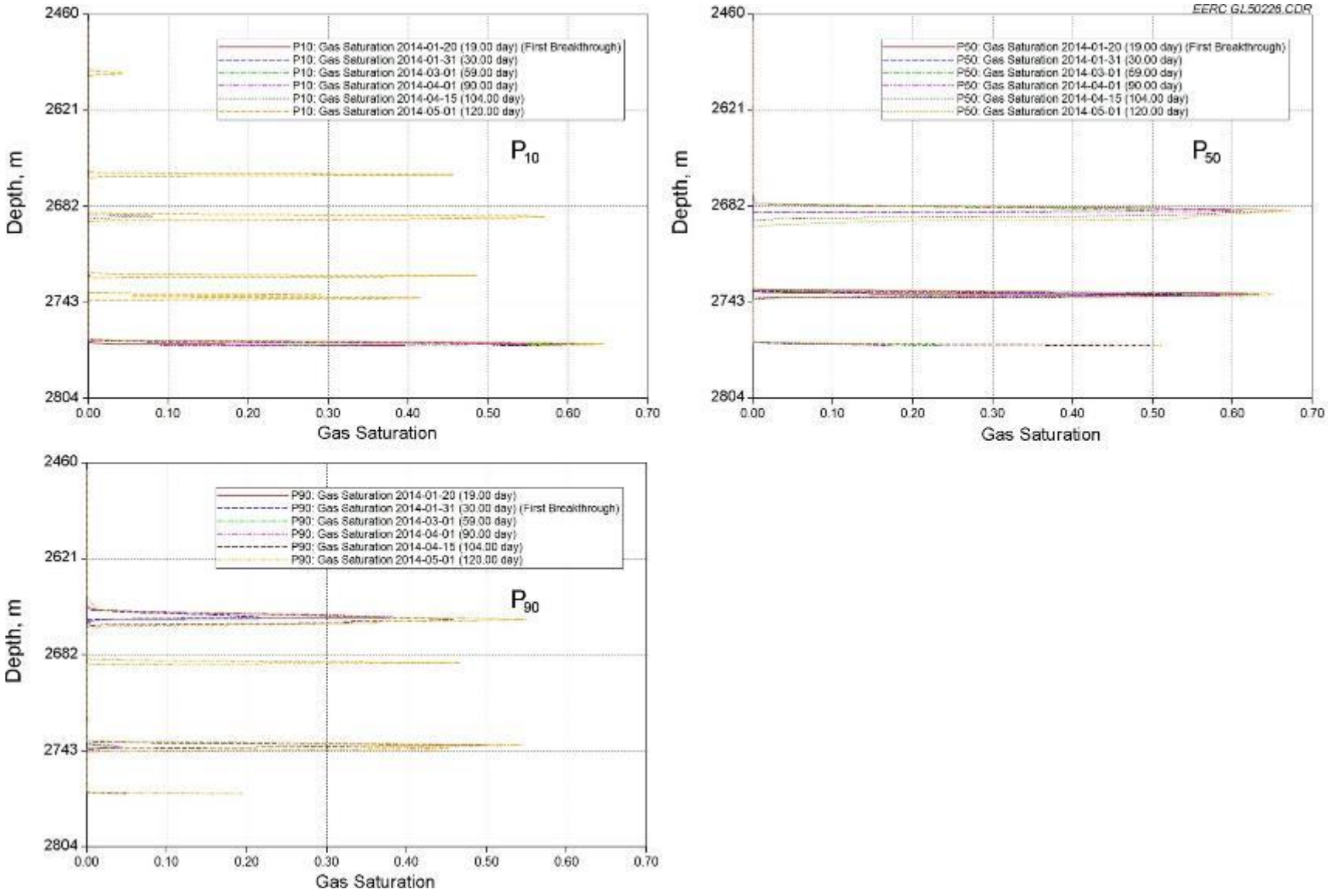

Figure A-25. CO_2 saturation plots along the observation well from top to bottom over time based on three geologic realizations.

Case 3 Pressure Change Monitoring

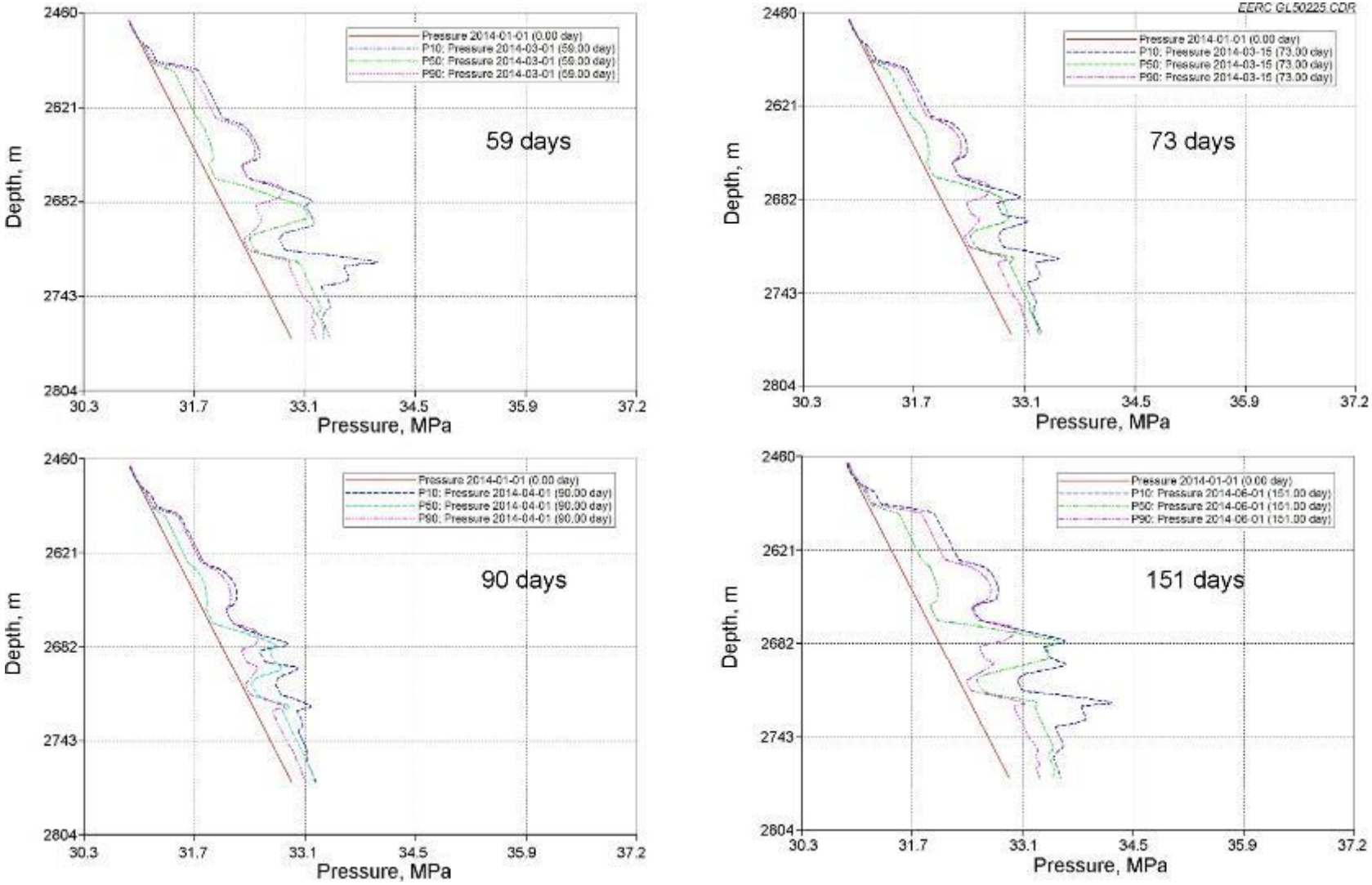

Figure A-26. Pressure plots along the observation well from top to bottom over time, starting from the injection beginning.

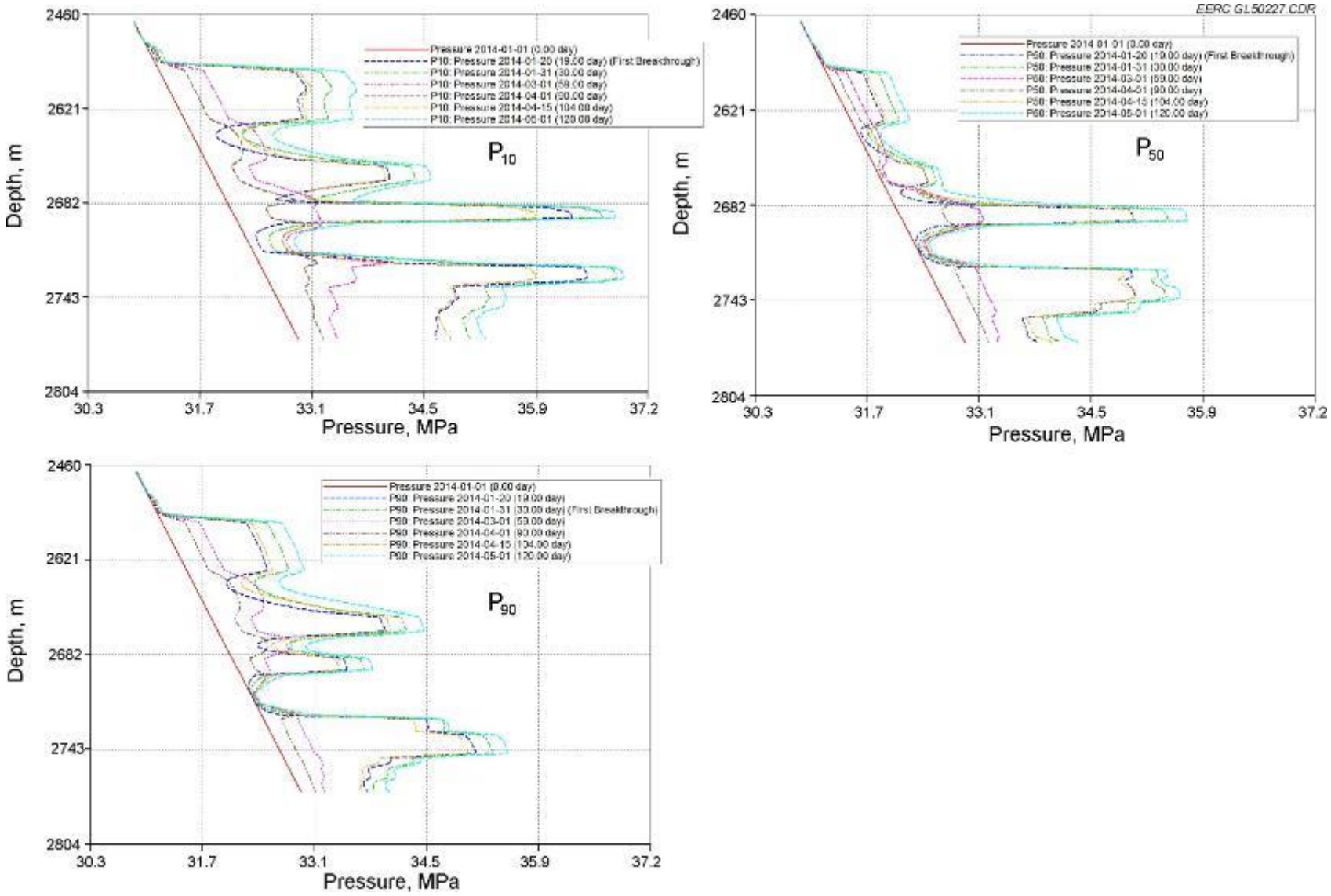

Figure A-27. CO_2 saturation plots along the observation well from top to bottom over time based on three geologic realizations.

Case 3 CO_2 Plume Movements

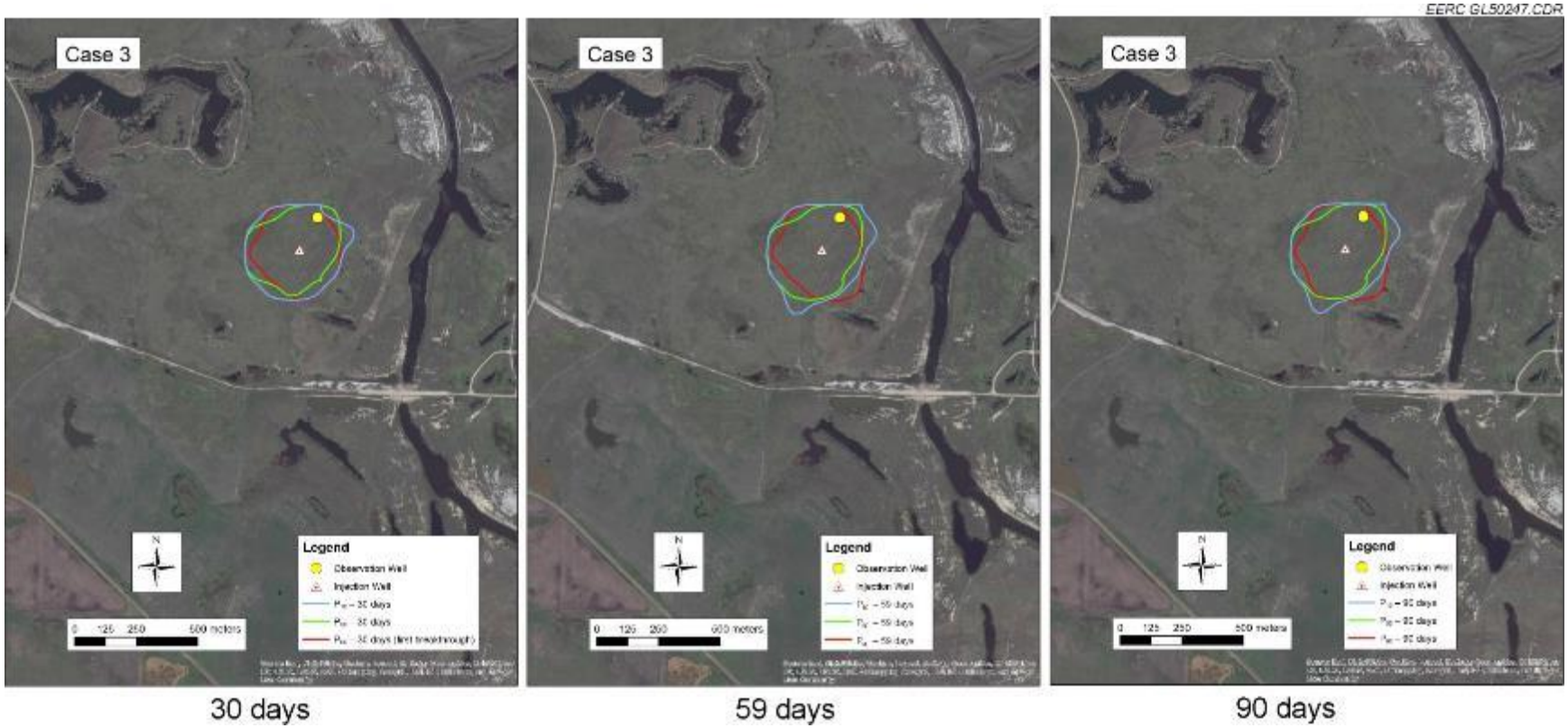

Figure A-28. CO_2 plume maps over time, starting from the injection beginning (continued).

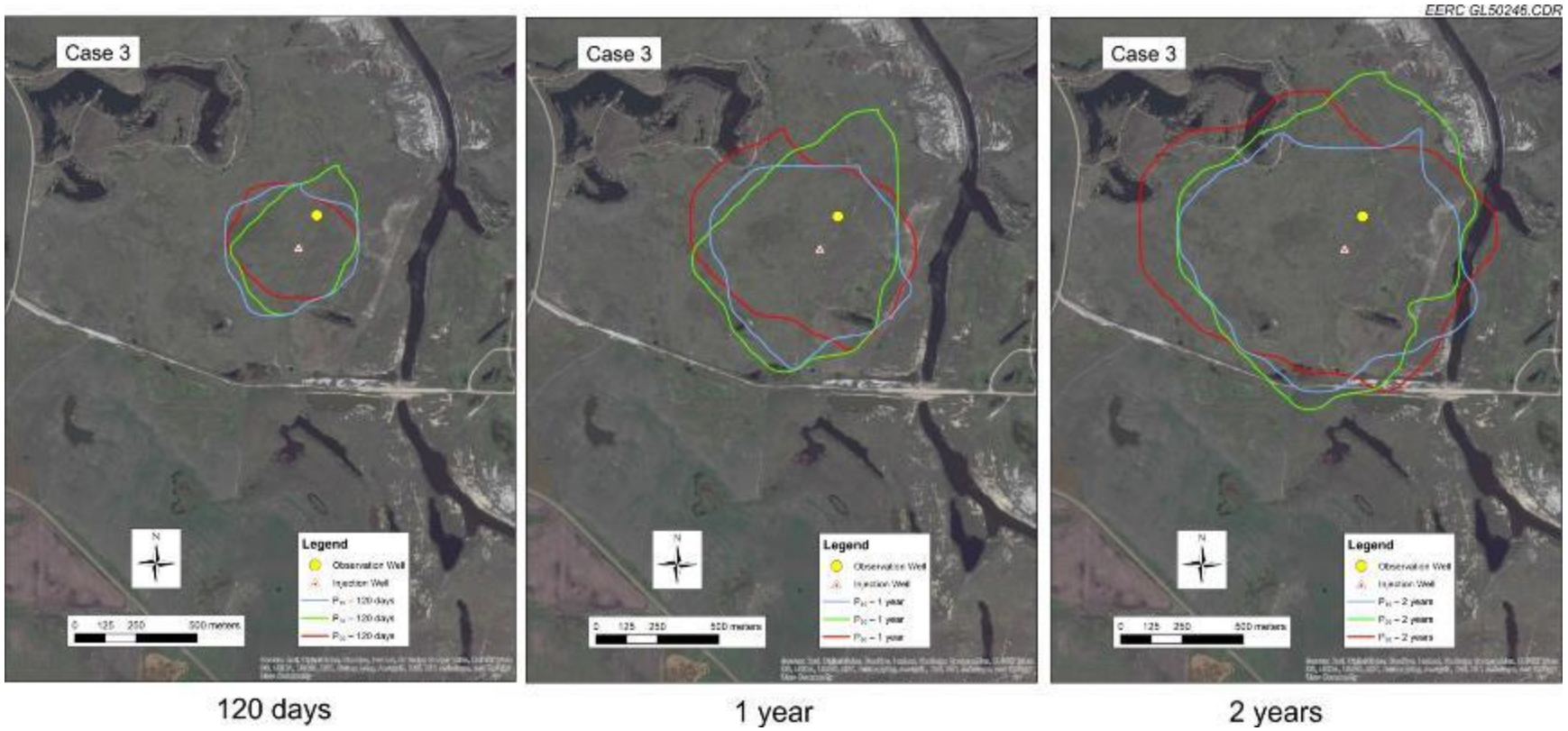

Figure A-28 (continued). CO_2 plume maps over time, starting from the injection beginning.

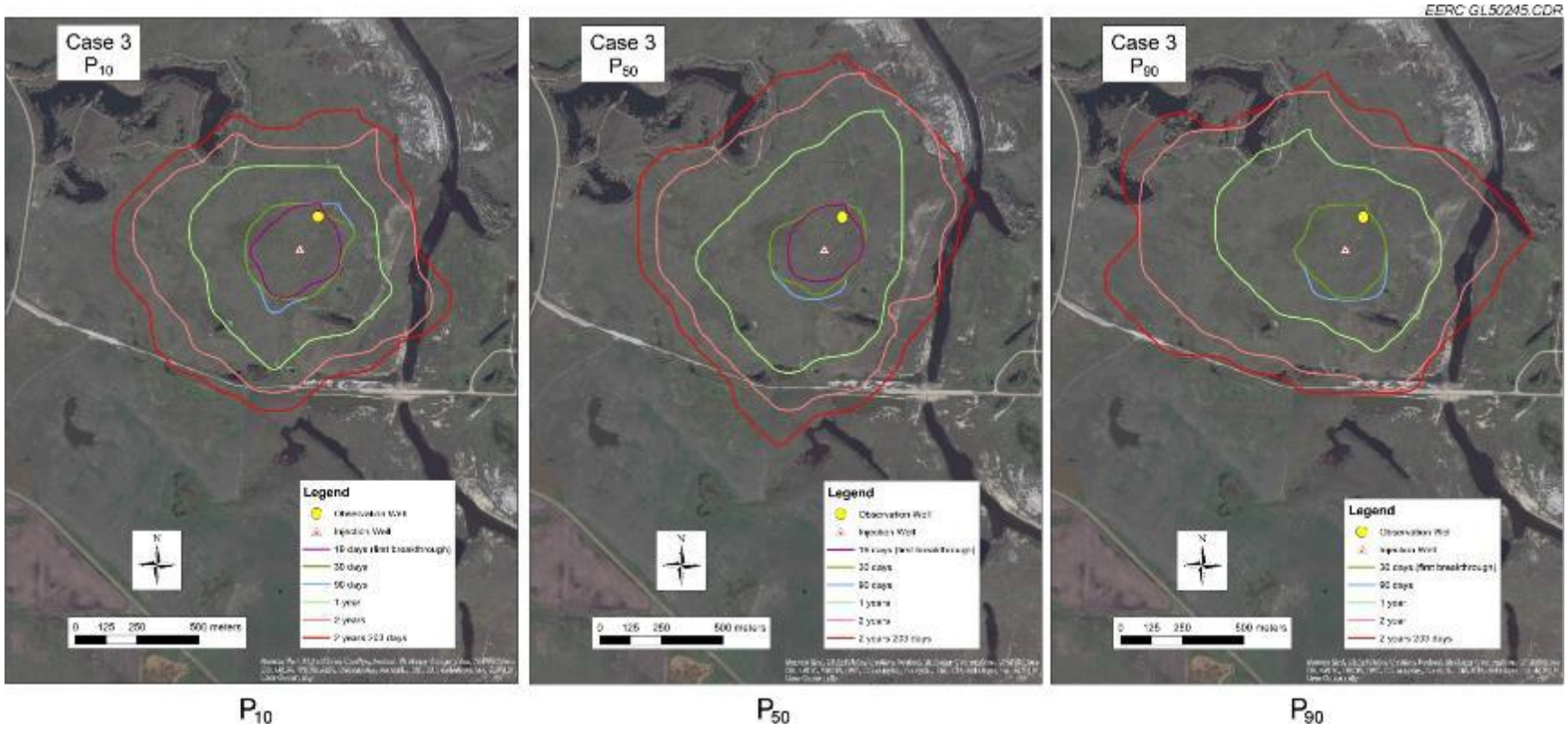

Figure A-29. CO_2 plume maps over three geologic realizations.

Case 3 Probability Distributions of CO_2 Movement

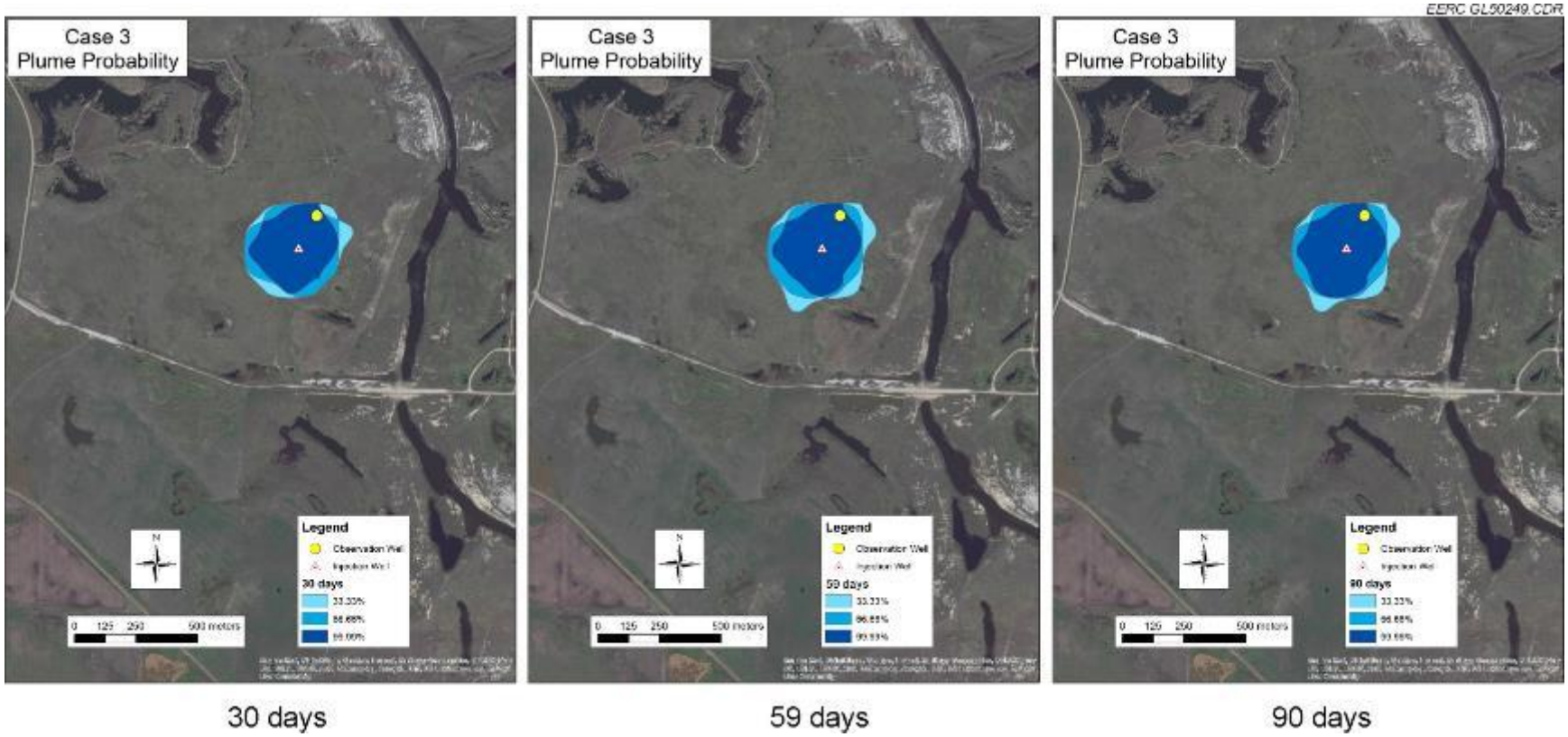

Figure A-30. Probability distributions of CO_2 movement over time (continued).

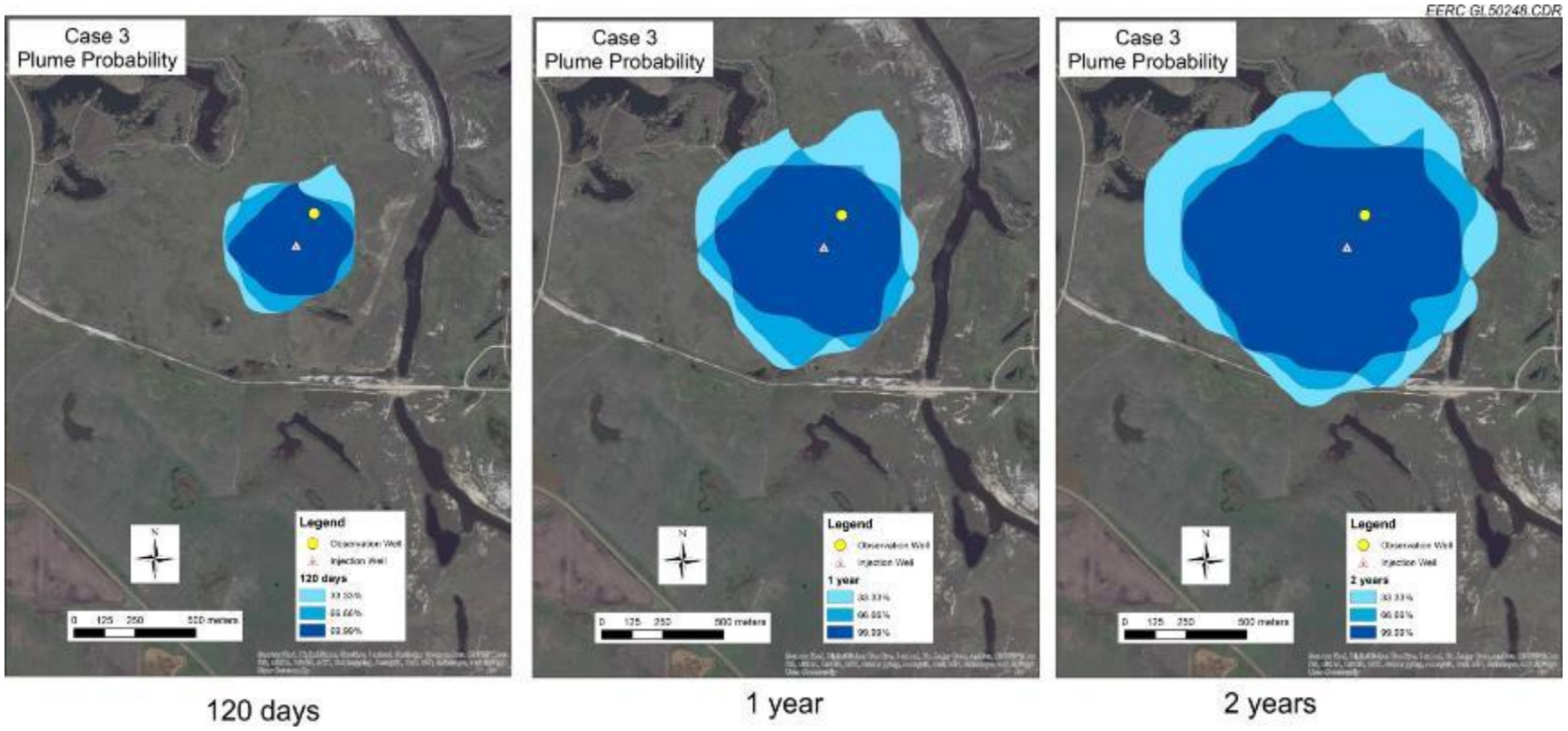

Figure A-30 (continued). Probability distributions of CO_2 movement over time (continued).

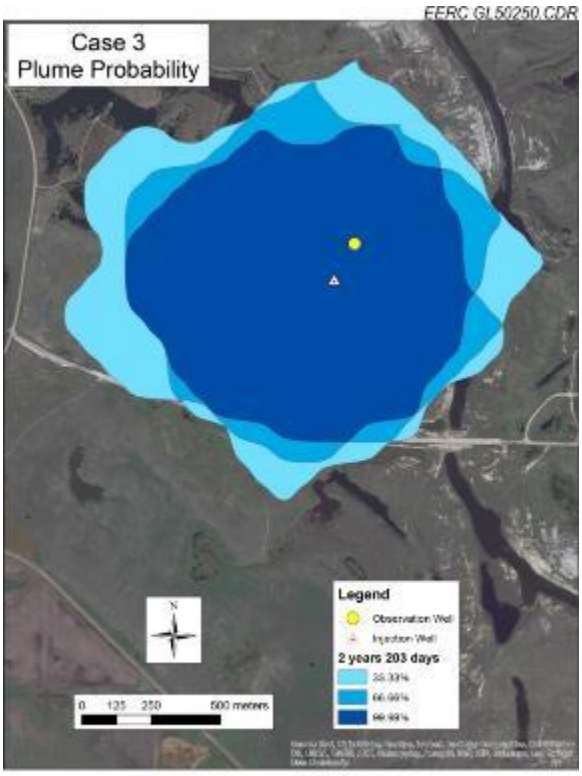

Figure A-30 (continued). Probability distributions of CO_2 movement over time.

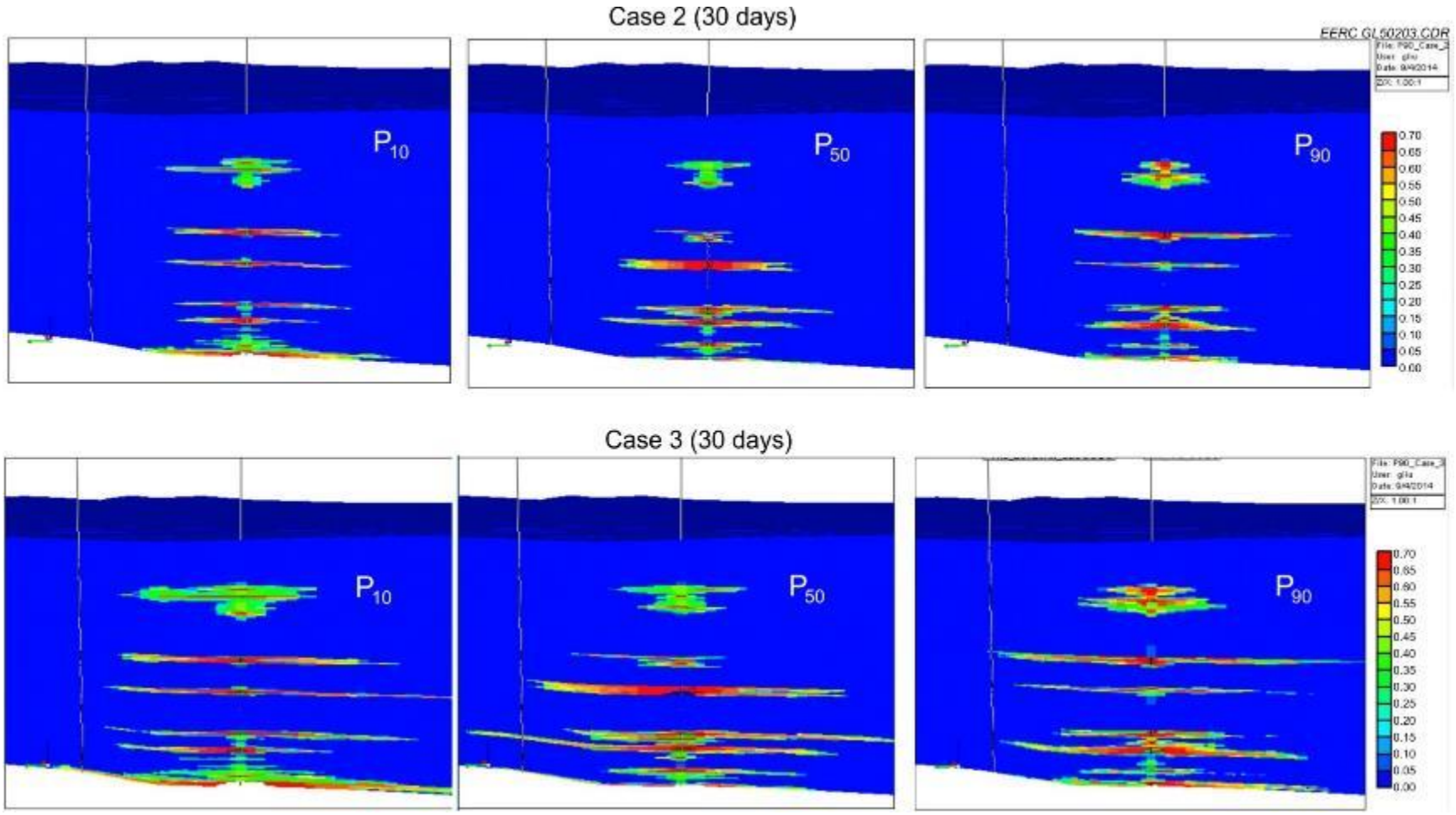

Figure A-31. Cross-section view of CO_2 saturation comparisons over time and realizations (continued).

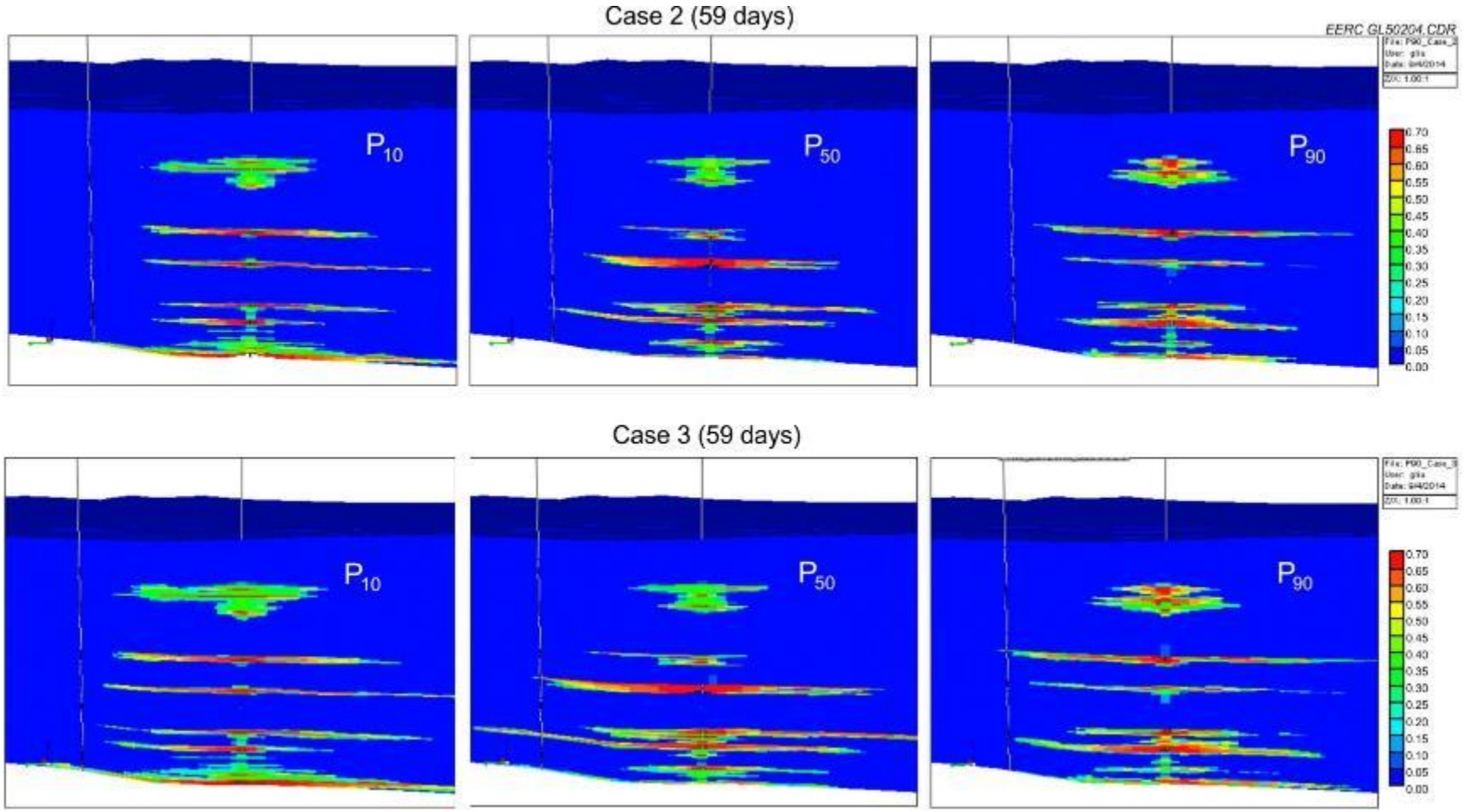

Figure A-31 (continued). Cross-section view of CO_2 saturation comparisons over time and realizations (continued).

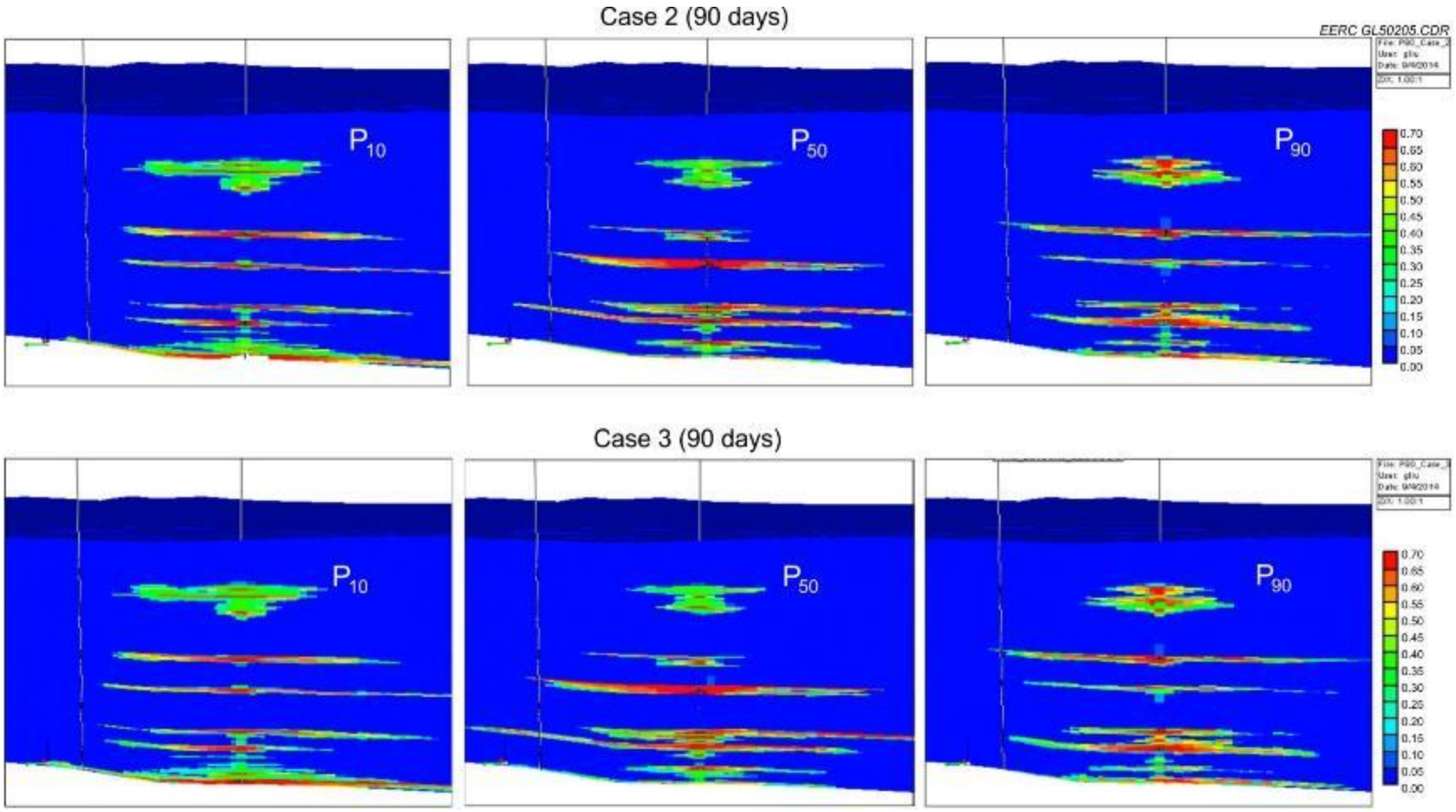

Figure A-31 (continued). Cross-section view of CO_2 saturation comparisons over time and realizations (continued).

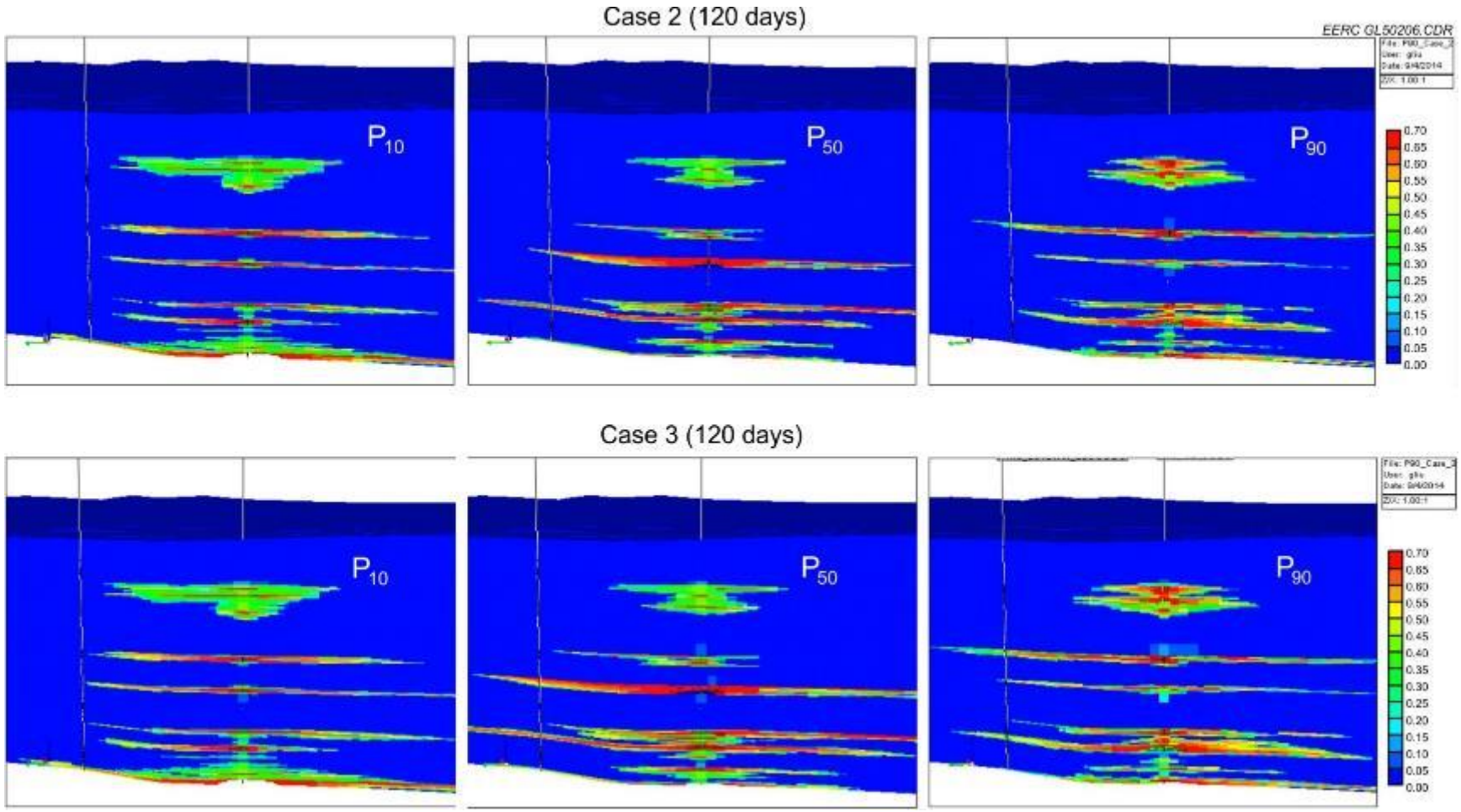

Figure A-31 (continued). Cross-section view of CO_2 saturation comparisons over time and realizations.

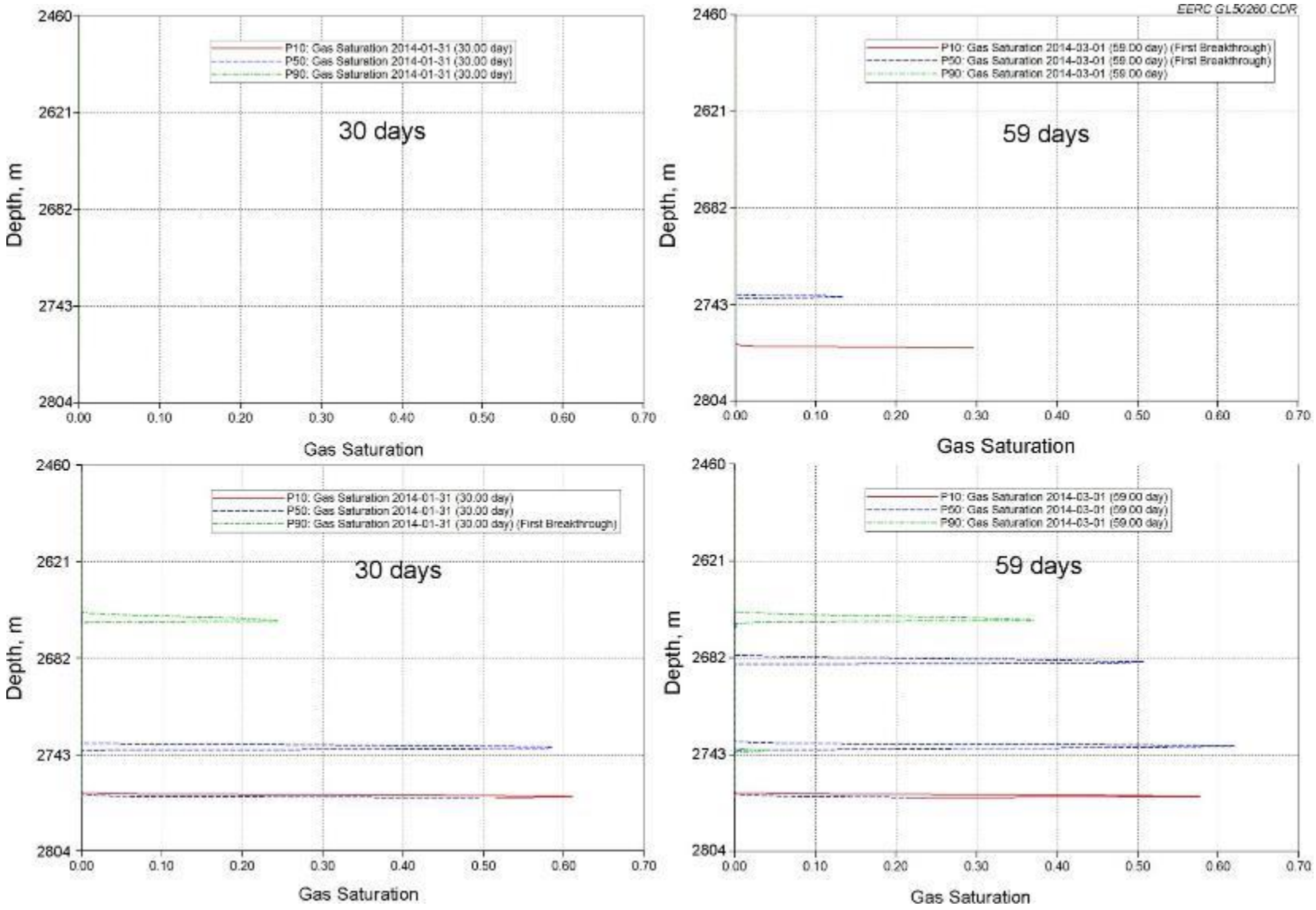

Figure A-32. Comparisons of CO_2 saturation plots along the observation well from top to bottom over time (continued).

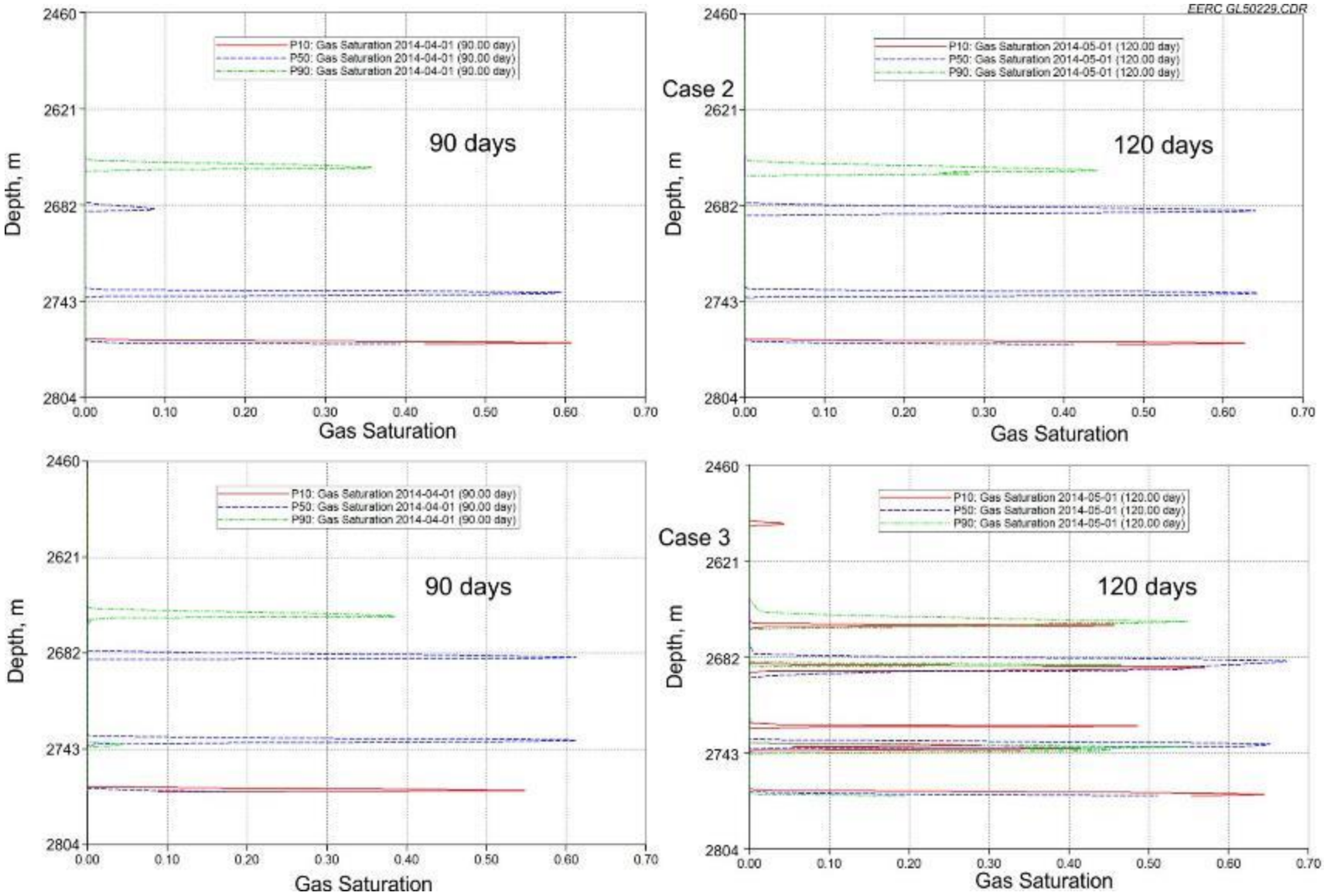

Figure A-32 (continued). Comparisons of CO_2 saturation plots along the observation well from top to bottom over time.

COMPARISONS OF PRESSURE CHANGE MONITORING

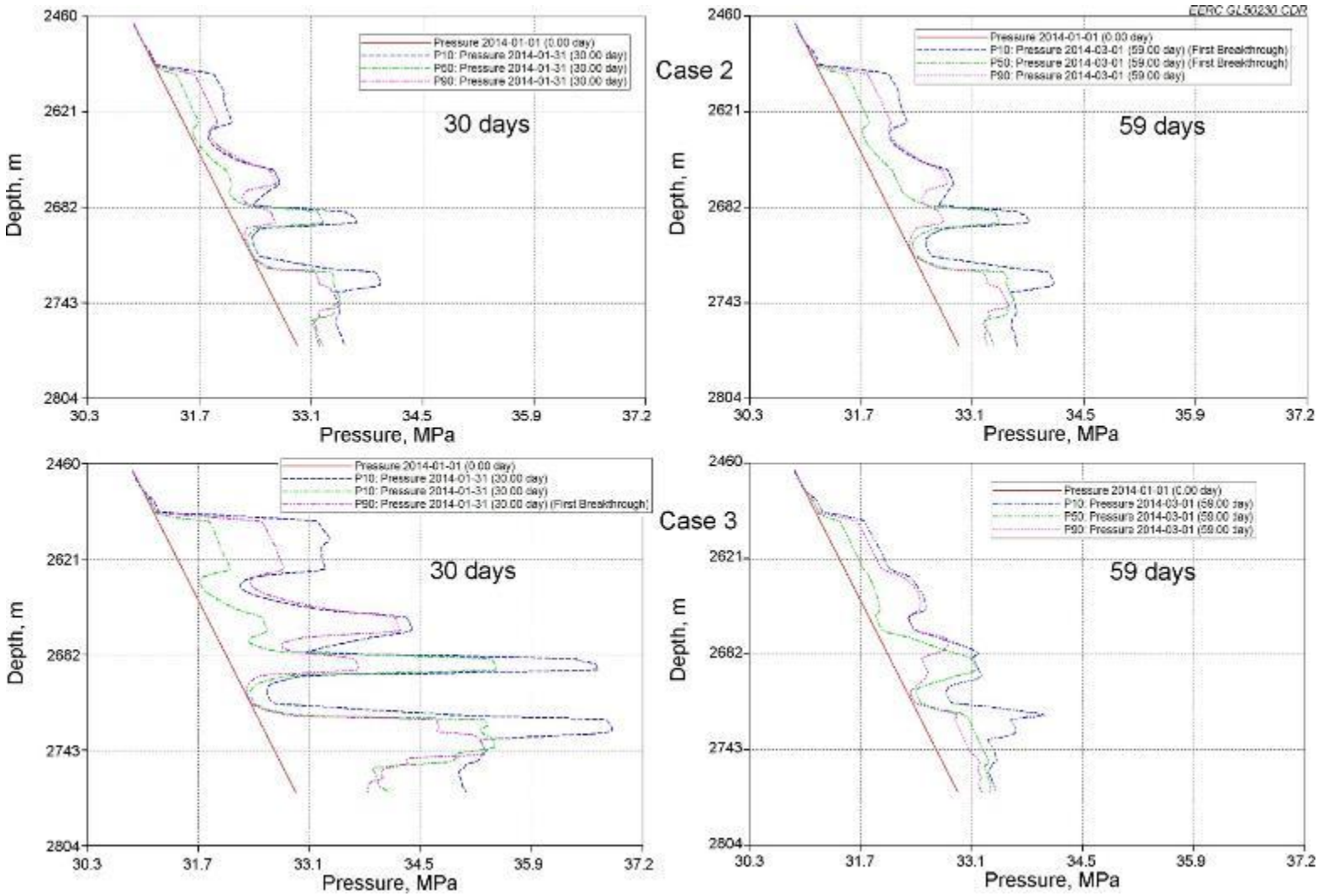

Figure A-33. Comparisons of pressure plots along the observation well from top to bottom over time, starting from the injection beginning (continued).

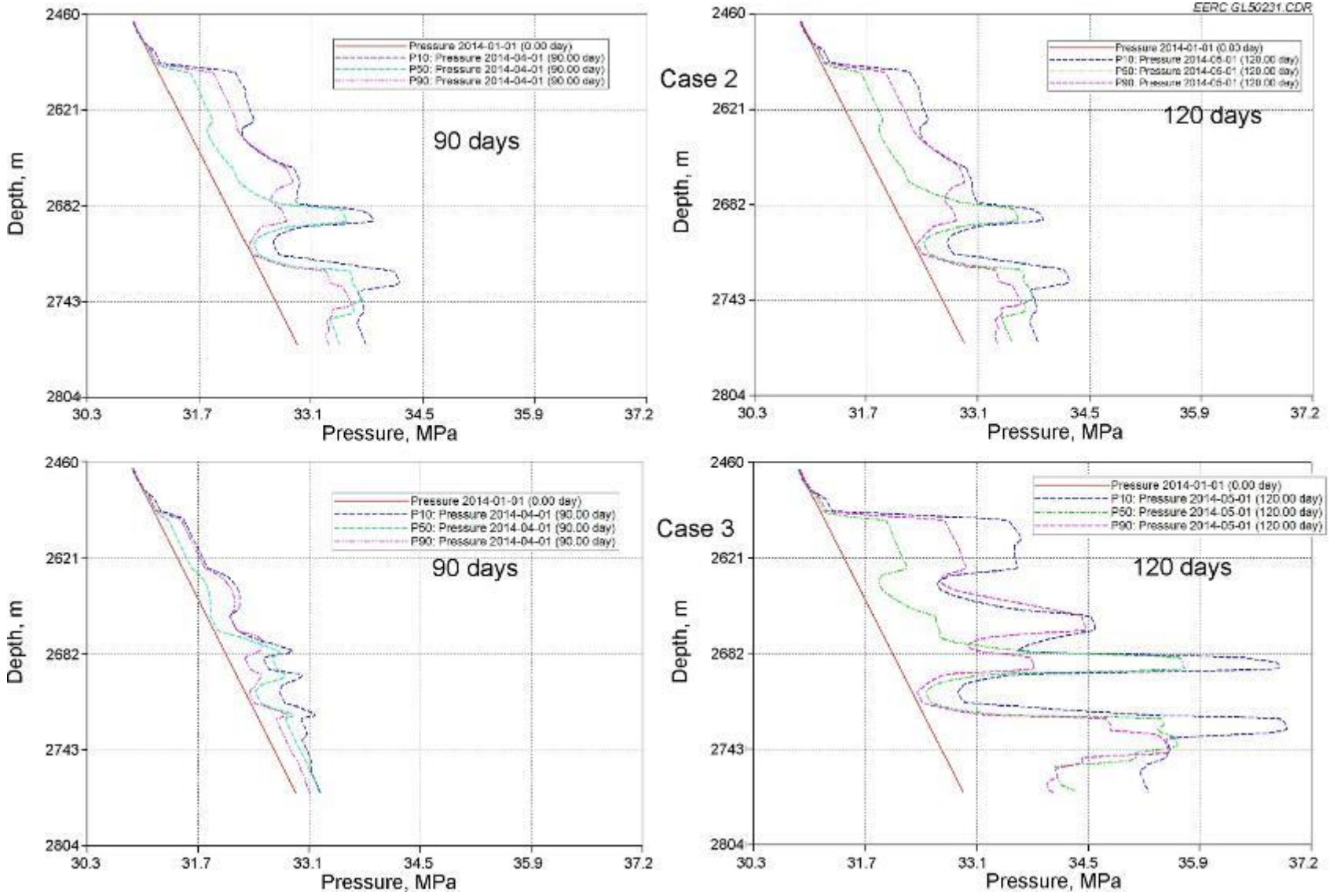

Figure A-33 (continued). Comparisons of pressure plots along the observation well from top to bottom over time, starting from the injection beginning.

COMPARISONS OF CO_2 PLUME MOVEMENTS

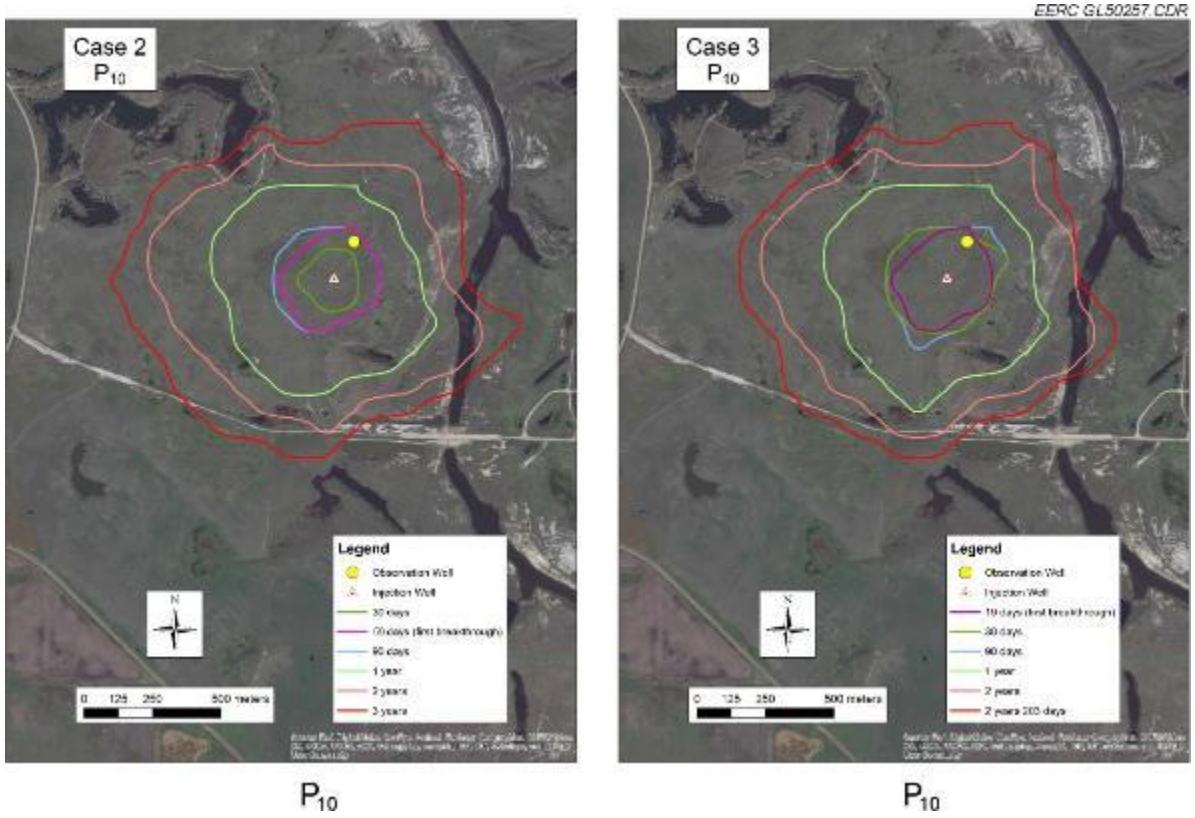

Figure A-34. Comparisons of CO_2 plume maps over three geologic realizations (continued).

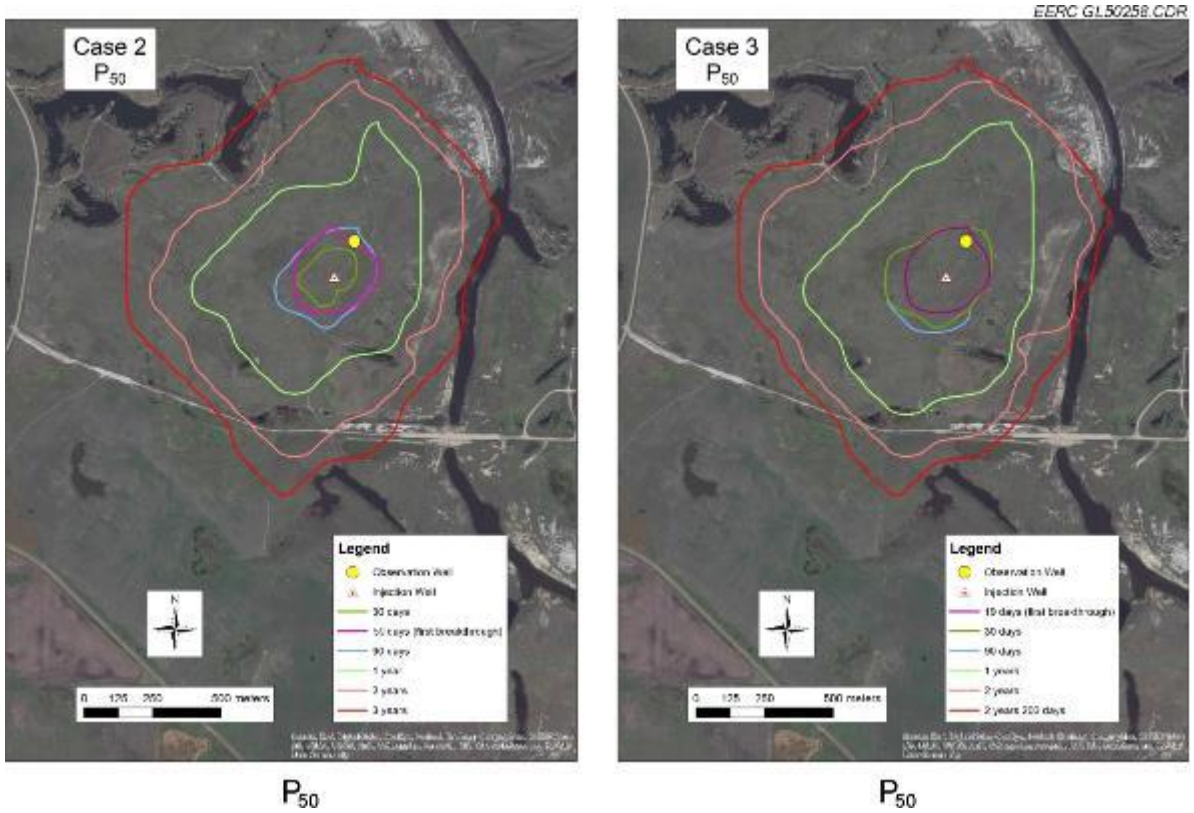

Figure A-34 (continued). Comparisons of CO_2 plume maps over three geologic realizations (continued).

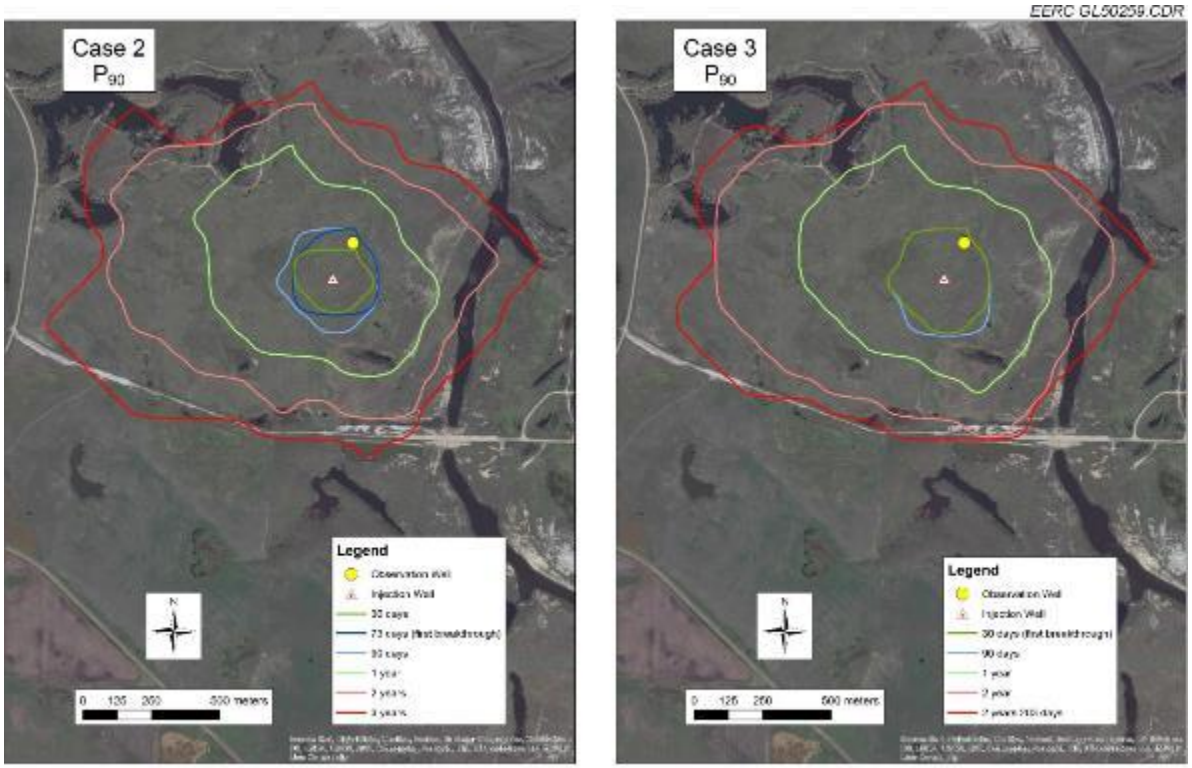

Figure A-34 (continued). Comparisons of CO_2 plume maps over three geologic realizations.

COMPARISONS OF PROBABILITY DISTRIBUTIONS OF CO_2 MOVEMENT

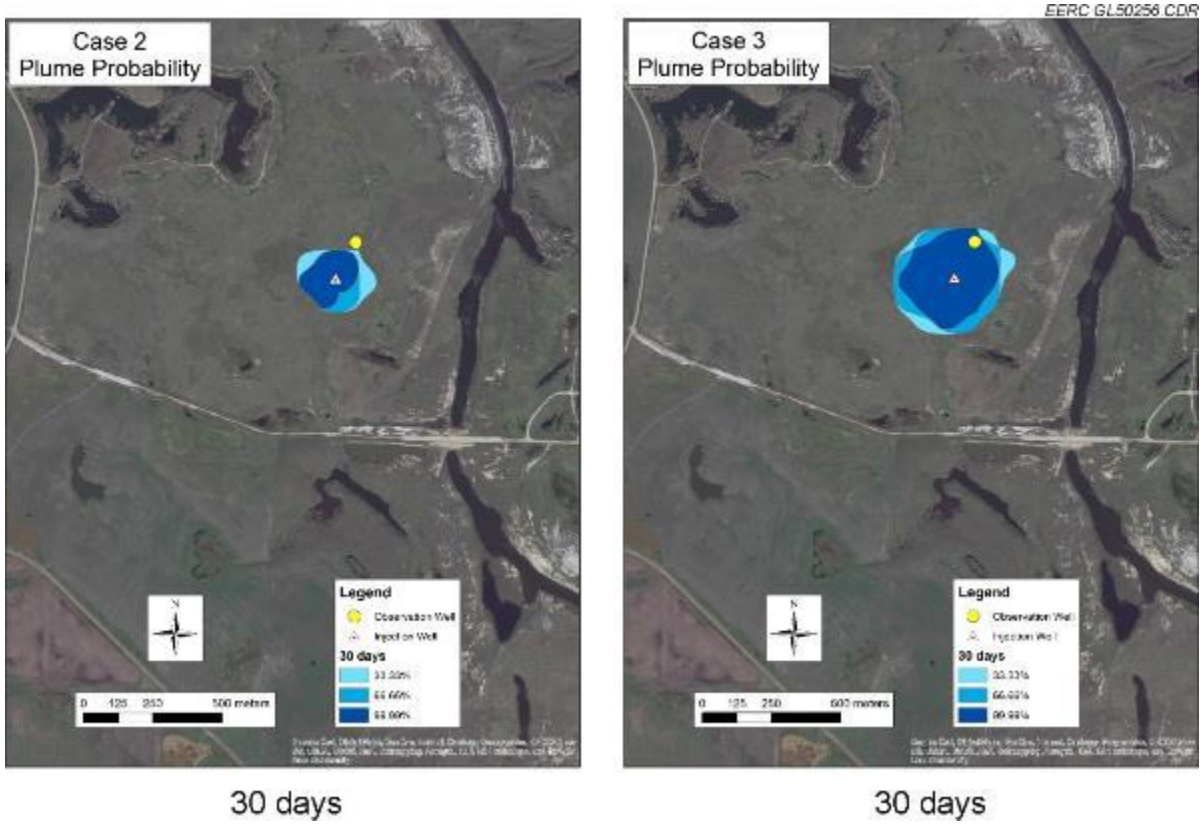

Figure A-35. Comparisons of probability distributions of CO_2 movement over time (continued).

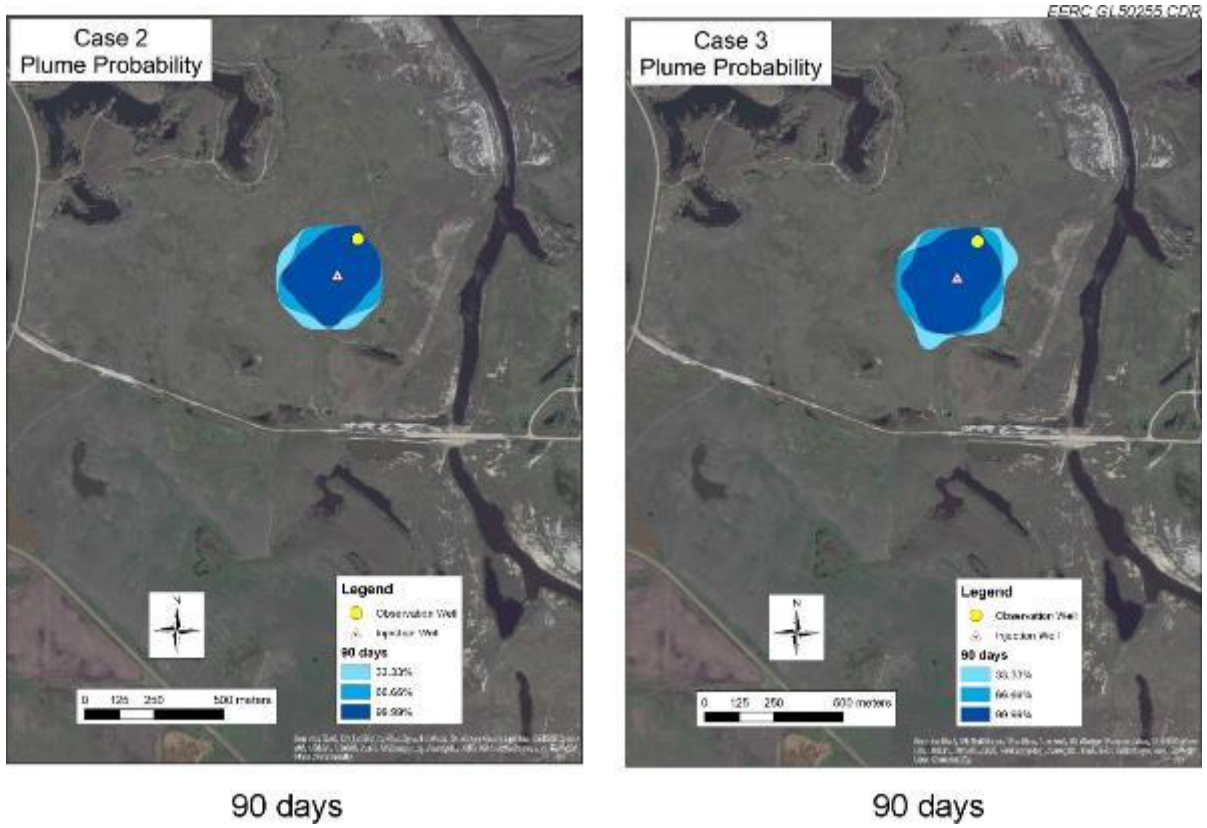

Figure A-35 (continued). Comparisons of probability distributions of CO_2 movement over time (continued).

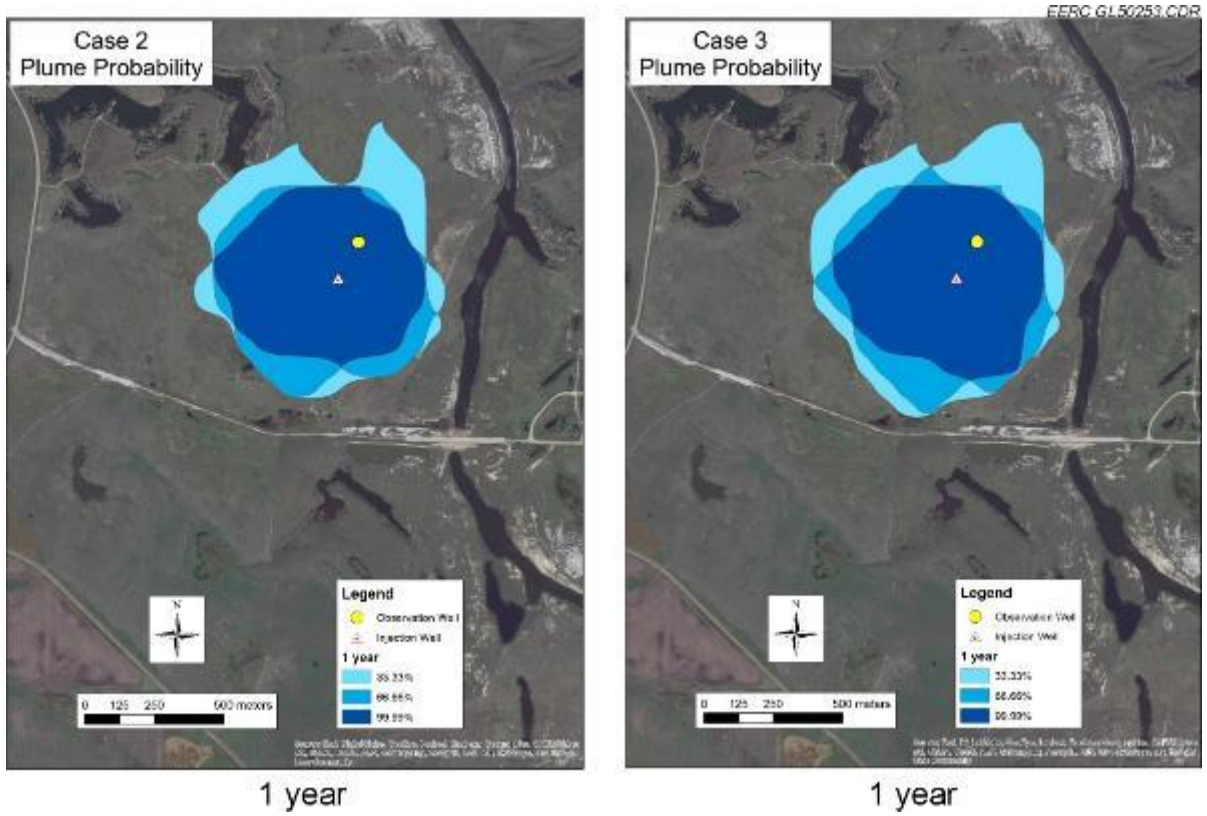

Figure A-35 (continued). Comparisons of probability distributions of CO_2 movement over time (continued).

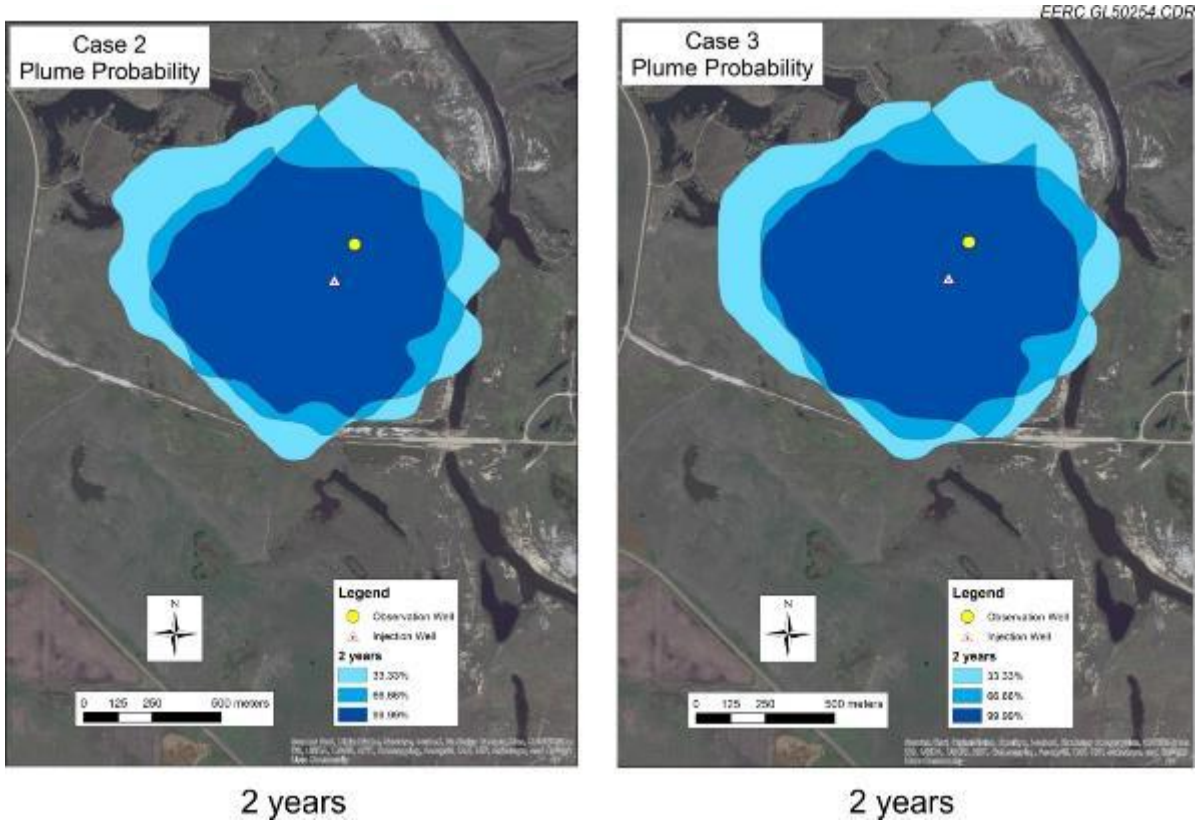

Figure A-35 (continued). Comparisons of probability distributions of CO_2 movement over time.